UNIVERSITY OF MINNESOTA

This is to certify that I have examined this copy of a doctoral thesis by

FATIH ECEVIT

and have found that it is complete and satisfactory in all respects,
and that any and all revisions required by the final
examining committee have been made.

DR. FERNANDO REITICH

Name of Faculty Adviser

Signature of Faculty Adviser

Date

GRADUATE SCHOOL

Integral Equation Formulations of Electromagnetic and Acoustic Scattering Problems: High-frequency Asymptotic Expansions and Convergence of Multiple Scattering Iterations

A THESIS
SUBMITTED TO THE GRADUATE SCHOOL
OF THE UNIVERSITY OF MINNESOTA
BY

Fatih Ecevit

IN PARTIAL FULFILLMENT OF THE REQUIREMENTS
FOR THE DEGREE OF
DOCTOR OF PHILOSOPHY

Dr. Fernando Reitich, Adviser

August 2005

Acknowledgements

I am grateful to the many people who helped me get to this stage and complete this thesis.

First and foremost, I would like to express my sincere gratitude to my Ph.D. thesis adviser, Professor Fernando Reitich, for I cannot overstate how much I appreciate the truly endless support and encouragement he provided through the last four years. I would like to thank him, on the one hand, for introducing me the marvellous field of computational electromagnetics and acoustics, and for the many fruitful discussions we had on the subject; and on the other hand, for demonstrating the essential nature and beauty of applied mathematics to a formerly pure mathematician.

I highly acknowledge Professors Bernardo Cockburn, Anand Gopinath and Fadil Santosa for their participation in my dissertation committee. My special thanks goes to Professor Markus Keel for his careful reading of the initial manuscript, and providing many helpful comments.

I am grateful to Professors Paul Garrett and Victor Reiner for their support and encouragement in the preliminary stages of my Ph.D. study.

Professor Mete Soner of Koç University - Istanbul has had a considerable influence on my carrier. I would like to thank him for helping me in making a decision among the graduate schools, and more importantly for drawing my attention to Professor Fernando Reitich. Professor Soner has also greatly influenced my decision to go to Max Planck Institute for Mathematics in the Sciences to pursue a postdoctoral research.

My M.S. thesis adviser, Professor Nilgün Işık of Boğaziçi University - Istanbul, was the person who motivated me to become a mathematician. Among many other things, this is what I am the most grateful to her.

The memory of my mother Hatice Ecevit, who kept our family united after my father Nureddin Ecevit's early departure, will always lead me in my life. Besides my mother, my sister Dilek and brother Murat have always supported me in all respects. I am indebted to and thankful to them all for their endless encouragement.

Finally, I want to thank my beloved wife Ebru for her love and patience. It is a true statement that it would not be possible to complete this thesis without her support. I am also grateful to her for giving me the most wonderful creature on earth, our son Kaan Giray.

Abstract

One of the main difficulties in high-frequency electromagnetic and acoustic scattering simulations is that any numerical scheme based on the full-wave model entails the resolution of wavelength. It is due to this challenge that simulations involving even very simple geometries are beyond the reach of classical numerical schemes. In this thesis, we present an analysis of a recently proposed integral equation method that bypasses the need for the resolution of wavelength, and thereby delivers solutions in frequency-independent computational times. Within single scattering configurations, the method is based on the use of an appropriate ansatz for the unknown surface densities and on suitable extensions of the method of stationary phase. The extension to multiple-scattering configurations, in turn, is attained through consideration of an iterative (Neumann) series that successively accounts for multiple reflections. We show that the convergence properties of this series in the high-frequency regime depends solely on geometrical characteristics. Moreover, for periodic orbits, we explicitly determine the convergence rate for two- and three-dimensional configurations. Finally, we show that this insight suggests the use of alternative summation mechanisms that can greatly accelerate the convergence of the series, and that it also provides connection to classical scattering theory.

Contents

List of Figures

Chapter 1

Introduction

Today, it is virtually impossible to find an area in technology that does not utilize the principles of electromagnetics and acoustics. Indeed, electromagnetism and acoustics find applications in a wide spectrum of areas in engineering and industry, including communications, material science, plasma physics, biology, radar and remote sensing to name but just a few. Advances in computer hardware and numerical algorithms during the last twenty years have made it possible to rely on computer simulations to guide the development of a variety of electromagnetic and acoustic devices. Consequently, computational electromagnetics and acoustics have claimed a central position in the mainstream of contemporary computational science [63].

Over the last two decades, accurate and efficient direct numerical schemes have been developed and successfully applied to the simulation of electromagnetic and acoustic wave propagation [4, 11, 20, 39, 71]. However, all of these methods require the resolution of wavelength, and this restricts their applicability to moderately low frequencies. For higher frequencies, accordingly, the only practical recourse is to resort to asymptotic methods (e.g. ray tracing) as these by-pass the need for frequency-dependent discretizations [3, 13, 46, 55]. These methods, on the other hand, are not error-controllable since they solve an approximate model instead of the original equations (e.g. the eikonal equation instead of the Helmholtz equation or the Maxwell system). Ideally, then, it would be desirable to design a numerical scheme that combines the advantages of rigorous solvers (error-controllability) with those of the asymptotic methods (frequency-independent discretization), and that will therefore allow for efficient and accurate simulations throughout the frequency spectrum.

Recently, an integral equation method that displays these capabilities has been proposed for the solution of surface-scattering problems [15, 16, 17, 18]. In single scattering configurations, the method is based on a combination of three main elements: 1) A *high-frequency ansatz* that captures, with coarse discretizations, the rapidly oscillatory progression of the surface currents; 2) A novel numerical integration method based on *localization principle* and extensions of the stationary phase method; and 3) A *change of variables around shadow boundaries*, that produces needed corrections of the phase extraction ansatz in these regions, and thus allows the method to account accurately for diffraction effects and creeping waves. The extension to multiple scattering configurations, in turn, are based on an iteratively computable (*Neumann*) series for the currents induced on the scattering surfaces, which accounts rigorously for multiple scattering; and reduces its treatment to a succession of single-scattering events.

This thesis is devoted to the analysis of these multiple-scattering iterations, their convergence properties, possible acceleration strategies and the connection of these with classical scattering theory.

The main part of the thesis relates to the determination of the rate of convergence of the iterated series for configurations that consist of several interacting convex structures. In this regard, we establish that, when a collection of obstacles are transversed periodically, the ratios of the (asymptotic representations of) iterated currents that differ by one period converge uniformly to a certain complex number. This number is independent of incidence, and in the limit of infinite frequency it depends solely on the geometrical arrangement. To derive these results, our mathematical strategy is based on the following three steps:

1. *Derivation of a high-frequency asymptotic recurrence for the terms of the series, in terms of the geometrical quantities determined by optical ray paths.* Specifically, we show that if a ray arrives at a point on the boundary of a scatterer after n-bounces, then (asymptotically) the current at that point equals the current at the (n-1)-th reflection-point of the ray times a continued fraction determined by geometric properties of the corresponding ray path.

2. *Analysis of ray paths.* Here we establish that if a group of rays traverse the objects periodically for a large number of reflections, then -except for the first and last few reflections- their reflection points accumulate on certain specific regions of the boundaries of the scatterers.

3. *Analysis of the recurrence on the iterated currents.* Here we use 2) to derive a rate from 1). More precisely, we demonstrate that, when a p-periodic orbit is traversed indefinitely, the ratio of iterated currents differing by one period converges uniformly to the product of a number p of "limit p-periodic continued fractions"; the convergence rate is then deduced appealing to the theory of limit p-periodic continued fractions [44].

As we said, this result shows, for instance, that in the high-frequency regime the convergence properties of the iterated series depend solely on the geometrical characteristics of the scatterers. For example, for a configuration consisting of two convex cylindrical bodies K_1 and K_2, the rate is

$$r = \left((1+\kappa_1 d)(1+\kappa_2 d) \left[1 + \sqrt{1 - \frac{1}{(1+\kappa_1 d)(1+\kappa_2 d)}} \;\right]^2 \right)^{-1/2}$$

where κ_i are the curvatures at the uniquely determined points a_1 and a_2 that minimize the distance between K_1 and K_2, and $d = |a_1 - a_2|$. We note that, while for practical purposes the analysis of the periodic orbits will generically yield a good estimate of the overall convergence rate, a full demonstration will necessitate an analogous study of non-periodic orbits.

Although, as our work has shown, the series converges spectrally, it is clearly desirable to design mechanisms to accelerate its convergence. The second part of the thesis provides an explanation for the enhanced convergence properties of one such procedure, namely Pade approximation [6] in this context. Indeed, appealing to our analysis of optical ray paths, we show that the ratio of iterated currents differing by one period stabilizes after a certain number of reflections. As we demonstrate, once stabilized, the behavior of the series resembles that of a geometric series which, in turn, can be exactly represented as a rational function. This observation suggests that beyond the point where currents become stationary, Pade approximation will deliver significantly more accurate solutions than those provided by the summation of the series.

The final part of the thesis relates to consequences of our work on the analysis of a fundamental operator in classical scattering theory, namely the *scattering operator* [75]. As it turns out, in the high-frequency regime, the rate of convergence of the Neumann series is directly linked to the location of the poles of the scattering operator. As we shall explain, our work on the rate of convergence of multiple-scattering iterations provides a simple method for the determination of the poles of the scattering operator for two strictly convex obstacles.

Chapter 2

Preliminaries

In this Chapter, we have collected the preliminaries for the thesis. In §2.1, we review the partial differential equations modelling the propagation of electromagnetic and acoustic waves. An overview of the state-of-the-art methods relating to the numerical treatment of these partial differential equations is provided in §2.2. Scattering problems, which constitute the main topic of this thesis, are discussed in §2.3. Finally, in regards to our integral equation approach to scattering problems, we display the classical integral equations for the solution of scattering problems.

2.1 Governing Equations

In this section, we briefly review the mathematical models relating to the propagation of electromagnetic and acoustic waves. In particular, we explain the fundamental role played by the Helmholtz equation, upon which we base our further developments.

2.1.1 Electromagnetic Waves

Electromagnetic wave propagation in a medium in $\mathbb{R}^3$ is governed by the equations

$$
\begin{aligned}
\nabla \times \mathbf{E} + \frac{\partial \mathbf{B}}{\partial t} &= 0 && (\textit{Faraday's law}) \\
\nabla \times \mathbf{H} - \frac{\partial \mathbf{D}}{\partial t} &= \mathbf{J} && (\textit{Ampere-Maxwell law}) \\
\nabla \cdot \mathbf{B} &= 0 && (\textit{absence of free magnetic poles}) \\
\nabla \cdot \mathbf{D} &= \rho && (\textit{Coulomb's law})
\end{aligned}
$$

known as *Maxwell equations* [43]. The scalar field ρ is the electric charge density, and the vector fields $\mathbf{E}$, $\mathbf{H}$, $\mathbf{D}$, $\mathbf{B}$, and $\mathbf{J}$ are, respectively, the electric field, magnetic field, electric displacement, magnetic induction, and conduction current density. In addition, there are the constitutive relations that express $\mathbf{D}$, $\mathbf{B}$ and $\mathbf{J}$ in terms of $\mathbf{E}$ and $\mathbf{H}$. In the case of an isotropic medium (i.e. when its physical properties at each point are independent of direction of propagation), they take on the relatively simple form

$$
\begin{aligned}
\mathbf{D} &= \epsilon \mathbf{E}, \\
\mathbf{B} &= \mu \mathbf{H}, \\
\mathbf{J} &= \sigma \mathbf{E}. \qquad (\textit{Ohm's law})
\end{aligned}
$$

The scalar fields ϵ, μ, and σ are, respectively, the electric permittivity, magnetic permeability, and electric conductivity.

For time-harmonic electromagnetic waves of the form

$$
\begin{aligned}
\mathbf{E}(x,t) &= \mathrm{Re}\left(\left(\epsilon + \frac{i\sigma}{\omega}\right)^{-1/2} e^{-i\omega t} E(x)\right), \\
\mathbf{H}(x,t) &= \mathrm{Re}\left(\mu^{-1/2} e^{-i\omega t} H(x)\right)
\end{aligned}
$$

with frequency $\omega > 0$, we deduce that the complex-valued space-dependent parts satisfy the *time-harmonic Maxwell equations*

$$\nabla \times E - ikH = 0, \tag{2.1.1a}$$

$$\nabla \times H + ikE = 0, \tag{2.1.1b}$$

$$\nabla \cdot (\epsilon E) = \rho, \tag{2.1.1c}$$

$$\nabla \cdot (\mu H) = 0 \tag{2.1.1d}$$

where the wave number k satisfies

$$k^2 = \left(\epsilon + \frac{i\sigma}{\omega}\right)\mu\omega^2$$

with k chosen such that $\operatorname{Im} k \geq 0$.

Typically, equations (2.1.1) must be supplemented with appropriate boundary conditions. For instance, at the interface between two different medium, the tangential component of the electric field E is ought to be continuous, while the tangential component of the magnetic field H must be discontinuous by an amount proportional to the magnitude of the surface current density. In particular, if the second medium is a perfect conductor, the tangential component of the total electric field E as well as the normal component of the total magnetic field H must vanish at the interface. This gives rise to the *perfect conductor boundary condition*

$$\nu \times E = 0, \quad \nu \cdot H = 0 \quad \text{on } \partial K$$

where ν denotes the unit exterior normal vector to the interface ∂K. More general boundary conditions can also be considered. For example, when the second interface is not perfectly conducting but does not allow the electromagnetic wave to penetrate deeply into the medium, then an *impedance boundary condition* of the form

$$\nu \times (\nabla \times E) - i\lambda(\nu \times E) \times \nu = 0$$

must be imposed at the interface ∂K with an appropriately chosen positive constant λ.

Naturally, studying Maxwell equations with constant coefficients is a prerequisite for studying them in general. In the case that the medium is homogeneous (i.e. ϵ, μ, and σ are constant) and free of charges (i.e. $\rho = 0$), the time-harmonic equations reduce to

$$\nabla \times E - ikH = 0,$$
$$\nabla \times H + ikE = 0.$$

In this case, E and H are divergence-free and satisfy the *vector Helmholtz equation*

$$\Delta E + k^2 E = 0,$$
$$\Delta H + k^2 H = 0.$$

Conversely, if E (or H) is a solution to the vector Helmholtz equation satisfying $\nabla \cdot E = 0$ (or $\nabla \cdot H = 0$), then E and $H = (1/ik)\nabla \times E$ (or H and $E = (-1/ik)\nabla \times H$) satisfy the time-harmonic Maxwell equations [25].

2.1.2 Acoustic Waves

Consider the propagation of sound waves of small amplitude in a homogeneous isotropic medium in $\mathbb{R}^3$ viewed as an inviscid fluid. Let $v = v(x, t)$ be the velocity field and let $p = p(x, t)$, $\rho = \rho(x, t)$ and $S = S(x, t)$ denote the pressure, density and specific entropy, respectively, of the fluid. The motion is then governed by the *Euler equations* [25]:

$$
\begin{aligned}
\frac{\partial v}{\partial t} + (v \cdot \nabla) v + \frac{1}{\rho} \nabla p = 0 & \qquad (\textit{equation of conservation of momentum}) \\
\frac{\partial \rho}{\partial t} + \nabla \cdot (\rho v) = 0 & \qquad (\textit{equation of continuity}) \\
p = f(\rho, S) & \qquad (\textit{state equation}) \\
\frac{\partial S}{\partial t} + v \cdot \nabla S = 0 & \qquad (\textit{adiabatic hypothesis})
\end{aligned}
$$

where f is a function depending on the nature of the fluid. We assume that v, p, ρ and S are small perturbations of the static state $v_0 = 0$, $p_0 =$ constant, $\rho_0 =$ constant and $S_0 =$ constant and linearize to obtain the *linearized Euler equations* :

$$
\begin{aligned}
\frac{\partial v}{\partial t} + \frac{1}{\rho_0} \nabla p &= 0, \\
\frac{\partial \rho}{\partial t} + \rho_0 \nabla \cdot v &= 0, \\
\frac{\partial p}{\partial t} &= \frac{\partial f}{\partial \rho}(\rho_0, S_0) \frac{\partial \rho}{\partial t}.
\end{aligned}
$$

From this we obtain the *wave equation*

$$
\frac{1}{c^2} \frac{\partial^2 p}{\partial t^2} = \Delta p
$$

where the speed of sound, c, is given by

$$
c^2 = \frac{\partial f}{\partial \rho}(\rho_0, S_0).
$$

From the linearized Euler equations, we observe that there exists a velocity potential $U = U(x,t)$ such that

$$
v = \frac{1}{\rho_0} \nabla U \quad \text{and} \quad p = -\frac{\partial U}{\partial t}.
$$

Clearly, the velocity potential also satisfies the wave equation

$$\frac{1}{c^2}\frac{\partial^2 U}{\partial t^2} = \Delta U.$$

For time-harmonic acoustic waves of the form

$$U(x,t) = \mathrm{Re}\left(e^{-i\omega t}u(x)\right)$$

with frequency $\omega > 0$, we deduce that the complex-valued, space-dependent part u satisfies the *Helmholtz equation*

$$\Delta u + k^2 u = 0 \tag{2.1.2}$$

where the wave number k is given by the positive constant

$$k = \omega/c.$$

As with the electromagnetic waves, equation (2.1.2) must be coupled with suitable boundary conditions. For instance, when the pressure of the total wave u vanishes on the interface ∂K between two different medium, the Dirichlet boundary condition

$$u = 0 \quad \text{on} \quad \partial K$$

must be imposed. Similarly, if the normal velocity of the acoustic wave vanishes on the interface ∂K, then the appropriate boundary condition is the *Neumann* boundary condition:

$$\partial u/\partial \nu = 0 \quad \text{on} \quad \partial K.$$

More generally, allowing interfaces on which the normal velocity is proportional to the excess pressure leads to an *impedance boundary condition* of the form

$$\frac{\partial u}{\partial \nu} + i\lambda u = 0 \quad \text{on} \quad \partial K$$

where, again, λ is a positive constant.

2.2 Computational Electromagnetics/Acoustics

Although the principles of electromagnetics and acoustics are well understood (cf. §2.1), their application to practical configurations of current interest is significantly complicated and far beyond manual calculation in all but the simplest aspects. The significant advances in computer modelling of electromagnetic and acoustic interactions that have taken place over the last two decades have made it possible to shift the classical "trial and error" design paradigm for electromagnetic and acoustic devices to one that heavily relies on computer simulation. *Computational Electromagnetics (CEM)* and *Computational Acoustics (CA)* have thus taken on great technological importance and, largely due to this, they have become a central problem in present-day computational science [63].

The continuously increasing industrial and engineering demands for sophisticated electromagnetic and acoustic modelling, have made CEM and CA into industries of their own, involving a large number of researchers in academic, government and industrial laboratories. Not surprisingly then, the number of methods, or variations thereof, is almost as large. Still, the most successful methodologies can be broadly categorized as belonging to one of the following classes:

1. Differential (DE) equation methods: These algorithms are based on direct discretization of differential formulations of electromagnetic and acoustic equations, e.g. *finite difference time-domain method (FDTD)* etc.

2. Variational formulation (VF) methods: These methods are based on the solution

of weak formulations of the equations. Examples of VF methods include *method of moments (MoM)*, *finite element methods (FEM)*, and *finite volume methods (FVM)*.

3. Integral equation (IE) methods: These schemes are based on the discretization of integral equation formulations of the problems, e.g. the *boundary integral equation method (BIEM)*, the *boundary element method (BEM)*, etc.

4. Asymptotic Methods (AM): In contrast with the methods above, these do not solve the full Maxwell or acoustic equations, but rather an approximation of them (e.g. the *eikonal equation* instead of the *Helmholtz equation*). Examples of AM algorithms include *ray-tracing methods*, *shooting-and-bouncing-ray method (SBR)*, etc.

Each of these display advantages and shortcomings. DE methods, for instance, are easy to implement and they are, therefore, extensively used for computing electromagnetic/acoustic scattering by general objects [50]. However, they typically require 10-20 grid points per wavelength to obtain sufficiently accurate solutions of the scattered fields [74]. Such requirements inhibit the use of the DE methods for accurately computing electromagnetic/acoustic scattering by large objects. In addition, DE methods are not very versatile as they are constrained to use structured grids [61]. Variational formulation methods, on the other hand, are better adapted to simulations involving complicated geometries [41, 45].

When using DE or VF methods in scattering simulations, an artificial surface must be introduced at a finite distance from the scatterers in order to limit the computational domain. As a result, proper boundary conditions, known as *artificial boundary conditions (ABC)*, enforcing the condition that the scattered field be outgoing, must be introduced on this surface. In fact, the imposition of *exact* ABC's is possible via *Dirichlet-to-Neumann (DtN)* maps [37, 41]. However, the resulting boundary conditions are non-local, since they are expressed as surface integrals, and consequently, the linear systems that arise upon discretization are partially dense. This, in turn, can significantly add to the computational cost for DE and VF methods.

The design of efficient and accurate *local* ABC's is a complex exercise, that still attracts significant attention as it constitutes one of the main challenges in the implementation of DE and VF algorithms. A *characteristic type* ABC, requiring the scattered field to vanish at the artificial surface, has often been used (see [38] and the references therein). However, this causes significant reflections from the artificial boundary that pollute the computational results unless the surface is placed very far away from the scatterer (i.e., at a distance of 10-20 wavelengths). To alleviate this problem, a number of high-order *local* ABC's have been proposed [36, 37, 56]. With the same objective, a different approach was introduced by Berenger [8, 9] which bypasses the need for ABC, replacing them by a suitably constructed absorbing medium known as a *perfectly matched layer (PML).* In its initial form, Berenger's PML utilized a non-physical splitting of the electromagnetic field which led to instability [1]; stable versions of the PML approach have since been proposed [26, 31, 32, 38].

It is partly due to these difficulties in enforcing the radiation condition that IE methods constitute an advantageous approach for scattering simulations. Indeed, in integral equation formulations, the radiation condition is explicitly enforced by simply choosing an appropriate ("outgoing") fundamental solution [24, 25]. Moreover, the solution space is confined to the scattering obstacles and the number of unknowns arising when discretizing such equations is relatively small compared to those of DE and VF methods, especially in surface scattering applications. However, in general, the discretization of integral equation formulations leads to dense matrices [57]. As is well known, inversion of a dense $n \times n$ matrix with a direct solver, such as the LU decomposition, is an $O(n^3)$ operation [60]; an iterative method can decrease this to $O(n^2)$ [34]. Still this, however, can quickly become prohibitive in scattering applications. In fact, a significant part of all recent efforts relating to the numerical solution of integral equations in this context has focused on the design of *fast methods,* i.e. methods that perform the matrix-vector multiplications in $O(n^r)$ operations, with r less than 2.

Indeed, a number of fast methods for IE simulations have been proposed in the past. These include the *wavelet expansion method (WEM)* [72, 77], the *impedance matrix localization scheme (IML)* [21], *the adaptive integral method (AIM)* [11], and *fast multiple methods (FMM)* [64]. The basic idea behind these methods is to obtain a sparse matrix starting with the classical *method of moments (MoM)* solution procedure. In WEM and IML, the generation of a sparse matrix is achieved by utilizing a special set of basis functions to represent the unknown quantity, while in AIM and FMM, this is achieved by handling the influence of the kernel function in a novel way. The use of wavelet basis functions in WEM reduces the solution time by a constant factor but not the computational complexity. The IML technique, on the other hand, allows the MoM matrix to be replaced by a matrix with localized clumps of large elements, but it achieves modest sparsity and only for simple geometries. The AIM, in turn, utilizes *fast Fourier transforms (FFT)* to reduce the computational cost to $O(n^{3/2} \log n)$ and $O(n \log n)$ complexities for surface and volumetric scattering problems, respectively. The FMM algorithm was originally proposed by Rokhlin for solving static problems [64] and then for particle simulations [35]. Its use can dramatically reduce the time and memory required to compute interactions. The method was extended again by Rokhlin [65] to solve acoustic wave scattering problems in 2-dimensions and then to solve electromagnetic scattering problems by a number of researchers in both 2-dimensions [23, 53] and 3-dimensions [22, 70]. A two-level FMM algorithm reduces both the complexity of a matrix multiplication and memory requirement from $O(n^2)$ to $O(n^{3/2})$ [66], while multilevel FMM algorithm require $O(n \log n)$ operations [71]. However, as has been shown [29, 51], while FMM is well adapted to the solution of low-frequency problems, it becomes unstable at higher frequencies.

Even with the present day super-computers, DE, VF and IE methods can reach their limits of capabilities at modest frequencies. For example, the most advanced implementations of these methods can compute *radar cross section (RCS)* of fighter aircraft up to only a few GHz. For higher frequencies, the state-of-the-art relies on AM methods.

2.3 Scattering Problems

One of the basic problems in electromagnetics/acoustics is the scattering of time-harmonic waves by impenetrable obstacles [25]. To formulate the problem, let $K \subset \mathbb{R}^3$ be a compact set with smooth boundary, and consider an incoming wave impinging on *the obstacle* K.

In electromagnetics, the incoming wave (E^{inc}, H^{inc}) corresponds to a free space solution to the time-harmonic Maxwell equations

$$\nabla \times E^{inc} - ikH^{inc} = 0, \quad \nabla \times H^{inc} + ikE^{inc} = 0 \quad \text{in} \ \ \mathbb{R}^3, \tag{2.3.1}$$

which generates a scattered field (E^s, H^s) in a manner so that the total electromagnetic field

$$(E, H) = (E^{inc}, H^{inc}) + (E^s, H^s) \tag{2.3.2}$$

satisfies the time-harmonic Maxwell equations

$$\nabla \times E - ikH = 0, \quad \nabla \times H + ikE = 0 \tag{2.3.3}$$

in the exterior domain $\Omega = \mathbb{R}^3 \backslash K$.

As with any exterior problem, the solution of the problem (2.3.1)-(2.3.3) is not unique unless a condition at infinity is imposed [25]; here the relevant condition is the *Silver-Muller radiation condition*

$$\lim_{r \to \infty} (H^s \times x - rE^s) = 0$$

or equivalently

$$\lim_{r\to\infty} (E^s \times x + rH^s) = 0$$

where $r = |x|$ and where the limit is assumed to hold uniformly in all directions $x/|x|$.

In the acoustic counterpart of the problem (2.3.1)-(2.3.3), the incident filed u^{inc} is a free space solution to the Helmholtz equation

$$\left(\Delta + k^2\right) u^{inc} = 0, \tag{2.3.4}$$

while the total field

$$u = u^{inc} + u^s \tag{2.3.5}$$

must satisfy the Helmholtz equation

$$\left(\Delta + k^2\right) u = 0 \quad \text{in} \quad \Omega. \tag{2.3.6}$$

The physical condition ensuring the uniqueness of solutions to the acoustic problem (2.3.4)-(2.3.6) is the *Sommerfeld radiation condition*

$$\lim_{r\to\infty} r\left(\frac{\partial u^s}{\partial r} - iku^s\right) = 0$$

where, again, $r = |x|$ and the limit is assumed to hold uniformly in all directions $x/|x|$. In fact, for solutions to the time-harmonic Maxwell equations in a homogeneous medium with no charges, the Silver-Muller radiation condition is equivalent to the Sommerfeld radiation condition for the Cartesian components (see [25] Theorem 6.7).

For the existence and uniqueness of solutions to the electromagnetic scattering problem (2.3.1)-(2.3.3) as well as that of the acoustic scattering problem (2.3.4)-(2.3.6), we refer to [25] and the references therein.

Finally, we note that mathematical treatment of the scattering of time-harmonic electromagnetic and acoustic waves by infinitely long cylindrical obstacles with a bounded cross-section $K \subset \mathbb{R}^2$ also leads to exterior value problems for the Helmholtz equation in $\Omega = \mathbb{R}^2 \backslash K$ with wave number $k > 0$ [12, 43]. So, the problem (2.3.4)-(2.3.6) is also relevant to electromagnetic scattering problems in two-dimensions. However, in two dimensional problems, the Sommerfeld radiation condition must be modified to

$$\lim_{r\to\infty} r^{1/2}(\frac{\partial u^s}{\partial r} - iku^s) = 0$$

where $r = |x|$ and the limit is assumed to hold uniformly in all directions $x/|x|$.

2.4 Integral Equations

A potential theoretic approach to scattering problems begins with a representation of the field in the form of a double- or single-layer potential [25]. For instance, considering the acoustic scattering problems (2.3.4)-(2.3.6), when the scattered field u^s is represented as a double-layer potential

$$u^s(x) = -\int_{\partial K} \frac{\partial \Phi(x,y)}{\partial \nu(y)} \mu(y) ds(y), \quad x \in \Omega, \tag{2.4.1}$$

where

$$\Phi(x,y) = \begin{cases} \dfrac{i}{4} H_0^{(1)}(k|x-y|) & \text{in } \mathbb{R}^2, \\ \\ \dfrac{1}{4\pi} \dfrac{e^{ik|x-y|}}{|x-y|} & \text{in } \mathbb{R}^3, \end{cases} \tag{2.4.2}$$

is the free-space outgoing Green's function for the Helmholtz equation (here, $H_0^{(1)}$ is the Hankel function of the first kind and of order zero [24, 25]), the density μ must be south to satisfy the integral equation of the second kind

$$\frac{1}{2}\mu(x) + \int_{\partial K} \frac{\partial \Phi(x,y)}{\partial \nu(y)} \mu(y) ds(y) = u^{inc}(x), \quad x \in \partial K. \tag{2.4.3}$$

On the other hand, if u^s is represented as a single-layer potential

$$u^s(x) = -\int_{\partial K} \Phi(x,y)\eta(y)ds(y), \;\; x \in \Omega, \tag{2.4.4}$$

then η must satisfy the integral equation of the first kind

$$\int_{\partial K} \Phi(x,y)\eta(y)ds(y) = u^{inc}(x), \quad x \in \partial K. \tag{2.4.5}$$

As it turns out, the density η is a physical quantity. For instance, when the Dirichlet boundary condition $u = 0$ is imposed on ∂K, η coincides with the normal velocity of the total field $\partial u/\partial \nu$ which is known as the surface current in electromagnetics. Indeed, for $x \in \Omega$, taking advantage of the fact that u^{inc} is a free space solution to the Helmholtz equation (so, in particular, in K) yields via an appeal to Green's second theorem that

$$\begin{aligned}\int_{\partial K} &\left(u^{inc}(y)\frac{\partial \Phi(x,y)}{\partial \nu(y)} - \frac{\partial u^{inc}}{\partial \nu}(y)\Phi(x,y)\right) ds(y) \\ &= \int_K \left(u^{inc}\Delta\Phi - \Phi\Delta u^{inc}\right) dx = \int_K u^{inc}\left(\Delta\Phi + k^2\Phi\right) dx = 0.\end{aligned} \tag{2.4.6}$$

On the other hand, since Φ is radiating, we also have

$$u^s(x) = \int_{\partial K} \left(u^s(y)\frac{\partial \Phi(x,y)}{\partial \nu(y)} - \frac{\partial u^s}{\partial \nu}(y)\Phi(x,y)\right) ds(y), \quad x \in \Omega. \tag{2.4.7}$$

Therefore, when the Dirichlet boundary condition is imposed, equations (2.4.6) and (2.4.7) give

$$\begin{aligned}u^s(x) = \int_{\partial K} &\left(u(y)\frac{\partial \Phi(x,y)}{\partial \nu(y)} - \frac{\partial u}{\partial \nu}(y)\Phi(x,y)\right) ds(y) \\ &= -\int_{\partial K} \frac{\partial u}{\partial \nu}(y)\Phi(x,y)ds(y), \quad x \in \Omega.\end{aligned} \tag{2.4.8}$$

Comparing (2.4.4) with (2.4.8), we conclude via uniqueness of solutions that

$$\eta = \frac{\partial u}{\partial \nu} \quad \text{on } \partial\Omega,$$

that is, the density η in the single-layer representation of the scattered field u^s is the physical surface current.

Although it differs significantly from that in (2.4.3), an integral equation of the second kind can also be derived for the current. Indeed, taking the exterior normal derivative in (2.4.8) using the *jump relation* for the derivatives of the single-layer potential (cf. [25] Theorem 3.1) yields

$$\frac{\partial u^s}{\partial \nu}(x) = \frac{1}{2}\frac{\partial u}{\partial \nu}(x) - \int_{\partial K} \frac{\partial \Phi(x,y)}{\partial \nu(x)} \frac{\partial u}{\partial \nu}(y) ds(y), \quad x \in \partial K$$

or equivalently

$$\frac{1}{2}\frac{\partial u}{\partial \nu}(x) + \int_{\partial K} \frac{\partial \Phi(x,y)}{\partial \nu(x)} \frac{\partial u}{\partial \nu}(y) ds(y) = \frac{\partial u^{inc}}{\partial \nu}(x), \quad x \in \partial K \tag{2.4.9}$$

which is an integral equation of the second kind. Yet, the solution of the integral equation (2.4.9) is not unique if k is a so-called *irregular wave number* or *internal resonance*, i.e., if there exist non-trivial solutions u to the Helmholtz equation in the interior domain K satisfying homogeneous Neumann boundary conditions $\partial u/\partial \nu = 0$ on $\partial\Omega$ [25]. This non-uniqueness problem can be avoided by combining the integral equations (2.4.5) and (2.4.9) with a real coupling parameter $\beta \neq 0$ yielding a uniquely solvable integral equation of the second kind for the surface current on ∂K (see [47] for an investigation on the proper choice of the coupling parameter β):

$$\frac{1}{2}\frac{\partial u}{\partial \nu}(x) + \int_{\partial K} \left(\frac{\partial \Phi(x,y)}{\partial \nu(x)} + i\beta\Phi(x,y) \right) \frac{\partial u}{\partial \nu}(y) ds(y) = \frac{\partial u^{inc}}{\partial \nu}(x) + i\beta u^{inc}(x). \tag{2.4.10}$$

Chapter 3

A High-frequency Integral Equation Method (HF-IEM)

Although the problems (2.3.1)-(2.3.3) and (2.3.4)-(2.3.6) are perhaps the simplest examples of physically realistic problems in scattering theory, they still cannot be considered completely solved, particularly in the high-frequency regime, and remain the subject matter of copious ongoing research [25, 63]. A major advance in this direction was recently attained in [15, 16, 17, 18] where a novel integral equation method for high-frequency scattering was developed. A central characteristic of this scheme is that it allows for the evaluation of solutions within any prescribed accuracy to be obtained in frequency-independent computational times. In this Chapter, we review the basic ideas behind this approach, whose analysis is the subject of this thesis. The details of this procedure in single-scattering configurations is provided in §3.1. As we show in §3.2, the extension to multiple-scattering configurations is naturally attained through an iteratively computable series. As will be clear from the discussion, the basic ideas naturally extend to other types of boundary conditions.

3.1 Single-scattering Configurations

As was mentioned in Chapter 1, the algorithm proposed in [15, 16] in connection with the single-scattering configurations is based on three main elements.

The first main element provides the *correct* choice between the integral equations utilizing the physical intuition that the density used to represent the scattered field as a layer potential should oscillate along with the incident field. Accordingly, the density must allow an ansatz in the form of a slowly varying envelope modulated by a highly-oscillatory phase term provided by the geometrical optics solution [46]. The slowly varying amplitude can then be represented by a number of degrees of freedom independent of the frequency. Moreover, the algorithm presented in [15, 16] accounts rigorously for the fact that the ansatz is only valid in certain regions of the scattering surface.

The second main element of the algorithm is a localized integration method related to the method of stationary phase [10]. This localized integration scheme, which reduces the support of integration to a small subset of the scattering surface, can be seen as a natural link between high-frequency approximate, nonconvergent methods such as the Kirchhoff approximation, and a direct integral equation method. As discussed below, the size of the reduced integration support is related to the wavelength, leading to a number of integration points independent of frequency, and thus, to a frequency-independent overall computational complexity.

The third main element is a change of variables around shadow boundaries in order to represent the slowly varying envelopes within a fixed error tolerance by means of a frequency-independent discretization density. Indeed, these slowly varying envelopes possess boundary layers of cubic order in wavelength around shadow boundaries, and the change of variables is based on the asymptotic expansions provided in [55].

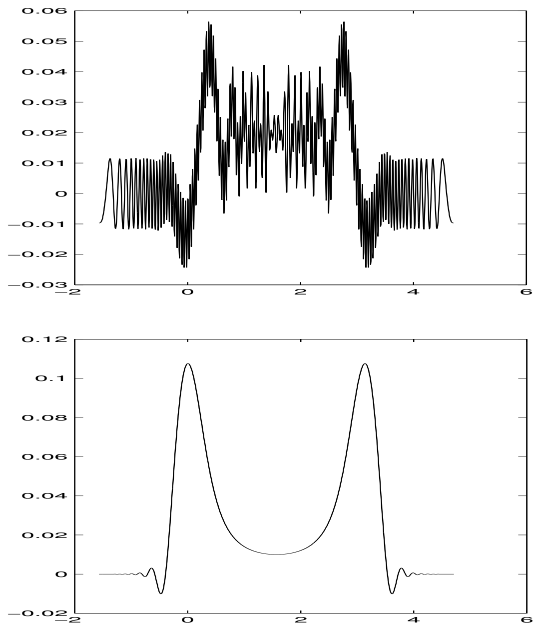

Figure 3.1: Real (top left) and Imaginary (top right) parts of μ/ku^{inc}; Real (bottom left) and Imaginary (bottom right) parts of η/ku^{inc}.

3.1.1 High-frequency Ansatz

As we said, based on the physical intuition, one expects the unknown densities μ and η in (2.4.1) and (2.4.4) to oscillate along with the incident field. This gives rise to the ansatz

$$\mu(x) = \mu_{slow}(x)e^{ik\alpha\cdot x},$$

and

$$\eta(x) = \eta_{slow}(x)e^{ik\alpha\cdot x}, \tag{3.1.1}$$

when the incident field is given by the plane wave

$$u^{inc}(x) = e^{ik\alpha\cdot x},\ x \in \mathbb{R}^n \tag{3.1.2}$$

with direction α, $|\alpha| = 1$. We display the graphs of these functions in Figure 3.1.

Interestingly, only the normalized density of η in (2.4.4) oscillates slowly, indicating that the function μ in (2.4.1) *does not* oscillate like the incoming field. These results can be easily explained. Indeed, as we showed in §2.4, the density η represents a physical quantity, namely the surface current; on the other hand, it was shown in [15] that the double-layer density μ has no such physical meaning. The advantage, then, that η delivers is that the slowly varying envelope

$$\rho := \eta_{slow},$$

can be represented by a number of degrees of freedom independent of frequency.

As will be explained in §3.2, the convergence analysis of our multiple scattering approach for the calculation of the surface current will be based on integral equations of the second kind. As we mentioned in §2.4, when the wave number k is an internal resonance, the solution $\eta = \partial u/\partial \nu$ of the integral equation (2.4.9) is not unique, and equation (2.4.10) must therefore be used. On the other hand, the ideas in what follows do not depend on the particular integral equation utilized. Therefore, for simplicity of our presentation, we will assume that the wave number k is not an internal resonance and work with the integral equation (2.4.9). Note that, with

$$G(x, y) := -2\Phi(x, y), \quad x \neq y \text{ in } \mathbb{R}^n,$$

the equation (2.4.9) can be written for η as

$$\eta(x) - \int_{\partial K} \frac{\partial G(x, y)}{\partial \nu(x)} \eta(y) ds(y) = 2 \frac{\partial u^{inc}}{\partial \nu}(x), \quad x \in \partial K; \tag{3.1.3}$$

and this, in turn, gives rise to the integral equation

$$\rho(x) - \int_{\partial K} \frac{\partial G(x, y)}{\partial \nu(x)} \, e^{ik\alpha \cdot (y-x)} \rho(y) ds(y) = 2ik\alpha \cdot \nu(x), \quad x \in \partial K \tag{3.1.4}$$

for the slowly oscillating density ρ when the incidence is given by (3.1.2).

3.1.2 Localization Principle

Despite the fact that the unknown in the modified boundary integral formulation (3.1.4) is a slowly oscillating function, a direct numerical evaluation of the integral in (3.1.4) would still require a number of quadrature points proportional to the wave number k. The method developed in [15, 16] reduces this requirement to a number independent of frequency by introducing an error-controllable extension of the classical method of stationary phase [10].

To this end, the approach begins evaluation of the critical points of the integral in (3.1.4) for each target point x. Clearly, the critical points are

1. the target (observation) point x itself, where the kernel is singular; and
2. the stationary points of the phase

$$\varphi(y) = \alpha \cdot (y - x) + |y - x|. \tag{3.1.5}$$

   These stationary points, which are given by the solution of a nonlinear system of equations, can be evaluated easily by means of Newton's method.

In view of the method of stationary phase, we know that, asymptotically, the only significant contributions to the integral in (3.1.4) arise from values of the slow integrands and their derivatives at the critical points. To derive an error-controllable (rather than asymptotic) integration strategy with a frequency-independent computational cost, the authors of [15, 16] introduce an approach based on *localization* around these critical points. Physically, for an observation point located away from the scatterer's surface, the critical points correspond to the points of specular reflection: there is only one such critical point on the surface of a convex scatterer. The critical points mentioned above constitute a generalization of this concept to the case in which the observation point lies on the scatterer's surface.

The concept of *localized integration* can be understood by considering the problem of integration of the one-dimensional smooth function $f_A(x)e^{ikx^p}$ depicted in Figure

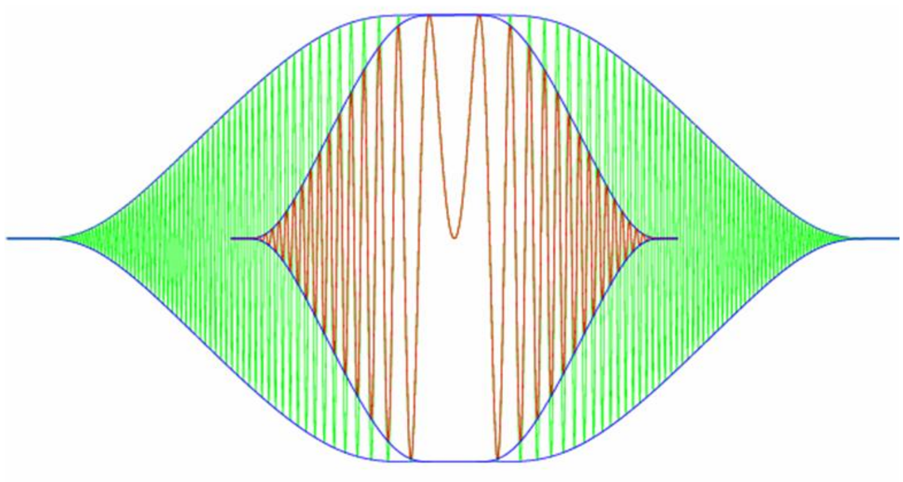

Figure 3.2: Real parts of functions $f_A(x)e^{ikx^p}$ and $f_\epsilon(x)e^{ikx^p}$ with upper envelopes $f_A(x)$ and $f_\epsilon(x)$, respectively; $p = 2$ [15].

3.2. This discussion applies to the integral in (3.1.4) rather directly, since, via expansion of the phase φ in Taylor series, the oscillatory behavior of the integration kernels around their critical points is well captured by an exponential of the form e^{ikx^p} with $p = 1$ (around the kernel singularity), $p = 2$ (around the stationary points other than the shadow boundaries), or $p = 3$ (around the shadow boundary stationary points, provided the curvature does not vanish). The basic result is the following.

Lemma 3.1.1 *[15] Given* positive *real numbers A, ϵ, c and p with $\epsilon < A$ and $c < 1 \leq p$, denote by $f_A(x)$ and $f_\epsilon(x)$ the upper enveloping curves in Figure 3.2. Then*

$$\int_{-A}^{A} f_A(x)e^{ikx^p}dx = \int_{-\epsilon}^{\epsilon} f_\epsilon(x)e^{ikx^p}dx + \mathcal{O}\left((k\epsilon^p)^{-n}\right), \qquad \forall n \geq 1.$$

That is, under certain conditions on the product $k\epsilon^p$, the integral between $-\epsilon$ and ϵ of $f_\epsilon(x)e^{ikx^p}$ is a good approximation of the integral of $f_A(x)e^{ikx^p}$ between $-A$ and A.

Error estimates for the integral (3.1.4), similar to that of Lemma 3.1.1, which can be obtained by Taylor-expanding the phase φ in (3.1.5) around the critical points, provide the criteria for the localized integration. For each target point the corresponding set of distinguished points is covered by a number of small regions, as indicated in what follows:

1. the target point is covered by a region U_t of radius proportional to the wavelength λ ($p = 1$);

2. the l-th stationary point is covered by a region U_s^l of radius proportional to $\sqrt{\lambda}$ ($p = 2$) or $\sqrt[3]{\lambda}$ ($p = 3$, at the shadow boundaries).

A partition of unity [19, 20] is used to smoothly split the integral over ∂K into a number of integrals over subsets of ∂K. This partition of unity is taken to be subordinated to the covering by open sets U_t and U_s^l and the complement V of a closed set which is contained in and closely approximates the union of the set $U_t \bigcup U_s^l$ (in other words, the set where each of the functions making up the partition of unity is not zero is contained in one of the sets U or V). The integral over all of ∂K is then split as a sum of integrals over V and each one of the U sets, with integrands which include the corresponding partitions of unity. The integral in the outside region V is neglected. Note that, for sufficiently small wave numbers, the U intervals cover the scatterer completely, and this high-frequency integral formulation reduces seamlessly to the original integral equation.

This localized integration scheme is exemplified in [16] by computing the following integral on a circle of unit radius, centered at the origin:

$$I(\theta_0) = \int_0^{2\pi} \left[H_0^1 \left(k|r(\theta) - r(\theta_0)| \right) e^{ik\alpha \cdot (r(\theta) - r(\theta_0))} \right] \cos(\theta) d\theta, \qquad (3.1.6)$$

with $r(\theta) = (\cos\theta, \sin\theta)$. Equation (3.1.6) corresponds to the two-dimensional single layer potential in the integral equation (3.1.3), with the unknown density substituted by $\cos(\theta)$. Table 3.1 demonstrates the fixed accuracy of the integrator for $\theta_0 = 0$ and $\alpha = (1, 0)$ throughout the frequency spectrum, using a *fixed* number of integration points for all values of k.

k	N	ϵ	Error
1000	2100	1	1.5e-6
2000	2100	0.5	4.8e-8
4000	2100	0.25	1.2e-7
8000	2100	0.125	9.8e-7
16000	2100	0.0625	1.5e-6

Table 3.1: Localized integrator, sinusoidal slow density. Error on $I(\theta_0 = 0)$ using N integration points [15].

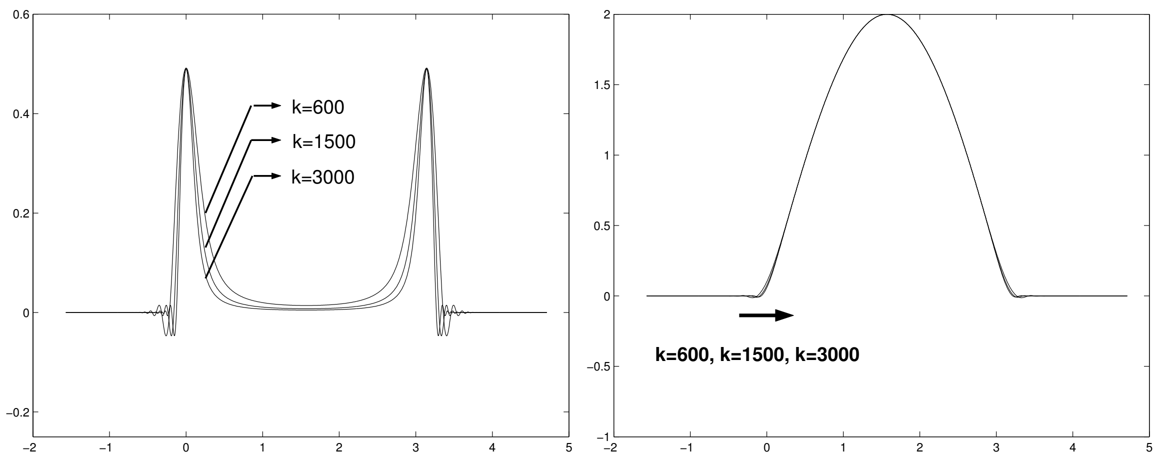

Figure 3.3: Real (left) and Imaginary (right) parts of $\rho/k^{2/3}$ for $k = 600$, 1500 and 3000.

3.1.3 Change of Variables around Shadow Boundaries

While the illuminated region (where $\alpha \cdot \nu << 0$) can be treated as explained above, shadow boundaries (where $\alpha \cdot \nu = 0$) require special consideration (cf. Figure 3.3). Indeed, in order to represent ρ within a fixed error tolerance by means of a frequency-independent discretization density, a cubic root singularity inherent in the slow density around such boundaries needs to be accounted for appropriately. This can be done by means of changes of variables which compensate for the $k^{1/3}$ increase of the slopes of the slow density phases $\varphi = \varphi_k(\theta)$ around the shadow boundaries as k increases (cf. Figure 3.4); see [15] for details.

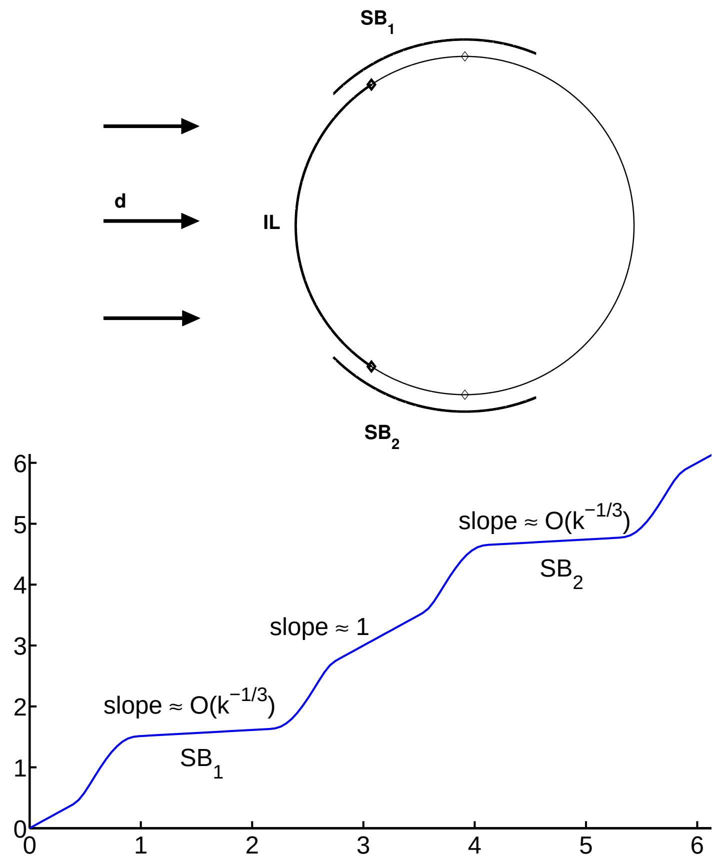

Figure 3.4: A convex obstacle illuminated by a plane wave (top); change of variables around shadow boundaries (bottom).

In view of the above discussions, ρ in (3.1.4) can be obtained, within a prescribed error tolerance, through interpolation from a fixed (independent of frequency) number of discretization points. In implementations, these points are associated with the nodes of Cartesian grids discretizing one or more (overlapping) patches covering the scatterer surface, as proposed by [19, 20]. Fast interpolations of very high order can then be obtained using refined FFTs and polynomial off-grid interpolation [14].

The integral in the region U_t, which contains the kernel singularity, is evaluated by means of a discretization with a mesh-size proportional to λ; the choice of singular integrator is that described by [25] in the two-dimensional case and by [19, 20] in the three-dimensional case. These methods provide high-order quadrature for the singular integrands arising in the integral equations under consideration. The integral in the region U_s^l , in turn, is evaluated by means of the trapezoidal rule with a discretization mesh-size proportional to $\sqrt{\lambda}$ or $\sqrt[3]{\lambda}$. In all cases, the values of the slow densities at the integration points are obtained through interpolation from the fixed discretization mesh mentioned above. Note that, because of the smooth cut-offs used, all integrands are smooth periodic functions for which the trapezoidal rule gives rise to high-order convergence. Also note that a special procedure is necessary to guarantee that the nonempty intersections occurring between the various U sets defined above do not cause difficulties: if the sets have identical discretizations, they are simply merged and the corresponding elements of the partition of unity are summed; otherwise, in a recursive manner, the integral on the set having the finer discretization is computed completely, and its partition of unity subtracted from the other sets.

3.1.4 Numerical Tests

In [16], a matrix free iterative solver was implemented by utilizing the two-dimensional version of the high-frequency integrator described above in conjunction with the GMRES algorithm [68]. Table 3.2 shows results produced by means of this two-dimensional solver on a 1.5GHz PC, applied to a circular cylinder of radius a. Errors are computed by comparison with an exact solution for the integral equation, and defined as

$$\left(\frac{\int_{\partial K} \mid \rho^{exact}(x) - \rho(x) \mid^2 ds(x)}{\int_{\partial K} \mid \rho^{exact}(x) \mid^2 ds(x)} \right)^{1/2} .$$

This example illustrates the asymptotically bounded complexity of the approach: the error for $k = 1000$ is almost identical to that for $k = 100000$, using the same number of unknowns and the same number of integration points. The high-frequency solver is well conditioned and requires a small number of GMRES iterations for arbitrarily large wave numbers, leading to nearly identical computation times for all values of

25 unknowns, $\epsilon = \epsilon_{ref}$			
ka	GMRES Iteration	Error	CPU Time
1	9	1.0e-12	< 1s
10	11	1.6e-4	< 1s
100	13	9.3e-4	3s
1000	13	8.3e-3	5s
10000	15	1.0e-2	6s
100000	14	1.1e-2	6s

100 unknowns, $\epsilon = 5\epsilon_{ref}$			
ka	GMRES Iteration	Error	CPU Time
1	9	1.0e-12	< 1s
10	17	3.0e-11	5s
100	22	1.5e-5	11s
1000	25	3.1e-5	2m30s
10000	27	8.4e-5	3m12s
100000	30	8.8e-5	3m43s

Table 3.2: Scattering of an incident plane wave on a circular cylinder of radius a [15].

$k > 1000$. The results given in the upper half of Table 3.2 are obtained using 25 discretization points for the slow density ρ and a local integration interval size $\epsilon_{ref} = 600(ka)^{-1}$, with 800 integration points.

3.2 Multiple-scattering Configurations

In this section, we review the basic ideas introduced in [17, 18] that allow for the extension of the approach explained in §3.1 to multiple-scattering configurations.

3.2.1 Multiple-scattering Formulation

Mathematically, the observations that enable the extension of the HF-IEM approach of [15, 16] to multiple-scattering configurations begins by noting that if the obstacle

K is decomposed into a collection of disjoint sets $K = \bigcup_{i=1}^{N} K_i$, then (3.1.3) can be written as

$$\eta_i - R_{ii}\eta_i - \sum_{j \neq i} R_{ij}\eta_j = f_i, \quad \text{on} \quad \partial K_i, \quad 1 \leq i \leq N \tag{3.2.1}$$

where, for $1 \leq i \leq N$, and $x \in \partial K_i$

$$\begin{aligned} \eta_i(x) &= \eta(x), \\ f_i(x) &= 2\frac{\partial u^{inc}(x)}{\partial \nu(x)} \\ R_{ij}\eta_j(x) &= \int_{\partial K_j} \frac{\partial G(x,y)}{\partial \nu(x)} \eta_j(y) ds(y). \end{aligned}$$

The diagonal operators R_{ii} correspond precisely to the scattering problems for each isolated sub-surface ∂K_i and are therefore invertible (away from internal resonances). Accordingly, (3.2.1) can be written for $1 \leq i \leq N$ on ∂K_i as

$$\eta_i - \sum_{j \neq i} (I - R_{ii})^{-1} R_{ij}\eta_j = (I - R_{ii})^{-1} f_i \tag{3.2.2}$$

or equivalently

$$\eta_i - \sum_{j \neq i} A_{ij}\eta_j = g_i. \tag{3.2.3}$$

For $1 \leq i \leq N$, the operators A_{ij} are defined on ∂K_i by the identities

$$A_{ij} = \begin{cases} (I - R_{ii})^{-1} R_{ij} & \text{if} \quad 1 \leq i \neq j \leq N \\ 0 & \text{if} \quad 1 \leq i = j \leq N \end{cases}$$

and the functions g_i are the unique solutions to $(I - R_{ii})g_i = f_i$ on ∂K_i, that is

$$g_i = (I - R_{ii})^{-1} f_i.$$

Alternatively, (3.2.3) can be written as

$$(I - A)\eta = g \quad \text{on } \partial K \tag{3.2.4}$$

with $\eta = [\eta_1 \ \eta_2 \ ... \ \eta_N]^T$, $A = [A_{ij}]$ and $g = [g_1 \ g_2 \ ... \ g_N]^T$. The series solution to (3.2.4) is given by the *Neumann series*

$$\eta = \sum_{n=0}^{\infty} [\eta_1^n \ \eta_2^n \ ... \ \eta_N^n]^T \quad \text{on } \partial K \tag{3.2.5}$$

where the terms are inductively defined as

$$\left[\eta_1^0 \ \eta_2^0 \ ... \ \eta_N^0\right]^T = [g_1 \ g_2 \ ... \ g_N]^T \tag{3.2.6}$$

and

$$[\eta_1^n \ \eta_2^n \ ... \ \eta_N^n]^T = A \left[\eta_1^{n-1} \ \eta_2^{n-1} \ ... \ \eta_N^{n-1}\right]^T . \tag{3.2.7}$$

More explicitly, relations (3.2.6) and (3.2.7) can be written in the form

$$\eta_i^0(x) - \int_{\partial K_i} \frac{\partial G(x,y)}{\partial \nu(x)} \ \eta_i^0(y) ds(y) = 2 \frac{\partial u^{inc}(x)}{\partial \nu(x)} \tag{3.2.8}$$

and

$$\eta_i^n(x) - \int_{\partial K_i} \frac{\partial G(x,y)}{\partial \nu(x)} \ \eta_i^n(y) ds(y) = \sum_{j \neq i} \int_{\partial K_j} \frac{\partial G(x,y)}{\partial \nu(x)} \ \eta_j^{n-1}(y) ds(y) \tag{3.2.9}$$

respectively, for $i = 1, \ldots, N$. At this stage, and using (3.2.8)-(3.2.9), it can be readily verified that, the n-th order correction $[\eta_1^n \ \eta_2^n \ ... \ \eta_N^n]^T$ in (3.2.5) corresponds precisely to the current generated on each structure by the n-th order reflection, that is, by the field generated after the incidence u^{inc} has undergone n bounces. Indeed, on the one hand, equations (3.2.8) correspond to the solution of the scattering problems for each isolated sub-surface in response to the incoming radiation, ignoring interactions. And, on the other hand, the right-hand sides of (3.2.9) are precisely the fields scattered by each sub-surface at the (n - 1)-st stage, evaluated on the complementary part of the structure. Thus the n-th order correction corresponds to the current generated by this latter incidence and this, in turn, can be used to inductively show that it also corresponds to the n-th order reflection.

Evidently then, for a fixed surface ∂K_i, the n-th correction η_i^n is the sum of $(N-1)^n$ corrections corresponding to each obstacle path of length n terminating precisely at ∂K_i. Accordingly, the *total* surface current η is the sum over all infinite sequences of obstacle paths $(K_m)_{m\geq 0}$ (i.e. each K_m is one of the objects in consideration, and no two consecutive objects are the same) of the solutions of the integral equations

$$\eta_0(x) - \int_{\partial K_0} \frac{\partial G(x,y)}{\partial \nu(x)}\, \eta_0(y) ds(y) = 2\frac{\partial u^{inc}(x)}{\partial \nu(x)} = 2ike^{ik\alpha\cdot x}\alpha\cdot\nu(x), \quad x \in \partial K_0 \quad (3.2.10)$$

and for $m = 1, 2, \ldots$

$$\begin{aligned}\eta_m(x) - \int_{\partial K_m} \frac{\partial G(x,y)}{\partial \nu(x)}\, \eta_m(y) ds(y) \\ = \int_{\partial K_{m-1}} \frac{\partial G(x,y)}{\partial \nu(x)}\, \eta_{m-1}(y) ds(y), \quad x \in \partial K_m. \quad (3.2.11)\end{aligned}$$

3.2.2 Generalized High-frequency Ansatz

The significance of the formulation in §3.2.1 stems from the fact that it guarantees that each of the problems in (3.2.10)-(3.2.11) entails the solution of problems within single scattering configurations for which the methods described in §3.1 provide an error-controllable scheme with fixed computational complexity. To apply this procedure, however, we must first identify the phase of each correction η_m to the current, to derive a representation analogous to (3.1.1). But this, once again, is facilitated by the interpretation of these corrections as corresponding to successive wave reflections, which suggests that the highly-oscillatory part of their phases must coincide with that provided by a geometrical optics solution.

For instance, when the obstacles are convex and "visible" (in the sense that none of them meets the convex hull generated by any other pair of objects), the geometrical optics solution provides a sequence of phase functions $\{\varphi_m\}_{m\geq 0}$ measuring the optical distance travelled by a ray arriving at $x_m \in \partial K_m$ after m reflections. More precisely, depending on $x_m \in \partial K_m$, the geometrical optics solution provides *uniquely* determined points $(x_0, x_1, \cdots, x_{m-1}) \in \partial K_0 \times \partial K_1 \times \cdots \times \partial K_{m-1}$ on the optical ray path arriving at x_m after m reflections. The m-tuple $(x_0, x_1, \cdots, x_{m-1})$ is characterized, for $m \geq 1$, by the following principles:

1. *Rays bounce off illuminated regions*:

$$\alpha \cdot \nu_0 < 0, \quad \text{and} \quad (x_{i+1} - x_i) \cdot \nu_i > 0, \quad i = 1, \ldots, m-1$$

2. *Law of reflection*:

$$\frac{x_1 - x_0}{|x_1 - x_0|} = \alpha - 2(\alpha \cdot \nu_0)\nu_0,$$

and

$$\frac{x_{i+1} - x_i}{|x_{i+1} - x_i|} = \frac{x_i - x_{i-1}}{|x_i - x_{i-1}|} - 2\left(\frac{x_i - x_{i-1}}{|x_i - x_{i-1}|} \cdot \nu_i\right)\nu_i, \quad i = 1, \ldots, m-1.$$

Here, we have chosen $\nu_i = \nu_i(x_i)$ to denote the outward unit normal to the surface ∂K_i at the point x_i. In this case, the phase at the point x_m is defined to be

$$\varphi_m = \varphi_m(x_m) = \begin{cases} \alpha \cdot x_0 & \text{if } m = 0, \\ \\ \alpha \cdot x_0 + \sum_{i=0}^{m-1} |x_{i+1} - x_i| & \text{if } m \geq 1; \end{cases} \tag{3.2.12}$$

see Figures 3.5 and 3.8 for examples. Using (3.2.12) and similar to (3.1.1), we write

$$\eta_m(x) = \rho_m(x) e^{ik\varphi_m(x)}, \tag{3.2.13}$$

and equations (3.2.10)-(3.2.11) read:

$$\rho_0(x) - \int_{\partial K_0} \frac{\partial G(x,y)}{\partial \nu(x)} \; e^{ik(\varphi_0(y)-\varphi_0(x))}\rho_0(y)ds(y) = 2ik\alpha \cdot \nu(x), \quad x \in \partial K_0 \quad (3.2.14)$$

and for $m = 1, 2, \ldots$

$$\rho_m(x) - \int_{\partial K_m} \frac{\partial G(x,y)}{\partial \nu(x)} \; e^{ik(\varphi_m(y)-\varphi_m(x))}\rho_m(y)ds(y)$$
$$= \int_{\partial K_{m-1}} \frac{\partial G(x,y)}{\partial \nu(x)} \; e^{ik(\varphi_{m-1}(y)-\varphi_m(x))}\rho_{m-1}(y)ds(y), \quad x \in \partial K_m. \quad (3.2.15)$$

3.2.3 Extension of the Single-scattering Algorithm

As we said, the slowly oscillatory character of the quantities ρ_m follows from the interpretation of the right-hand side of (3.2.11) as the normal derivative of the field scattered by ∂K_{m-1} after $(m-1)$ reflections, so that its phase is precisely given by φ_m. Equation (3.2.15) is then amenable to the treatment described in §3.2 the only difference being that the evaluation of the right hand side of (3.2.15), for $m \geq 1$, entails an integral of a highly oscillatory function. This, however, can again be treated with the aforementioned strategies of localized integration. In fact, in this case the integrand is regular and only integrations around stationary points of the overall phase must be performed. Moreover, as is to be expected from the asymptotic limit, for any given target point $x_m \in \partial K_m$ there will be exactly one stationary point $x_{m-1} \in \partial K_{m-1}$ of the corresponding integral. Indeed, this point will coincide with the point in ∂K_{m-1} from which a geometrical ray that has experienced $(m-1)$ reflections goes through x_m upon an additional reflection at x_{m-1}.

3.2.4 Numerical Tests

In Figures 3.6 and 3.7 (taken from [62]), we exemplify this procedure in the specific instance of Figure 3.5 for the wave number $k = 40$. In Figure 3.6, we display the graphs of the functions $\eta^m(x)$, $\rho^m(x)$ and $\varphi^m(x)$ on the obstacle K_1, namely the ellipse located on top, (left, middle and right panels, respectively) for different values of m ($m = 0$, 10, 20, 40 in the first, second and third rows, respectively). In particular, the figure demonstrates the slowly oscillatory character of the envelopes that result from the generalized phase extraction described above. Indeed, the figure shows that the functions $\rho^m(x)$ are slowly oscillatory throughout the region of K_1 that is illuminated after m reflections, that they vanish in the corresponding deep shadow zones, and that they exhibit sharp transitions (of the order of $k^{-1/3}$) about shadow boundaries, exactly as in the single scattering case. Finally, Figure 3.7 illustrates the convergence properties of the series (3.2.5). More precisely, there we display the values of truncated approximations η^{approx}, and of the error

$$\text{Max. Error} = \frac{1}{k}\ max \mid \eta(x) - \eta^{approx}(x) \mid,$$

where η is the solution (converged to machine precision) obtained by means of the algorithm proposed in [25], and where the error is normalized by the wave number since the solution η grows linearly with k. In addition, Figure 3.7 demonstrates the spectral rate of convergence of the series which, in this case, translates in an error of less than 1% in less than 15 iterations.

A similar example is provided in Figures 3.8, 3.9 and 3.10.

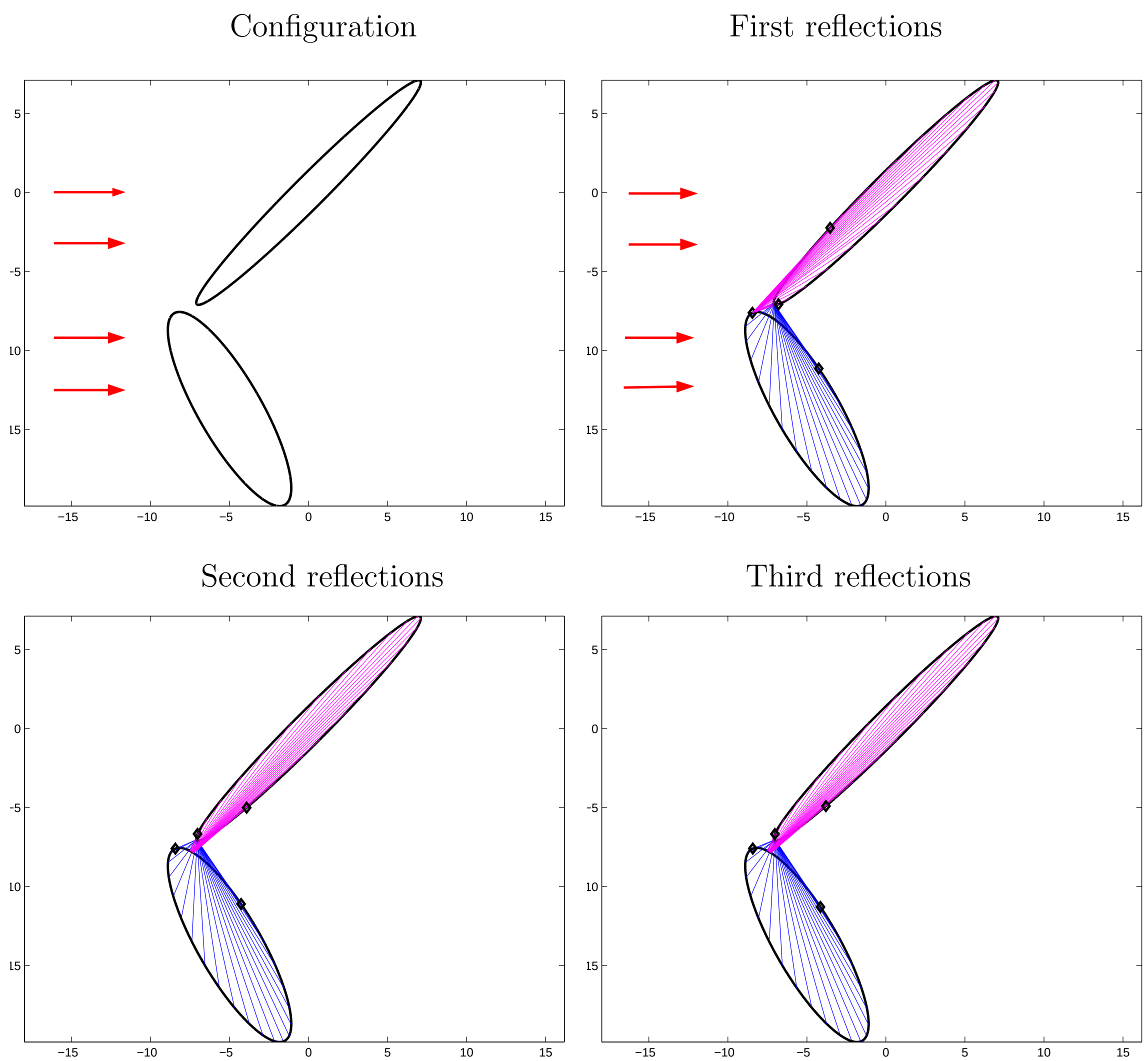

Figure 3.5: A configuration consisting of two ellipses, and the corresponding geometrical rays.

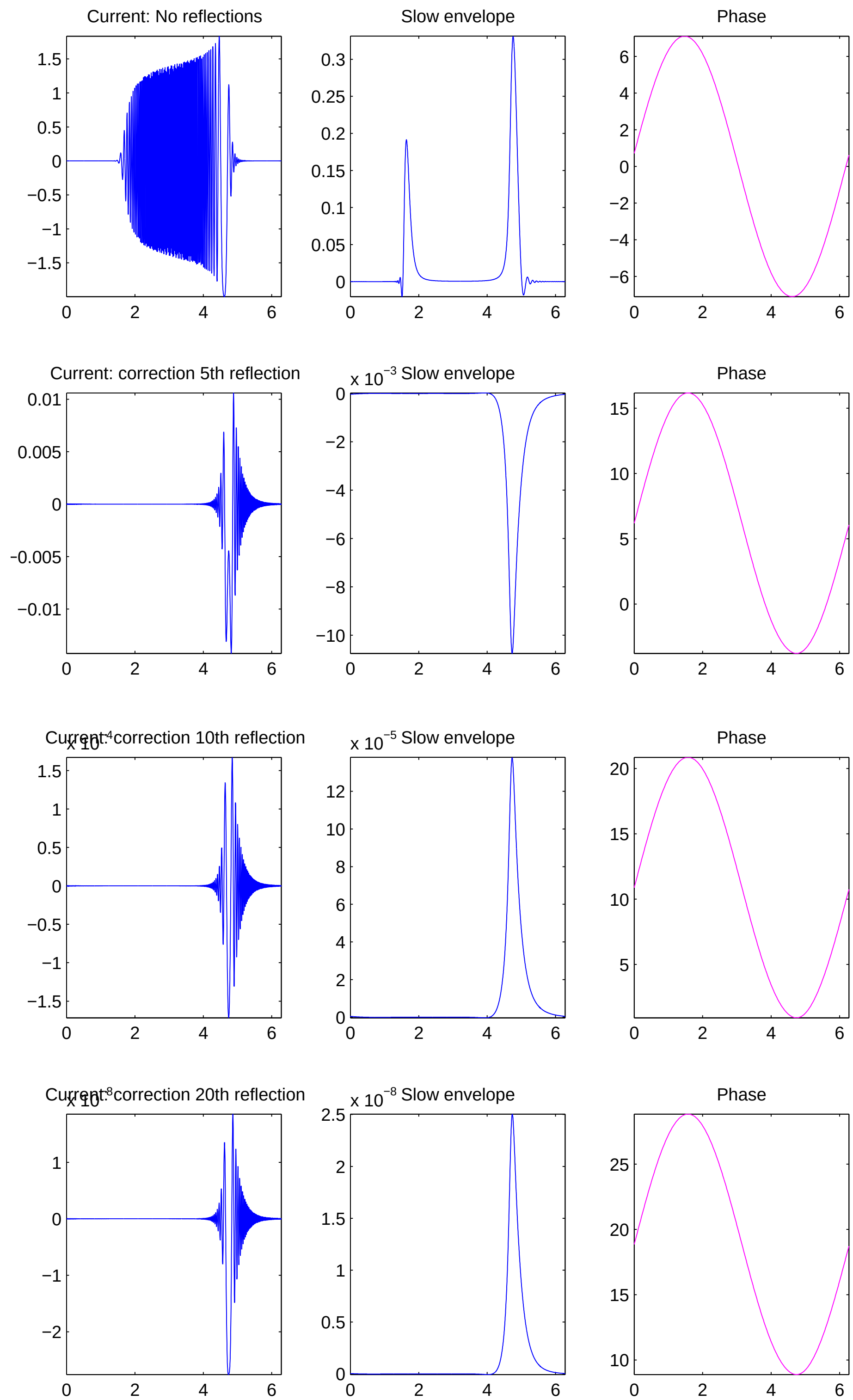

Figure 3.6: Corrections η_m(left), slow envelopes ρ_m (middle), and phases φ_m (right) corresponding to reflections $m = 0,\ 10,\ 20,\ 40$ for the configuration in Figure 3.5 (data corresponds to the ellipse on top).

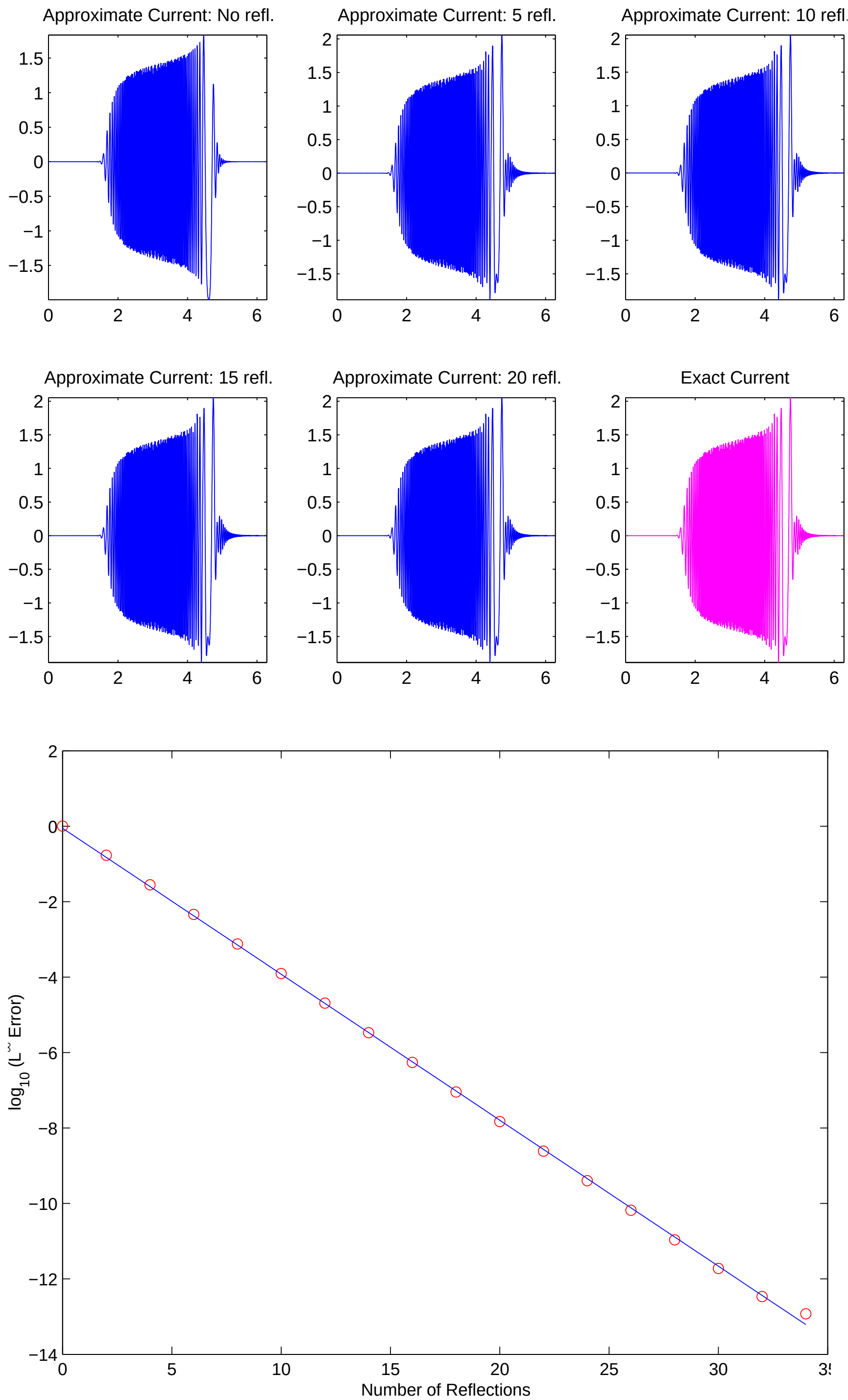

Figure 3.7: Top and middle rows: Approximate current η^m for reflections $m = 0$, 10, 20, 30, 40; middle right is the exact current; Bottom: Number of reflections versus the L^∞ error (data corresponds to the upper ellipse in Figure 3.5).

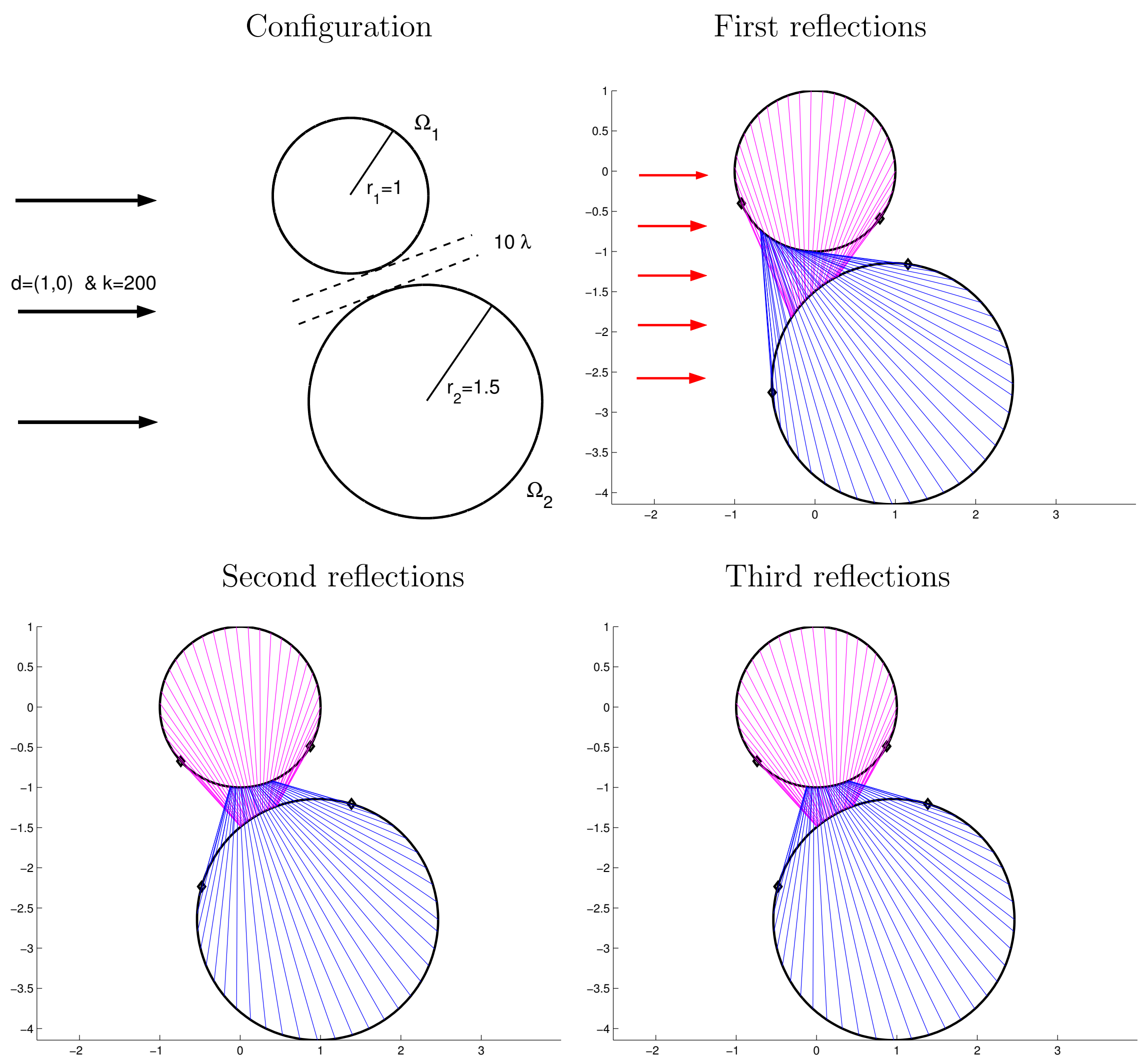

Figure 3.8: A configuration consisting of two circles, and the corresponding geometrical rays.

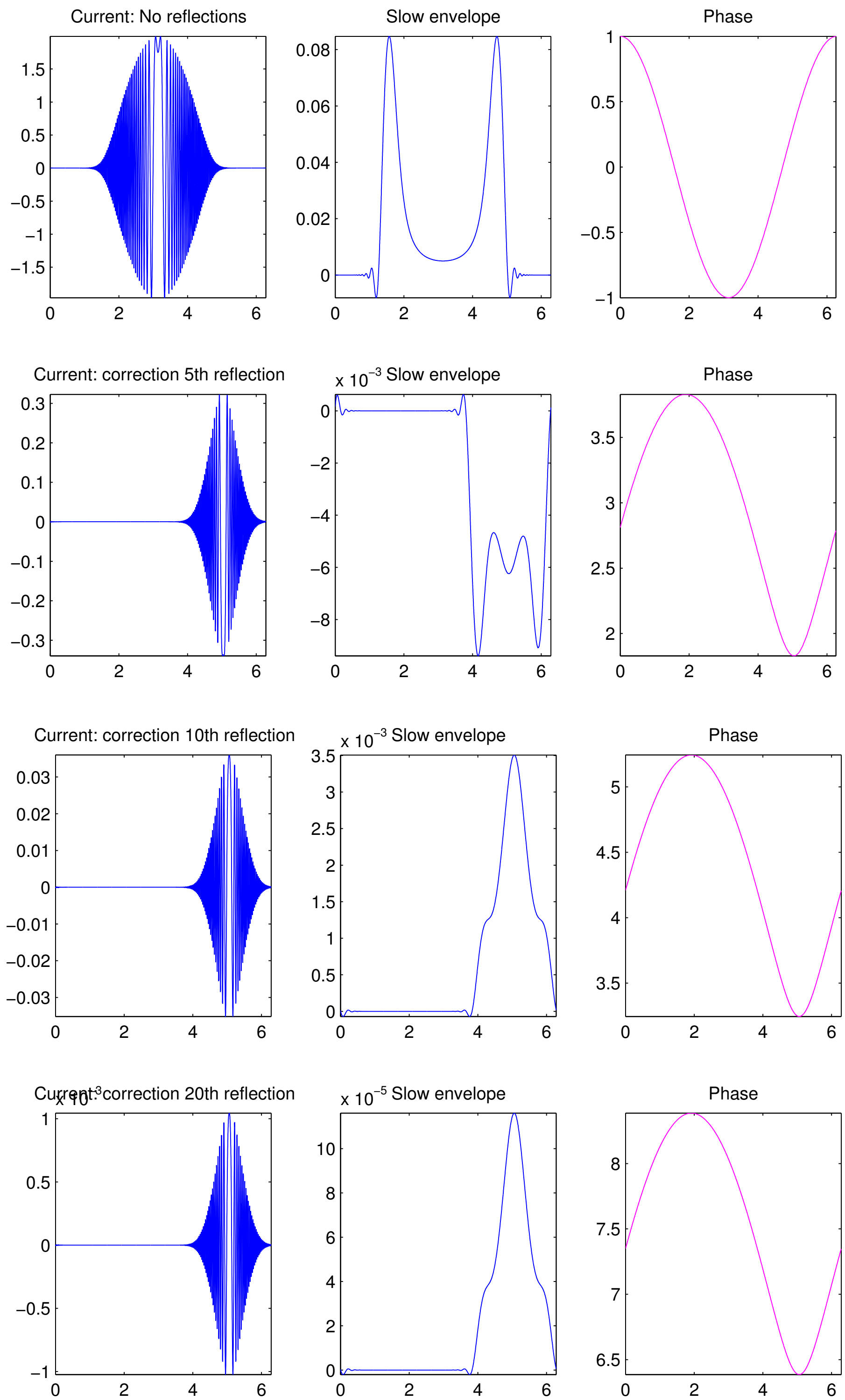

Figure 3.9: Corrections η_m(left), slow envelopes ρ_m (middle), and phases φ_m (right) corresponding to reflections $m = 0, 5, 10, 20$ for the configuration in Figure 3.8 (data corresponds to the upper circle).

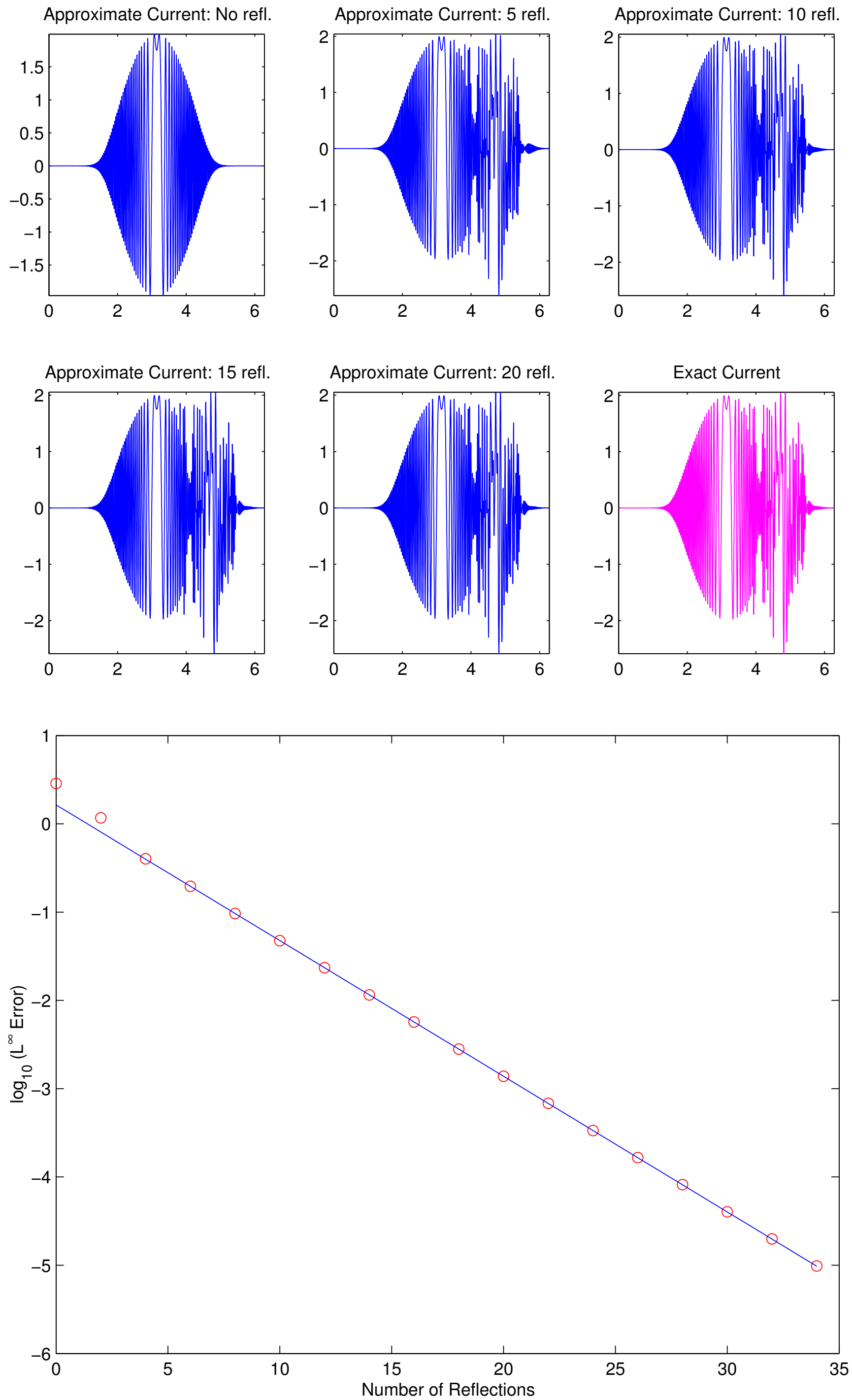

Figure 3.10: Top and middle rows: Approximate current η^m for reflections $m = 0$, 5, 10, 15, 20; middle right is the exact current; Bottom: Number of reflections versus the L^∞ error (data corresponds to the upper circle in Figure 3.8).

Chapter 4

Asymptotic Expansions of the Two-dimensional Multiple Scattering Iterations in HF-IEM

In this Chapter, we derive the asymptotic expansions of the solutions η_m of the integral equations (3.2.10)-(3.2.11) in a two-dimensional setting for a finite collection of convex obstacles. In order to simplify the calculations, we assume the *visibility condition*, that is, no obstacle meets with the closed convex hull generated by any other pair of objects. Under these assumptions, and utilizing the notation set in §3.2.2, the main result of this chapter reads as follows:

Theorem 4.0.1 (Asymptotic Expansions of Iterated Currents) *At each reflection, the asymptotic expansions of iterated currents $\eta_m = \eta_m(x_m)$ are given on the m-th illuminated regions (off the $\mathcal{O}(k^{-1/3})$ shadow boundaries) by*

$$\eta_0 = 2ike^{ik\alpha \cdot x_0} \ \alpha \cdot \nu_0 \ \left(1 + \mathcal{O}\left(k^{-1}\right)\right),$$

and for $m = 1, 2, \ldots$

$$\eta_m = e^{ik|x_m - x_{m-1}|}\ Q_m\ R_m\ \eta_{m-1}\left(1 + \mathcal{O}\left(k^{-1}\right)\right)$$

where

$$Q_m = \frac{x_m - x_{m-1}}{|x_m - x_{m-1}|} \cdot \nu_m \left(\frac{x_m - x_{m-1}}{|x_m - x_{m-1}|} \cdot \nu_{m-1}\right)^{-1},$$

and R_i*'s are defined recursively as*

$$R_1 = 1 + 2\kappa_0 |x_1 - x_0| \left(\frac{x_1 - x_0}{|x_1 - x_0|} \cdot \nu_0\right)^{-1},$$

and, for $1 \leq i \leq m-1$,

$$R_{i+1} = 1 + 2\kappa_i |x_{i+1} - x_i| \left(\frac{x_{i+1} - x_i}{|x_{i+1} - x_i|} \cdot \nu_i\right)^{-1} + \frac{|x_{i+1} - x_i|}{|x_i - x_{i-1}|}\left(1 - \frac{1}{R_i}\right).$$

On the other hand, the iterated current η_m *vanishes to first order in wavelength on the m-th shadow region (off the* $\mathcal{O}(k^{-1/3})$ *shadow boundaries).*

The proof of Theorem 4.0.1 is based on an analysis of the integral equations (3.2.14) and (3.2.15). Indeed, the integrals contained in these equations are generalized Fourier integrals. Accordingly, their asymptotic evaluations in the high-frequency regime require the determination of the corresponding critical points (where the kernel is singular or the phase is stationary); once these points are found, the integrals can be evaluated appealing to classical techniques relating to the treatment of oscillatory integrals [10].

One of the key points in determining the critical points is the behavior of *creeping waves* as given by the classical *geometrical theory of diffraction* (GTD): "creeping waves travel along geodesics into the shadow region" [46]. In particular, then, the phase functions φ_m must be redefined on the shadow regions of ∂K_m as follows: the phase at a point $x_m \in \partial K_m$ in the shadow region is the phase at the shadow boundary plus the geodesic distance in between. Using this new definition, in §4.1.2,

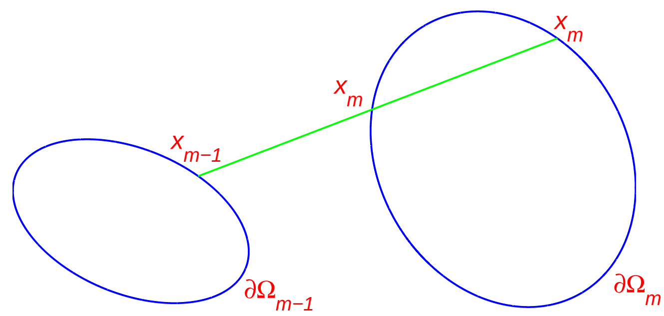

Figure 4.1: Stationary points.

we characterize the stationary points. As it turns out, for a target point $x_m \in \partial K_m$, the phase is stationary at a point $x_{m-1} \in \partial K_{m-1}$ if the ray that bounces off x_{m-1} at the $(m$ - $1)$-th reflection arrives x_m in one of the following ways (cf. Figure 4.1):

1) the ray bounces off the point x_{m-1} in accordance with the law of reflection;

2) the ray passes through x_{m-1} without altering its direction;

3) the point x_{m-1} is in the $(m$ - $1)$-th shadow region, and the ray is a creeping ray that leaves ∂K_{m-1} at x_{m-1} making a tangential contact with the corresponding geodesic.

These classify all the stationary points of the right-hand side (RHS) integrals in (3.2.14)-(3.2.15).

The characterization of the stationary points for the left-hand side (LHS) integrals, on the other hand, is more complicated. Indeed, appealing to the rules above, we see that the LHS integral has no stationary point when the target point x_m is located in the m-th illuminated region, and has only one stationary point when the target point is in the m-th shadow region (cf. Figure 4.1). As we show in §4.3, however, for a target point $x_m \in \partial K_m$ in the m-th shadow region, the contribution coming from the stationary point x_{m-1} of the RHS integral cancels to first order in wavelength that of the stationary point (located in the m-th illuminated region) of the LHS integral.

Kernel singularities are characterized easily appealing to (2.4.2) and (3.2.13): both the kernels of RHS and LHS integrals in (3.2.14)-(3.2.15) are singular at the shadow boundaries on account of a discontinuity in the third derivative of the phases; and the LHS integrals are singular at the corresponding target point x_m. However, as we show in §4.2, the integrals in a neighborhood of the singular points behave asymptotically as $\eta_m \mathcal{O}(k^{-1})$, and therefore their contributions can be neglected.

As a consequence, at each reflection, the only important contributions to the asymptotic expansions come from the stationary points of the phases. In §4.3, we use the *method of stationary phase* [10] to evaluate the integrals around stationary points which require the calculation of the second derivatives of phase functions. These calculations are performed in §4.1.3.

4.1 Properties of Phase Functions

The aim of this section is two fold. First, in §4.1.2 we characterize the stationary points of the phase functions. Then, we use this characterization to calculate the second derivatives of these functions explicitly.

To begin, suppose that we are given a sequence of obstacles $\{K_m\}_{m\geq 0}$. We assume that the boundary curves ∂K_m possess regular analytic and 2π-periodic parametric representations of the form

$$x_m(t_m) = (x_m^1(t_m), x_m^2(t_m)), \qquad 0 \leq t \leq 2\pi$$

in counterclockwise orientation. For a *fixed* $x_{m+1} = x_{m+1}(t_{m+1}) \in \partial K_{m+1}$, with $m \geq 0$, consider the phase functions

$$\varphi_{t_{m+1}}(t_m) = \alpha \cdot x_0 + \sum_{i=0}^{m} |x_{i+1} - x_i|, \tag{4.1.1}$$

of the RHS integrals in (3.2.15) where the points $x_0, \dots, x_m$ are assumed to be on the same optical ray path and belong to the illuminated regions of their corresponding boundary curves; and

$$\varphi^s_{t_{m+1}}(t_m) = \varphi_m(x^{sb}_m) + \int_{t^{sb}_m}^{t_m} |\dot{x}_m(\xi)| d\xi + |x_{m+1} - x_m|, \tag{4.1.2}$$

where we assume that $x^{sb}_m = x_m(t^{sb}_m) \in \partial K_m$ is at the m-th shadow boundary, and the points $x_m \in \partial K_m$ belong to the m-th shadow region. The functions $\varphi^s_{t_{m+1}}(t_m)$ correspond to the creeping rays, and are utilized in §4.1.2 to deduce that *creeping rays diffract tangentially while travelling along the geodesics*. An immediate consequence of this result is that, the visibility condition ensures that, in the high-frequency regime, contributions to asymptotic expansions coming from creeping rays are negligible.

4.1.1 First Derivatives

In the rest of the Chapter, we use the notation:

$$\dot{x}_i = \frac{d}{dt_i} x_i(t_i).$$

Lemma 4.1.1 *Derivatives of the phase functions (4.1.1) are given by*

$$\frac{d}{dt_0}\varphi_{t_1}(t_0) = \left(\alpha - \frac{x_1 - x_0}{|x_1 - x_0|}\right) \cdot \dot{x}_0, \tag{4.1.3}$$

and

$$\frac{d}{dt_m}\varphi_{t_{m+1}}(t_m) = \left(\frac{x_m - x_{m-1}}{|x_m - x_{m-1}|} - \frac{x_{m+1} - x_m}{|x_{m+1} - x_m|}\right) \cdot \dot{x}_m, \quad m \geq 1. \tag{4.1.4}$$

On the other hand, the derivatives of the phase functions (4.1.2) are

$$\frac{d}{dt_m}\varphi^s_{t_{m+1}}(t_m) = \left(\frac{\dot{x}_m}{|\dot{x}_m|} - \frac{x_{m+1} - x_m}{|x_{m+1} - x_m|}\right) \cdot \dot{x}_m, \quad m \geq 0. \tag{4.1.5}$$

Proof. The proofs of (4.1.3) and (4.1.5) are straightforward. To obtain (4.1.4), we differentiate (4.1.1) with respect to t_m:

$$\frac{d}{dt_m}\varphi_{t_{m+1}}(t_m) = \left(\alpha - \frac{x_1 - x_0}{|x_1 - x_0|}\right) \cdot \dot{x}_0 \frac{dt_0}{dt_m}$$
$$+ \sum_{i=0}^{m-2} \left(\frac{x_{i+1} - x_i}{|x_{i+1} - x_i|} - \frac{x_{i+2} - x_{i+1}}{|x_{i+2} - x_{i+1}|}\right) \cdot \dot{x}_{i+1} \frac{dt_{i+1}}{dt_m}$$
$$+ \left(\frac{x_m - x_{m-1}}{|x_m - x_{m-1}|} - \frac{x_{m+1} - x_m}{|x_{m+1} - x_m|}\right) \cdot \dot{x}_m.$$

Since the points $x_0, \ldots, x_m$ are assumed to be on the same optical ray path, this equation reduces to (4.1.4). ■

4.1.2 Characterization of Stationary Points

The first result of this section states that the phase function $\varphi_{t_{m+1}}(t_m)$ is stationary at a point x_m if and only if the points $x_0, \ldots, x_m, x_{m+1}$ are on the same optical ray path.

Lemma 4.1.2 i) (First Reflections) *For $m = 0$, the phase given by (4.1.1) is stationary at a point x_0 with $x_0 = x_0(t_0)$ if and only if*

$$\frac{x_1 - x_0}{|x_1 - x_0|} = \alpha + 2\frac{x_1 - x_0}{|x_1 - x_0|} \cdot \nu_0\ \nu_0 \tag{4.1.6}$$

or

$$\frac{x_1 - x_0}{|x_1 - x_0|} = \alpha. \tag{4.1.7}$$

ii) (Further Reflections) *For $m \geq 1$, the phase given by (4.1.1) is stationary at a point x_m with $x_m = x_m(t_m)$ if and only if*

$$\frac{x_{m+1} - x_m}{|x_{m+1} - x_m|} = \frac{x_m - x_{m-1}}{|x_m - x_{m-1}|} + 2\frac{x_{m+1} - x_m}{|x_{m+1} - x_m|} \cdot \nu_m\ \nu_m \tag{4.1.8}$$

or

$$\frac{x_{m+1} - x_m}{|x_{m+1} - x_m|} = \frac{x_m - x_{m-1}}{|x_m - x_{m-1}|}. \tag{4.1.9}$$

Proof. Equation (4.1.3) implies

$$\frac{d}{dt_0}\varphi_{t_1}(t_0) = 0 \;\Leftrightarrow\; \alpha = \lambda_0\nu_0 + \frac{x_1 - x_0}{|x_1 - x_0|}$$

for some λ_0. Also, since $|\alpha| = 1$, we have

$$1 = \alpha \cdot \alpha = \lambda_0^2 + 2\lambda_0\frac{x_1 - x_0}{|x_1 - x_0|} \cdot \nu_0 + 1$$

so that

$$\lambda_0 = -2\frac{x_1 - x_0}{|x_1 - x_0|} \cdot \nu_0 \qquad \text{or} \qquad \lambda_0 = 0.$$

Similarly, for $m \geq 1$, equation (4.1.4) gives

$$\frac{d}{dt_m}\varphi_{t_{m+1}}(t_m) = 0 \;\Leftrightarrow\; \frac{x_m - x_{m-1}}{|x_m - x_{m-1}|} = \lambda_m\nu_m + \frac{x_{m+1} - x_m}{|x_{m+1} - x_m|}$$

for some λ_m. Since

$$1 = \frac{x_m - x_{m-1}}{|x_m - x_{m-1}|} \cdot \frac{x_m - x_{m-1}}{|x_m - x_{m-1}|} = \lambda_m^2 + 2\lambda_m\frac{x_{m+1} - x_m}{|x_{m+1} - x_m|} \cdot \nu_m + 1,$$

we get

$$\lambda_m = -2\frac{x_{m+1} - x_m}{|x_{m+1} - x_m|} \cdot \nu_m \qquad \text{or} \qquad \lambda_m = 0,$$

completing the proof. ■

The next result states that a ray incident precisely on the shadow boundary (assuming that it travels along the geodesics into the shadow region as in GTD) diffracts tangentially along its path.

Lemma 4.1.3 (Creeping Rays Diffract Tangentially) *For $m \geq 0$, the phase* *given by (4.1.2) is stationary at a point x_m with $x_m = x_m(t_m)$ if and only if*

$$\frac{\dot{x}_m}{|\dot{x}_m|} - \frac{x_{m+1} - x_m}{|x_{m+1} - x_m|} = 0.$$

Proof. Immediate from (4.1.5). ■

4.1.3 Second Derivatives at Stationary Points

In this section, we derive explicit formulas for the second derivatives of phase functions given by (4.1.1). These formulas will be used in §4.3 to obtain the asymptotic expansions of iterated currents appealing to the method of stationary phase. The formulas will be stated in terms of the quantities S_m defined by the identities

$$\frac{d^2}{dt_m^2}\varphi_{t_{m+1}}(t_m) = \frac{|\dot{x}_m|^2}{|x_{m+1} - x_m|}\left(\frac{x_{m+1} - x_m}{|x_{m+1} - x_m|} \cdot \nu_m\right)^2 S_m,$$

for $m = 0, 1, \ldots$. With this notation, our main result reads:

Theorem 4.1.4 i) (Second Derivatives in First Reflections) *For $m = 0$, if (4.1.6) holds, then*

$$S_0 = 1 + 2\kappa_0 |x_1 - x_0| \left(\frac{x_1 - x_0}{|x_1 - x_0|} \cdot \nu_0\right)^{-1}, \tag{4.1.10}$$

while if (4.1.7) holds, then

$$S_0 = 1. \tag{4.1.11}$$

ii) (Second Derivatives in Further Reflections) *For $m \geq 1$, if (4.1.8) holds, then*

$$S_m = 2\kappa_m |x_{m+1} - x_m| \left(\frac{x_{m+1} - x_m}{|x_{m+1} - x_m|} \cdot \nu_m\right)^{-1} + T_m, \tag{4.1.12}$$

while if (4.1.9) holds, then

$$S_m = T_m, \tag{4.1.13}$$

where

$$T_m = 1 + \frac{|x_{m+1} - x_m|}{|x_m - x_{m-1}|}\left(1 - \frac{1}{S_{m-1}}\right). \tag{4.1.14}$$

Proof. Differentiating (4.1.3) yields

$$\begin{aligned}\frac{d^2}{dt_0^2}\varphi_{t_1}(t_0) &= \left(\alpha - \frac{x_1 - x_0}{|x_1 - x_0|}\right)\cdot \ddot{x}_0 + \frac{|\dot{x}_0|^2}{|x_1 - x_0|}\left(1 - \left(\frac{x_1 - x_0}{|x_1 - x_0|}\cdot\frac{\dot{x}_0}{|\dot{x}_0|}\right)^2\right)\\ &= \left(\alpha - \frac{x_1 - x_0}{|x_1 - x_0|}\right)\cdot \ddot{x}_0 + \frac{|\dot{x}_0|^2}{|x_1 - x_0|}\left(\frac{x_1 - x_0}{|x_1 - x_0|}\cdot \nu_0\right)^2\end{aligned}$$

from which (4.1.11) is immediate in case (4.1.7) holds. On the other hand, if (4.1.6) holds, then

$$\begin{aligned}\frac{d^2}{dt_0^2}\varphi_{t_1}(t_0) &= \lambda_0\nu_0\cdot\ddot{x}_0 + \frac{|\dot{x}_0|^2}{|x_1 - x_0|}\left(\frac{x_1 - x_0}{|x_1 - x_0|}\cdot \nu_0\right)^2\\ &= 2\frac{x_1 - x_0}{|x_1 - x_0|}\cdot\nu_0\kappa_0|\dot{x}_0|^2 + \frac{|\dot{x}_0|^2}{|x_1 - x_0|}\left(\frac{x_1 - x_0}{|x_1 - x_0|}\cdot \nu_0\right)^2,\end{aligned}$$

from which (4.1.10) follows at once. ■

To prove the result for further reflections we need several additional lemmas. We begin by proving a simple geometrical identity which will be very useful in the sequel.

Lemma 4.1.5 *Let u, v and w be three* unit *vectors, and let Θ be the matrix of rotation by $\pi/2$ radians in the counterclockwise direction. Then*

$$\Theta u\cdot\Theta v - (w\cdot\Theta u)(w\cdot\Theta v) = (w\cdot u)(w\cdot v). \tag{4.1.15}$$

Proof. Let $\alpha_1 = \cos^{-1}(w\cdot u)$ and $\alpha_2 = \cos^{-1}(w\cdot v)$. Then, (4.1.15) is equivalent to the trigonometric difference formula

$$\cos(\alpha_1 - \alpha_2) - \sin\alpha_1\sin\alpha_2 = \cos\alpha_1\cos\alpha_2.$$

■

The next result provides a representation for the second derivatives of phase functions in further reflections in terms of the relative coordinate derivatives dt_{m-1}/dt_m. To this end, for $m \geq 1$, we denote by V_m the quantities defined by the identities

$$\frac{dt_{m-1}}{dt_m} = \frac{|\dot{x}_m|}{|\dot{x}_{m-1}|} \frac{x_m - x_{m-1}}{|x_m - x_{m-1}|} \cdot \nu_m \left(\frac{x_m - x_{m-1}}{|x_m - x_{m-1}|} \cdot \nu_{m-1} \right)^{-1} V_m.$$

Lemma 4.1.6 (Second Derivatives in terms of Coordinate Derivatives) *For $m \geq 1$, if (4.1.8) holds, then*

$$S_m = 2\kappa_m |x_{m+1} - x_m| \left(\frac{x_{m+1} - x_m}{|x_{m+1} - x_m|} \cdot \nu_m \right)^{-1} + U_m, \tag{4.1.16}$$

while if (4.1.9) holds, then

$$S_m = U_m,$$

where

$$U_m = 1 + \frac{|x_{m+1} - x_m|}{|x_m - x_{m-1}|} \left(1 - V_m\right). \tag{4.1.17}$$

Proof. Differentiating (4.1.4) yields

$$\begin{aligned}
\frac{d^2}{dt_m^2} \varphi_{t_{m+1}}(t_m) = &\left(\frac{x_m - x_{m-1}}{|x_m - x_{m-1}|} - \frac{x_{m+1} - x_m}{|x_{m+1} - x_m|} \right) \cdot \ddot{x}_m \\
&+ \frac{|\dot{x}_m|^2}{|x_m - x_{m-1}|} \left(1 - \left(\frac{x_m - x_{m-1}}{|x_m - x_{m-1}|} \cdot \frac{\dot{x}_m}{|\dot{x}_m|} \right)^2 \right) \\
&+ \frac{|\dot{x}_m|^2}{|x_{m+1} - x_m|} \left(1 - \left(\frac{x_{m+1} - x_m}{|x_{m+1} - x_m|} \cdot \frac{\dot{x}_m}{|\dot{x}_m|} \right)^2 \right) \\
&- \frac{|\dot{x}_{m-1}||\dot{x}_m|}{|x_m - x_{m-1}|} \frac{dt_{m-1}}{dt_m} \\
&\times \left(\frac{\dot{x}_{m-1}}{|\dot{x}_{m-1}|} \cdot \frac{\dot{x}_m}{|\dot{x}_m|} - \frac{x_m - x_{m-1}}{|x_m - x_{m-1}|} \cdot \frac{\dot{x}_{m-1}}{|\dot{x}_{m-1}|} \frac{x_m - x_{m-1}}{|x_m - x_{m-1}|} \cdot \frac{\dot{x}_m}{|\dot{x}_m|} \right).
\end{aligned}$$

Appealing to Lemma 4.1.5 for the last term, we obtain

$$\begin{aligned}\frac{d^2}{dt_m^2}\varphi_{t_{m+1}}(t_m) = &\left(\frac{x_m - x_{m-1}}{|x_m - x_{m-1}|} - \frac{x_{m+1} - x_m}{|x_{m+1} - x_m|}\right) \cdot \ddot{x}_m \\ &+ \frac{|\dot{x}_m|^2}{|x_m - x_{m-1}|}\left(\frac{x_m - x_{m-1}}{|x_m - x_{m-1}|} \cdot \nu_m\right)^2 \\ &+ \frac{|\dot{x}_m|^2}{|x_{m+1} - x_m|}\left(\frac{x_{m+1} - x_m}{|x_{m+1} - x_m|} \cdot \nu_m\right)^2 \\ &- \frac{|\dot{x}_{m-1}||\dot{x}_m|}{|x_m - x_{m-1}|}\frac{x_m - x_{m-1}}{|x_m - x_{m-1}|} \cdot \nu_{m-1}\frac{x_m - x_{m-1}}{|x_m - x_{m-1}|} \cdot \nu_m \frac{dt_{m-1}}{dt_m}.\end{aligned}$$

Now, if (4.1.8) holds, then

$$\begin{aligned}\frac{d^2}{dt_m^2}\varphi_{t_{m+1}}(t_m) = &\, 2\frac{x_{m+1} - x_m}{|x_{m+1} - x_m|} \cdot \nu_m \kappa_m |\dot{x}_m|^2 \\ &+ \frac{|\dot{x}_m|^2}{|x_m - x_{m-1}|}\left(\frac{x_m - x_{m-1}}{|x_m - x_{m-1}|} \cdot \nu_m\right)^2 \\ &+ \frac{|\dot{x}_m|^2}{|x_{m+1} - x_m|}\left(\frac{x_{m+1} - x_m}{|x_{m+1} - x_m|} \cdot \nu_m\right)^2 \\ &- \frac{|\dot{x}_{m-1}||\dot{x}_m|}{|x_m - x_{m-1}|}\frac{x_m - x_{m-1}}{|x_m - x_{m-1}|} \cdot \nu_{m-1}\frac{x_m - x_{m-1}}{|x_m - x_{m-1}|} \cdot \nu_m \frac{dt_{m-1}}{dt_m} \\ = &\, 2\frac{x_{m+1} - x_m}{|x_{m+1} - x_m|} \cdot \nu_m \kappa_m |\dot{x}_m|^2 \\ &+ |\dot{x}_m|^2\left(\frac{1}{|x_m - x_{m-1}|} + \frac{1}{|x_{m+1} - x_m|}\right)\left(\frac{x_{m+1} - x_m}{|x_{m+1} - x_m|} \cdot \nu_m\right)^2 \\ &- \frac{|\dot{x}_{m-1}||\dot{x}_m|}{|x_m - x_{m-1}|}\frac{x_m - x_{m-1}}{|x_m - x_{m-1}|} \cdot \nu_{m-1}\frac{x_m - x_{m-1}}{|x_m - x_{m-1}|} \cdot \nu_m \frac{dt_{m-1}}{dt_m} \\ = &\, \frac{|\dot{x}_m|^2}{|x_{m+1} - x_m|}\left(\frac{x_{m+1} - x_m}{|x_{m+1} - x_m|} \cdot \nu_m\right)^2 \left(\frac{2\kappa_m |x_{m+1} - x_m|}{\frac{x_{m+1} - x_m}{|x_{m+1} - x_m|} \cdot \nu_m} + U_m\right).\end{aligned}$$

Note that the term next to U_m vanishes in case (4.1.9) holds. This completes the proof. ■

Finally, on account of the previous lemma, to obtain the explicit expressions in (4.1.12) and (4.1.13), we need only determine the coefficients V_m in (4.1.17). This is provided by the next two lemmas.

Lemma 4.1.7 (Time Derivatives in First Reflections) *For $m = 1$, if (4.1.6) holds, then*

$$V_1 = \left(1 + 2\kappa_0|x_1 - x_0|\left(\frac{x_1 - x_0}{|x_1 - x_0|}\cdot\nu_0\right)^{-1}\right)^{-1}, \tag{4.1.18}$$

while if (4.1.7) holds, then

$$V_1 = 1. \tag{4.1.19}$$

Proof. Differentiating the identity

$$\left(\alpha - \frac{x_1 - x_0}{|x_1 - x_0|}\right)\cdot \dot{x}_0 = 0$$

with respect to t_1 yields

$$\begin{aligned}
0 =& \left(\left(\alpha - \frac{x_1 - x_0}{|x_1 - x_0|}\right)\cdot \ddot{x}_0 + \frac{|\dot{x}_0|^2}{|x_1 - x_0|}\left(\frac{x_1 - x_0}{|x_1 - x_0|}\cdot\nu_0\right)^2\right)\frac{dt_0}{dt_1} \\
&- \frac{|\dot{x}_0||\dot{x}_1|}{|x_1 - x_0|}\left(\frac{\dot{x}_0}{|\dot{x}_0|}\cdot\frac{\dot{x}_1}{|\dot{x}_1|} - \frac{x_1 - x_0}{|x_1 - x_0|}\cdot\frac{\dot{x}_0}{|\dot{x}_0|}\,\frac{x_1 - x_0}{|x_1 - x_0|}\cdot\frac{\dot{x}_1}{|\dot{x}_1|}\right) \\
=& \left(\left(\alpha - \frac{x_1 - x_0}{|x_1 - x_0|}\right)\cdot \ddot{x}_0 + \frac{|\dot{x}_0|^2}{|x_1 - x_0|}\left(\frac{x_1 - x_0}{|x_1 - x_0|}\cdot\nu_0\right)^2\right)\frac{dt_0}{dt_1} \\
&- \frac{|\dot{x}_0||\dot{x}_1|}{|x_1 - x_0|}\frac{x_1 - x_0}{|x_1 - x_0|}\cdot\nu_0\frac{x_1 - x_0}{|x_1 - x_0|}\cdot\nu_1
\end{aligned}$$

where we made use of Lemma 4.1.5 in the last identity. Therefore

$$\begin{aligned}
\frac{dt_0}{dt_1} =& \frac{|\dot{x}_0||\dot{x}_1|}{|x_1 - x_0|}\frac{x_1 - x_0}{|x_1 - x_0|}\cdot\nu_0\frac{x_1 - x_0}{|x_1 - x_0|}\cdot\nu_1 \\
&\left(\left(\alpha - \frac{x_1 - x_0}{|x_1 - x_0|}\right)\cdot \ddot{x}_0 + \frac{|\dot{x}_0|^2}{|x_1 - x_0|}\left(\frac{x_1 - x_0}{|x_1 - x_0|}\cdot\nu_0\right)^2\right)^{-1}
\end{aligned}$$

Now, if (4.1.6) holds, then

$$\frac{dt_0}{dt_1} = \frac{|\dot{x}_0||\dot{x}_1|}{|x_1 - x_0|}\frac{x_1 - x_0}{|x_1 - x_0|} \cdot \nu_0 \frac{x_1 - x_0}{|x_1 - x_0|} \cdot \nu_1$$
$$\left(2\frac{x_1 - x_0}{|x_1 - x_0|} \cdot \nu_0 \kappa_0 |\dot{x}_0|^2 + \frac{|\dot{x}_0|^2}{|x_1 - x_0|}\left(\frac{x_1 - x_0}{|x_1 - x_0|} \cdot \nu_0\right)^2\right)^{-1}.$$

Rearranging the terms in this identity yields (4.1.18). On the other hand, if (4.1.7) holds, then

$$\begin{aligned}\frac{dt_0}{dt_1} &= \frac{|\dot{x}_0||\dot{x}_1|}{|x_1 - x_0|}\frac{x_1 - x_0}{|x_1 - x_0|} \cdot \nu_0 \frac{x_1 - x_0}{|x_1 - x_0|} \cdot \nu_1 \left(\frac{|\dot{x}_0|^2}{|x_1 - x_0|}\left(\frac{x_1 - x_0}{|x_1 - x_0|} \cdot \nu_0\right)^2\right)^{-1} \\ &= \frac{|\dot{x}_1|}{|\dot{x}_0|}\frac{x_1 - x_0}{|x_1 - x_0|} \cdot \nu_1 \left(\frac{x_1 - x_0}{|x_1 - x_0|} \cdot \nu_0\right)^{-1}\end{aligned}$$

completing the proof. ■

Lemma 4.1.8 (Time Derivatives in Further Reflections) *For $m > 1$, if (4.1.8) holds, then*

$$V_m = \left(2\kappa_{m-1}|x_m - x_{m-1}|\left(\frac{x_m - x_{m-1}}{|x_m - x_{m-1}|} \cdot \nu_{m-1}\right)^{-1} + U_{m-1}\right)^{-1} \tag{4.1.20}$$

while if (4.1.9) holds, then

$$V_m = U_{m-1}^{-1}, \tag{4.1.21}$$

where U_m is as given in Lemma 4.1.6.

Proof. Differentiating the identity

$$\left(\frac{x_{m-1} - x_{m-2}}{|x_{m-1} - x_{m-2}|} - \frac{x_m - x_{m-1}}{|x_m - x_{m-1}|}\right) \cdot \dot{x}_{m-1} = 0$$

with respect to t_m yields

$$
\begin{aligned}
0 &= \frac{\dot{x}_{m-1}}{|x_{m-1}-x_{m-2}|} \cdot \dot{x}_{m-1} \frac{dt_{m-1}}{dt_m} - \frac{\dot{x}_{m-2}}{|x_{m-1}-x_{m-2}|} \cdot \dot{x}_{m-1} \frac{dt_{m-2}}{dt_{m-1}} \frac{dt_{m-1}}{dt_m} \\
&+ \frac{x_{m-1}-x_{m-2}}{|x_{m-1}-x_{m-2}|} \cdot \ddot{x}_{m-1} \frac{dt_{m-1}}{dt_m} \\
&- \frac{x_{m-1}-x_{m-2}}{|x_{m-1}-x_{m-2}|} \cdot \dot{x}_{m-1} \frac{\dot{x}_{m-1}}{|x_{m-1}-x_{m-2}|} \cdot \frac{x_{m-1}-x_{m-2}}{|x_{m-1}-x_{m-2}|} \frac{dt_{m-1}}{dt_m} \\
&+ \frac{x_{m-1}-x_{m-2}}{|x_{m-1}-x_{m-2}|} \cdot \dot{x}_{m-1} \frac{\dot{x}_{m-2}}{|x_{m-1}-x_{m-2}|} \cdot \frac{x_{m-1}-x_{m-2}}{|x_{m-1}-x_{m-2}|} \frac{dt_{m-2}}{dt_{m-1}} \frac{dt_{m-1}}{dt_m} \\
&+ \frac{\dot{x}_{m-1}}{|x_m-x_{m-1}|} \cdot \dot{x}_{m-1} \frac{dt_{m-1}}{dt_m} - \frac{\dot{x}_m}{|x_m-x_{m-1}|} \cdot \dot{x}_{m-1} - \frac{x_m-x_{m-1}}{|x_m-x_{m-1}|} \cdot \ddot{x}_{m-1} \frac{dt_{m-1}}{dt_m} \\
&- \frac{x_m-x_{m-1}}{|x_m-x_{m-1}|} \cdot \dot{x}_{m-1} \frac{\dot{x}_{m-1}}{|x_m-x_{m-1}|} \cdot \frac{x_m-x_{m-1}}{|x_m-x_{m-1}|} \frac{dt_{m-1}}{dt_m} \\
&+ \frac{x_m-x_{m-1}}{|x_m-x_{m-1}|} \cdot \dot{x}_{m-1} \frac{\dot{x}_m}{|x_m-x_{m-1}|} \cdot \frac{x_m-x_{m-1}}{|x_m-x_{m-1}|}.
\end{aligned}
$$

Rearranging the terms gives

$$
\begin{aligned}
0 &= \left(\frac{x_{m-1}-x_{m-2}}{|x_{m-1}-x_{m-2}|} - \frac{x_m-x_{m-1}}{|x_m-x_{m-1}|} \right) \cdot \ddot{x}_{m-1} \frac{dt_{m-1}}{dt_m} \\
&+ \frac{1}{|x_{m-1}-x_{m-2}|} \left(|\dot{x}_{m-1}|^2 - \left(\frac{x_{m-1}-x_{m-2}}{|x_{m-1}-x_{m-2}|} \cdot \dot{x}_{m-1} \right)^2 \right) \frac{dt_{m-1}}{dt_m} \\
&+ \frac{1}{|x_m-x_{m-1}|} \left(|\dot{x}_{m-1}|^2 - \left(\frac{x_m-x_{m-1}}{|x_m-x_{m-1}|} \cdot \dot{x}_{m-1} \right)^2 \right) \frac{dt_{m-1}}{dt_m} \\
&- \frac{1}{|x_{m-1}-x_{m-2}|} \frac{dt_{m-2}}{dt_{m-1}} \frac{dt_{m-1}}{dt_m} \\
&\times \left(\dot{x}_{m-2} \cdot \dot{x}_{m-1} - \frac{x_{m-1}-x_{m-2}}{|x_{m-1}-x_{m-2}|} \cdot \dot{x}_{m-2} \frac{x_{m-1}-x_{m-2}}{|x_{m-1}-x_{m-2}|} \cdot \dot{x}_{m-1} \right) \\
&- \frac{1}{|x_m-x_{m-1}|} \left(\dot{x}_{m-1} \cdot \dot{x}_m - \frac{x_m-x_{m-1}}{|x_m-x_{m-1}|} \cdot \dot{x}_{m-1} \frac{x_m-x_{m-1}}{|x_m-x_{m-1}|} \cdot \dot{x}_m \right),
\end{aligned}
$$

or equivalently

$$\begin{aligned}
0 &= \left(\frac{x_{m-1}-x_{m-2}}{|x_{m-1}-x_{m-2}|} - \frac{x_m - x_{m-1}}{|x_m - x_{m-1}|}\right)\cdot \ddot{x}_{m-1}\frac{dt_{m-1}}{dt_m} \\
&+ |\dot{x}_{m-1}|^2\left(\frac{1}{|x_{m-1}-x_{m-2}|}+\frac{1}{|x_m-x_{m-1}|}\right)\left(\frac{x_m-x_{m-1}}{|x_m-x_{m-1}|}\cdot\nu_{m-1}\right)^2\frac{dt_{m-1}}{dt_m} \\
&- \frac{|\dot{x}_{m-2}||\dot{x}_{m-1}|}{|x_{m-1}-x_{m-2}|}\frac{dt_{m-2}}{dt_{m-1}}\frac{dt_{m-1}}{dt_m} \\
&\times\left(\frac{\dot{x}_{m-2}}{|\dot{x}_{m-2}|}\cdot\frac{\dot{x}_{m-1}}{|\dot{x}_{m-1}|} - \frac{x_{m-1}-x_{m-2}}{|x_{m-1}-x_{m-2}|}\cdot\frac{\dot{x}_{m-2}}{|\dot{x}_{m-2}|}\frac{x_{m-1}-x_{m-2}}{|x_{m-1}-x_{m-2}|}\cdot\frac{\dot{x}_{m-1}}{|\dot{x}_{m-1}|}\right) \\
&- \frac{|\dot{x}_{m-1}||\dot{x}_m|}{|x_m-x_{m-1}|}\left(\frac{\dot{x}_{m-1}}{|\dot{x}_{m-1}|}\cdot\frac{\dot{x}_m}{|\dot{x}_m|} - \frac{x_m-x_{m-1}}{|x_m-x_{m-1}|}\cdot\frac{\dot{x}_{m-1}}{|\dot{x}_{m-1}|}\frac{x_m-x_{m-1}}{|x_m-x_{m-1}|}\cdot\frac{\dot{x}_m}{|\dot{x}_m|}\right).
\end{aligned}$$

Appealing to Lemma 4.1.5 once more yields

$$\begin{aligned}
0 &= \left(\frac{x_{m-1}-x_{m-2}}{|x_{m-1}-x_{m-2}|} - \frac{x_m - x_{m-1}}{|x_m - x_{m-1}|}\right)\cdot \ddot{x}_{m-1}\frac{dt_{m-1}}{dt_m} \\
&+ |\dot{x}_{m-1}|^2\left(\frac{1}{|x_{m-1}-x_{m-2}|}+\frac{1}{|x_m-x_{m-1}|}\right)\left(\frac{x_m-x_{m-1}}{|x_m-x_{m-1}|}\cdot\nu_{m-1}\right)^2\frac{dt_{m-1}}{dt_m} \\
&- \frac{|\dot{x}_{m-2}||\dot{x}_{m-1}|}{|x_{m-1}-x_{m-2}|}\frac{x_{m-1}-x_{m-2}}{|x_{m-1}-x_{m-2}|}\cdot\nu_{m-2}\frac{x_{m-1}-x_{m-2}}{|x_{m-1}-x_{m-2}|}\cdot\nu_{m-1}\frac{dt_{m-2}}{dt_{m-1}}\frac{dt_{m-1}}{dt_m} \\
&- \frac{|\dot{x}_{m-1}||\dot{x}_m|}{|x_m-x_{m-1}|}\frac{x_m-x_{m-1}}{|x_m-x_{m-1}|}\cdot\nu_{m-1}\frac{x_m-x_{m-1}}{|x_m-x_{m-1}|}\cdot\nu_m
\end{aligned}$$

Therefore, if (4.1.8) holds, then

$$\begin{aligned}
0 &= 2\frac{x_m-x_{m-1}}{|x_m-x_{m-1}|}\cdot\nu_{m-1}\kappa_{m-1}|\dot{x}_{m-1}|^2\frac{dt_{m-1}}{dt_m} \\
&+ |\dot{x}_{m-1}|^2\left(\frac{1}{|x_{m-1}-x_{m-2}|}+\frac{1}{|x_m-x_{m-1}|}\right)\left(\frac{x_m-x_{m-1}}{|x_m-x_{m-1}|}\cdot\nu_{m-1}\right)^2\frac{dt_{m-1}}{dt_m} \\
&- \frac{|\dot{x}_{m-2}||\dot{x}_{m-1}|}{|x_{m-1}-x_{m-2}|}\frac{x_{m-1}-x_{m-2}}{|x_{m-1}-x_{m-2}|}\cdot\nu_{m-2}\frac{x_{m-1}-x_{m-2}}{|x_{m-1}-x_{m-2}|}\cdot\nu_{m-1}\frac{dt_{m-2}}{dt_{m-1}}\frac{dt_{m-1}}{dt_m} \\
&- \frac{|\dot{x}_{m-1}||\dot{x}_m|}{|x_m-x_{m-1}|}\frac{x_m-x_{m-1}}{|x_m-x_{m-1}|}\cdot\nu_{m-1}\frac{x_m-x_{m-1}}{|x_m-x_{m-1}|}\cdot\nu_m
\end{aligned}$$

which is equivalent to

$$0 = \frac{|\dot{x}_{m-1}|^2}{|x_m - x_{m-1}|} \left(\frac{x_m - x_{m-1}}{|x_m - x_{m-1}|} \cdot \nu_{m-1} \right)^2 \left(\frac{2\kappa_{m-1}|x_m - x_{m-1}|}{\frac{x_m - x_{m-1}}{|x_m - x_{m-1}|} \cdot \nu_{m-1}} + U_{m-1} \right) \frac{dt_{m-1}}{dt_m}$$
$$- \frac{|\dot{x}_{m-1}||\dot{x}_m|}{|x_m - x_{m-1}|} \frac{x_m - x_{m-1}}{|x_m - x_{m-1}|} \cdot \nu_{m-1} \frac{x_m - x_{m-1}}{|x_m - x_{m-1}|} \cdot \nu_m$$

Simplifying this last expression yields (4.1.20). In this last identity, in case (4.1.9) holds, the curvature term should be dropped from which we get (4.1.21). This completes the proof. ■

Finally, combining Lemmas 4.1.6, 4.1.7 and 4.1.8, we deduce that, in each case,

$$V_m = S_{m-1}^{-1}, \quad m \geq 1. \tag{4.1.22}$$

Therefore, using (4.1.22) in (4.1.17), we obtain the equations (4.1.12) and (4.1.13). This completes the proof of Theorem 4.1.4.

4.2 Integration around Kernel Singularities

As was mentioned above, the kernels of RHS integrals in (3.2.15) are singular only at the shadow boundary of ∂K_{m-1}, and these singularities are due to a discontinuity in the third derivative of the phases. However, the visibility assumption ensures that, in sufficiently high frequencies, the rays bouncing off $\mathcal{O}(k^{-1/3})$ neighborhoods of the shadow boundary of ∂K_{m-1} at the m-th reflection never reaches ∂K_m. Accordingly, the contributions of the RHS integrals around shadow boundaries of ∂K_{m-1} to the asymptotic expansions of ρ_m in (3.2.15) are negligible. Indeed, smoothing the phase functions around shadow boundaries if necessary, and utilizing the method of stationary phase, it can be easily verified that these contributions are of the form $\rho_{m-1}(x_{m-1})\mathcal{O}(k^{-1})$.

Note that the asymptotic expansion proposed in Theorem 4.0.1 relates to target points $x_m \in \partial K_m$ off the corresponding $\mathcal{O}(k^{-1/3})$ shadow boundaries. As with the RHS integrals, then, the contributions of LHS integrals (in equations (3.2.14)-(3.2.15)) coming from $\mathcal{O}(k^{-1/3})$ neighborhoods of the m-th shadow boundaries for such target points are of the form $\rho_m(x_m)\mathcal{O}(k^{-1})$, and are therefore negligible.

All of the kernel singularities discussed so far relate to singularities of phase functions. In addition to these, the kernels of LHS integrals are singular at the target points $x_m \in \partial K_m$. When the target point x_m is located away from shadow boundaries, one can choose a small enough neighborhood ∂K_m^ε (of the order $\mathcal{O}(1)$ with respect to k as $k \to \infty$) around x_m containing no stationary points and no other kernel singularities. More precisely, we choose ∂K_m^A to be a subset of ∂K_m in which $k|x_m - y| \gg 1$, and let

$$\partial K_m^\varepsilon = \partial K_m - \partial K_m^A.$$

As we show next, the LHS integrals on ∂K_m^ε are negligible too.

Lemma 4.2.1 *For a target point $x_m \in \partial K_m$ located off the m-th shadow boundaries (that are of order $\mathcal{O}(k^{-1/3})$), the LHS integrals in equations (3.2.14)-(3.2.15) restricted to ∂K_m^ε are of the from $\rho_m(x_m)\mathcal{O}(k^{-1})$.*

Proof. We will present the proof for target points located in illuminated regions as the proof for points in shadow regions follow the same lines.

Suppose now that the boundary ∂K_m is parametrized by $x = x(\tau)$, that $x_m = x(t)$, and write the integral in parametric form:

$$\int_{\partial K_m^\varepsilon} \frac{\partial G(x_m, y)}{\partial \nu(x_m)}\, e^{ik(\varphi_m(y)-\varphi_m(x_m))} \rho_m(y) ds(y) = \int_{t-\varepsilon}^{t+\varepsilon} F(t,\tau)\rho_m(\tau)d\tau \qquad (4.2.1)$$

where we used the notation

$$F(t,\tau) = \frac{ik}{2} H_1^{(1)}(k|x(\tau)-x(t)|)\frac{x(\tau)-x(t)}{|x(\tau)-x(t)|}\cdot \nu(t) e^{ik(\varphi_m(x(\tau))-\varphi_m(x(t)))}|\dot{x}(\tau)| \; . \quad (4.2.2)$$

We will consider the integral on $[t, t+\varepsilon]$ as its analysis is the same as that of the integral on $[t-\varepsilon, t]$.

To this end, first we introduce the change of variables

$$u = k|x(\tau) - x(t)|;$$

we shall expand $x(\tau)$ in a Taylor series around $x(t)$, and use this expansion to approximate function F given by (4.2.2). To complete the proof, we shall calculate the exact integral of this approximate quantity, and appeal to the asymptotic expansions of generalized hypergeometric series [69] to obtain the desired result.

Indeed, the Taylor expansion of $x(\tau)$ around $x(t)$ reads

$$x(\tau) - x(t) = (\tau - t)\dot{x}(t) + (\tau - t)^2 \frac{\ddot{x}(t)}{2} + \cdots \ ,$$

so that, near $u = 0$, we have

$$\tau - t \sim \frac{u}{k|\dot{x}(t)|} \ .$$

It follows that

$$\begin{aligned} \frac{x(\tau) - x(t)}{|x(\tau) - x(t)|} \cdot \nu(t) &= \frac{k}{u}\ (x(\tau) - x(t)) \cdot \nu(t) \\ &\sim \frac{k}{u}\ (\tau - t)^2\ \frac{\ddot{x}(t) \cdot \nu(t)}{2} \sim \frac{k}{u}\ \frac{u^2}{k^2}\ \frac{\ddot{x}(t) \cdot \nu(t)}{2|\dot{x}(t)|^2} = -\ \frac{\kappa_m(t)}{2}\ \frac{u}{k} \ . \end{aligned}$$

The term $|\dot{x}(\tau)|$ is simply approximated as $|\dot{x}(\tau)| \sim |\dot{x}(t)|$. It remains to approximate the exponential term in (4.2.2). Indeed,

$$\varphi_m(x(\tau)) - \varphi_m(x(t)) = o(\alpha \cdot (x(\tau) - x(t)))$$

where we have set

$$\alpha = \frac{x_{m-1}(t) - x_m(t)}{|x_{m-1}(t) - x_m(t)|} \ ,$$

and where $x_{m-1}(t) \in \partial K_{m-1}$ is on the geometrical optics path arriving at $x_m = x(t)$ after (m - 1) reflections. Consequently, we have

$$
\begin{aligned}
&ik\ (\varphi_m(x(\tau)) - \varphi_m(x(t))) \sim ik\ \alpha \cdot (x(\tau) - x(t)) \\
&\quad \sim ik \left(\alpha \cdot \dot{x}(t) + \alpha \cdot \frac{\ddot{x}(t)}{2}(\tau - t) \right) (\tau - t) \sim i \left(\alpha \cdot \frac{\dot{x}(t)}{|\dot{x}(t)|} + \alpha \cdot \frac{\ddot{x}(t)}{2|\dot{x}(t)|^2} \frac{u}{k} \right) u\ .
\end{aligned}
$$

These calculations complete the approximation of the function F in (4.2.2) yielding

$$
F(t,\tau) \sim \frac{\kappa_m(t)\ |\dot{x}(t)|}{4i}\ H_1^{(1)}(u)\ u\ \exp\left[i \left(\alpha \cdot \frac{\dot{x}(t)}{|\dot{x}(t)|} + \alpha \cdot \frac{\ddot{x}(t)}{2|\dot{x}(t)|^2} \frac{u}{k} \right) u \right] . \qquad (4.2.3)
$$

On the other hand, as we did for $|\dot{x}(\tau)|$, the last term in the integral (4.2.1), namely $\rho_m(\tau)$, is approximated as $\rho_m(\tau) \sim \rho_m(t)$. Finally, the approximation of $d\tau/du$ is found as follows:

$$
\begin{aligned}
&\frac{du}{d\tau} = k \frac{x(\tau) - x(t)}{|x(\tau) - x(t)|} \cdot \dot{x}(\tau) = \frac{k^2}{u}(x(\tau) - x(t)) \cdot \dot{x}(\tau) \\
&\quad \sim \frac{k^2}{u} \dot{x}(t) \cdot \dot{x}(\tau)(\tau - t) \sim \frac{k^2}{u} |\dot{x}(t)|^2 (\tau - t) \sim \frac{k^2}{u} |\dot{x}(t)|^2 \frac{u}{k|\dot{x}(t)|} = k|\dot{x}(t)|\ . \qquad (4.2.4)
\end{aligned}
$$

We conclude appealing to (4.2.3) and (4.2.4) that the integrals (4.2.1) are approximately equal to

$$
\frac{1}{4ik} \kappa_m(t) \rho_m(t) \int_0^{\varepsilon k |\dot{x}(t)|} H_1^{(1)}(u)\ u\ \exp\left[i \left(\alpha \cdot \frac{\dot{x}(t)}{|\dot{x}(t)|} + \alpha \cdot \frac{\ddot{x}(t)}{2|\dot{x}(t)|^2} \frac{u}{k} \right) u \right] du\ . \quad (4.2.5)
$$

Therefore, it remains to prove that the integral in (4.2.5) is of $\mathcal{O}(1)$. To this end, we write this integral as

$$
\int_0^{\varepsilon k |\dot{x}(t)|} = \int_0^C + \int_C^{\varepsilon k |\dot{x}(t)|} \qquad (4.2.6)
$$

where the constant C is chosen so that $1 \ll C$ and is independent of k. In particular, asymptotically, we may assume that $C \ll \varepsilon k |\dot{x}(t)|$. The integrand in (4.2.6) is asymptotically independent of k on the interval $[0, C]$, and accordingly the integral on $[0, C]$ is of $\mathcal{O}(1)$.

Concerning the integral on the interval $[C,\ \varepsilon k|\dot{x}(t)|\ ]$, we recall that [10] the Hankel function $H_1^{(1)}(z)$ possesses the asymptotic expansion

$$H_1^{(1)}(z) = \left(\frac{2}{\pi z}\right)^{1/2} e^{i(z-3\pi/4)} + \mathcal{O}(z^{-3/2}) \tag{4.2.7}$$

as $z \to \infty$ with $|\arg z| < \pi$. Therefore, the integral on $[C,\ \varepsilon k|\dot{x}(t)|\ ]$ is approximately equal to the integral

$$e^{-i3\pi/4}\left(\frac{2}{\pi}\right)^{1/2}\int_C^{\varepsilon k|\dot{x}(t)|} u^{1/2}\exp\left[i\left(1+\alpha\cdot\frac{\dot{x}(t)}{|\dot{x}(t)|}+\alpha\cdot\frac{\ddot{x}(t)}{2|\dot{x}(t)|^2}\frac{u}{k}\right)u\right]du\ . \tag{4.2.8}$$

On the other hand, as $x(t)$ is away from the shadow boundaries, and $u/k \leq \varepsilon|\dot{x}(t)|$ on $[C,\ \varepsilon k|\dot{x}(t)|\ ]$, the exponential in (4.2.8) behaves like $\exp(i\omega u)$ for some positive ω (independent of k). Since we have

$$\begin{aligned}
\int_0^a u^{1/2}e^{i\omega u}du &= a^{1/2}\int_0^1 u^{1/2}e^{ia\omega u}du = a^{1/2}\ {}_1F_1(3/2, 3/2+1, ia\omega)\\
&= \frac{2a^{1/2}}{3}\sum_{n=0}^{\infty}\frac{\Gamma(3/2+n)/\Gamma(3/2)}{\Gamma(3/2+1+n)/\Gamma(3/2+1)}\frac{(ia\omega)^n}{n!}\\
&= \frac{2a^{1/2}}{3}\sum_{n=0}^{\infty}\frac{3/2}{3/2+n}\frac{(ia\omega)^n}{n!} = a^{1/2}\sum_{n=0}^{\infty}\frac{1}{3/2+n}\frac{(ia\omega)^n}{n!}\\
&= a^{1/2}\ \mathcal{O}\left(\frac{e^{ia\omega}-1}{ia\omega}\right) = \mathcal{O}\left(\frac{e^{ia\omega}-1}{i\omega\sqrt{a}}\right)\ ,
\end{aligned}$$

where ${}_1F_1$ is a generalized hypergeometric series [69], we conclude that the integral on the interval $[C, \varepsilon k|\dot{x}(t)|]$ is of $\mathcal{O}(1)$. ■

4.3 Integration around Stationary Points

In this section, applying the method of stationary phase to the integrals in equations (3.2.14) and (3.2.15), we obtain the asymptotic expansions of the LHS and RHS integrals in equations (3.2.10) and (3.2.11).

As we explained above, the integrals in (3.2.14) and (3.2.15) being generalized Fourier integrals, the only important contribution to their asymptotic expansions come from the critical points of the corresponding integration kernels. As was proved in §4.2, however, among these critical points the only points that contribute to the asymptotic expansions are precisely the points where the phases φ_m are stationary. These stationary points were characterized in Lemma 4.1.2.

As we explained, when the LHS integrals are considered, whether there is a stationary point or not depends on where the target point is located. More precisely, if the target point $x_m \in \partial K_m$ is located in the m-th illuminated region, then the corresponding LHS integral has no stationary point. On account of the method of stationary phase and of Lemma 4.2.1, then, the LHS integral is of the form $\eta_m(x_m)\mathcal{O}(k^{-1})$.

On the other hand, when the target point $x_m^s \in \partial K_m$ is located in the m-th shadow region, the corresponding LHS integral has a point $x_m \in \partial K_m$ located in the m-th illuminated region as its only stationary point. Moreover, for these two points, the corresponding RHS integrals have the same stationary points, say $x_{m-1} \in \partial K_{m-1}$. Interestingly, as we shall see next, for the target point x_m^s, the contribution of the RHS integral coming from the stationary point x_{m-1} cancels the contribution of the LHS integral coming from the stationary point x_m. It follows that the iterated current η_m vanishes to first order in k on the m-th shadow region (off the $\mathcal{O}(k^{-1/3})$ shadow boundaries).

Let us consider the RHS integral in equation (3.2.15) for an *arbitrary* target point $x_m \in \partial K_m$. On account of the asymptotic expansion (4.2.7) of the Hankel function

$H_1^{(1)}(z)$, equation (2.4.2) yields

$$\int_{\partial K_{m-1}} \frac{\partial G(x_m, y)}{\partial \nu(x_m)} \rho_{m-1}(y) e^{ik(\varphi_{m-1}(y)-\varphi_m(x_m))} ds(y)$$
$$\sim \sqrt{\frac{k}{2\pi}} e^{-i(k\varphi_m(x_m)+\pi/4)} \int_{\partial K_{m-1}} Z(x_m, y) \rho_{m-1}(y) e^{ik(|x_m-y|+\varphi_{m-1}(y))} ds(y)$$

where we have set

$$Z(x_m, y) = \frac{1}{\sqrt{|x_m - y|}} \frac{x_m - y}{|x_m - y|} \cdot \nu(x_m), \quad y \in \partial K_{m-1}.$$

By Lemma 4.1.2, the only stationary point of the combined phase function $\varphi_{t_m}(t_{m-1}) = |x_m - y(t_{m-1})| + \varphi_{m-1}(y(t_{m-1}))$ is x_{m-1}. Thus, utilizing the stationary phase method gives

$$\int_{\partial K_{m-1}} Z(x_m, y) \rho_{m-1}(y) e^{ik(|x_m-y|+\varphi_{m-1}(y))} ds(y)$$
$$\sim Z(x_m, x_{m-1}) \rho_{m-1}(x_{m-1}) |\dot{x}_{m-1}| e^{ik\varphi_m(x_m)} e^{i\pi/4} \left[\frac{k}{2\pi} \left| \frac{d^2 \varphi_{t_m}(t_{m-1})}{dt_{m-1}^2} \right| \right]^{-1/2} ,$$

on account of the fact that $\varphi_m(x_m) = |x_m - x_{m-1}| + \varphi_{m-1}(x_{m-1})$. Thus, using Theorem 4.1.4 together with the relation (3.2.13) completes proof of the part of Theorem 4.0.1 concerning illuminated regions.

For the second part, we begin with proving that ρ_0 in (3.2.14) vanishes to first order in k in the shadow region. To this end, for a target point $x_0^s \in \partial K_0$ in the shadow region, we shall denote the corresponding stationary point of the LHS integral in (3.2.14) by x_0. By what we have shown above, we have

$$\rho_0(x_0)(1 + \mathcal{O}(k^{-1})) = 2ik\alpha \cdot \nu_0.$$

Therefore, using the method of stationary phase, we see that the LHS integral in

(3.2.14) satisfies

$$\begin{aligned}
&\int_{\partial K_0} \frac{\partial G(x_0^s, y)}{\partial \nu(x_0^s)}\, e^{ik(\varphi_0(y)-\varphi_0(x_0^s))}\rho_0(y)ds(y) \\
&\quad = \frac{x_0^s - x_0}{|x_0^s - x_0|}\cdot \nu(x_0^s)|\dot{x}_0| \left| \frac{d^2\varphi_{t_0^s}(t_0)}{dt_0^2}|x_0^s - x_0| \right|^{-1/2} \rho_0(x_0) + \mathcal{O}(k^{-1}) \\
&\quad = \frac{x_0^s - x_0}{|x_0^s - x_0|}\cdot \nu(x_0^s)|\dot{x}_0| \left| \frac{d^2\varphi_{t_0^s}(t_0)}{dt_0^2}|x_0^s - x_0| \right|^{-1/2} 2ik\alpha\cdot\nu_0 + \mathcal{O}(k^{-1}) \\
&\quad = \frac{x_0^s - x_0}{|x_0^s - x_0|}\cdot \nu(x_0^s)|\dot{x}_0| \left| |\dot{x}_0|^2 \left(\frac{x_0^s - x_0}{|x_0^s - x_0|}\cdot\nu_0\right)^2 \right|^{-1/2} 2ik\alpha\cdot\nu_0 + \mathcal{O}(k^{-1}) \\
&\quad = -\alpha\cdot\nu(x_0^s)(\alpha\cdot\nu_0)^{-1}2ik\alpha\cdot\nu_0 + \mathcal{O}(k^{-1}) \\
&\quad = -2ik\alpha\cdot\nu(x_0^s) + \mathcal{O}(k^{-1}).
\end{aligned}$$

Thus equation (3.2.14) implies

$$\rho_0(x_0^s) = \mathcal{O}(k^{-1}),$$

and thereby proves the second part of Theorem 4.0.1 for $m = 0$.

Let us now consider the evaluation of the integrals in (3.2.15) in the first reflection and for a target point $x_1^s \in \partial K$ in the shadow region. Let x_0 and x_1 be the stationary points of the RHS and LHS integrals. Then the RHS integral is given up to an error of magnitude $\rho_0(x_0)\mathcal{O}(k^{-1})$ by

$$\begin{aligned}
&\frac{x_1^s - x_0}{|x_1^s - x_0|}\cdot \nu(x_1^s)|\dot{x}_0| \left| \frac{d^2\varphi_{t_1^s}(t_0)}{dt_0^2}|x_1^s - x_0| \right|^{-1/2} \rho_0(x_0) \\
&= \frac{x_1^s - x_0}{|x_1^s - x_0|}\cdot \nu(x_1^s)|\dot{x}_0| \left| |\dot{x}_0|^2 \left(\frac{x_1^s - x_0}{|x_1^s - x_0|}\cdot\nu_0\right)^2 \left(1 + \frac{2\kappa_0|x_1^s - x_0|}{\frac{x_1^s - x_0}{|x_1^s - x_0|}\cdot\nu_0}\right) \right|^{-1/2} \rho_0(x_0) \\
&= \frac{\frac{x_1^s - x_0}{|x_1^s - x_0|}\cdot\nu(x_1^s)}{\frac{x_1^s - x_0}{|x_1^s - x_0|}\cdot\nu_0} \left(1 + \frac{2\kappa_0|x_1^s - x_0|}{\frac{x_1^s - x_0}{|x_1^s - x_0|}\cdot\nu_0}\right)^{-1/2} \rho_0(x_0)
\end{aligned}$$

On the other hand, the LHS integral is given up to an error of magnitude $\rho_1(x_1^s)\mathcal{O}(k^{-1})$ (and up to a phase term) by

$$
\begin{aligned}
&\frac{x_1^s - x_1}{|x_1^s - x_1|} \cdot \nu(x_1^s)|\dot{x}_1| \left| \frac{d^2\varphi_{t_1^s}(t_1)}{dt_1^2} |x_1^s - x_1| \right|^{-1/2} \rho_1(x_1) \\
&\sim \frac{x_1^s - x_1}{|x_1^s - x_1|} \cdot \nu(x_1^s)|\dot{x}_1| \left| \frac{d^2\varphi_{t_1^s}(t_1)}{dt_1^2} |x_1^s - x_1| \right|^{-1/2} \frac{\frac{x_1 - x_0}{|x_1 - x_0|} \cdot \nu_1}{\frac{x_1 - x_0}{|x_1 - x_0|} \cdot \nu_0} \left(1 + \frac{2\kappa_0 |x_1 - x_0|}{\frac{x_1 - x_0}{|x_1 - x_0|} \cdot \nu_0} \right)^{-1/2} \rho_0(x_0) \\
&= \frac{x_1^s - x_1}{|x_1^s - x_1|} \cdot \nu(x_1^s)|\dot{x}_1| \\
&\quad \left\{ \left(\frac{x_1^s - x_1}{|x_1^s - x_1|} \cdot \nu_1 \right)^2 |\dot{x}_1|^2 \left[1 + \frac{|x_1^s - x_1|}{|x_1 - x_0|} \left(1 - \left(\frac{2\kappa_0 |x_1 - x_0|}{\frac{x_1 - x_0}{|x_1 - x_0|} \cdot \nu_0} \right)^{-1} \right) \right] \right\}^{-1/2} \\
&\quad \frac{\frac{x_1 - x_0}{|x_1 - x_0|} \cdot \nu_1}{\frac{x_1 - x_0}{|x_1 - x_0|} \cdot \nu_0} \left(1 + \frac{2\kappa_0 |x_1 - x_0|}{\frac{x_1 - x_0}{|x_1 - x_0|} \cdot \nu_0} \right)^{-1/2} \rho_0(x_0) \\
&= -\frac{\frac{x_1^s - x_1}{|x_1^s - x_1|} \cdot \nu(x_1^s)}{\frac{x_1 - x_0}{|x_1 - x_0|} \cdot \nu_0} \\
&\quad \left[1 + \frac{|x_1^s - x_1|}{|x_1 - x_0|} \left(1 - \left(\frac{2\kappa_0 |x_1 - x_0|}{\frac{x_1 - x_0}{|x_1 - x_0|} \cdot \nu_0} \right)^{-1} \right) \right]^{-1/2} \left(1 + \frac{2\kappa_0 |x_1 - x_0|}{\frac{x_1 - x_0}{|x_1 - x_0|} \cdot \nu_0} \right)^{-1/2} \rho_0(x_0) \\
&= -\frac{\frac{x_1^s - x_1}{|x_1^s - x_1|} \cdot \nu(x_1^s)}{\frac{x_1 - x_0}{|x_1 - x_0|} \cdot \nu_0} \left(1 + \frac{2\kappa_0 |x_1 - x_0|}{\frac{x_1 - x_0}{|x_1 - x_0|} \cdot \nu_0} + \frac{2\kappa_0 |x_1^s - x_1|}{\frac{x_1 - x_0}{|x_1 - x_0|} \cdot \nu_0} \right)^{-1/2} \rho_0(x_0) \\
&= -\frac{\frac{x_1^s - x_1}{|x_1^s - x_1|} \cdot \nu(x_1^s)}{\frac{x_1^s - x_0}{|x_1^s - x_0|} \cdot \nu_0} \left(1 + \frac{2\kappa_0 |x_1^s - x_0|}{\frac{x_1^s - x_0}{|x_1^s - x_0|} \cdot \nu_0} \right)^{-1/2} \rho_0(x_0).
\end{aligned}
$$

Therefore, taking into account of the phase terms, we see that the RHS and LHS integrals cancel each other up to an error of magnitude $\rho_1(x_1^s)\mathcal{O}(k^{-1})$. The proof for further reflections follows the same lines.

Chapter 5

Asymptotic Expansions of the Three-dimensional Multiple Scattering Iterations in HF-IEM

In this Chapter, we derive the asymptotic expansions of the solutions η_m of the integral equations (3.2.10)-(3.2.11) in a three-dimensional setting. As in the previous Chapter, we will consider a finite collection of convex obstacles satisfying the visibility condition. We utilize a slightly different notation: indices of the points will be super-indices instead of sub-indices. The main result of this Chapter reads as follows:

Theorem 5.0.1 (Asymptotic Expansions of Iterated Currents) *At each reflection, the asymptotic expansions of iterated currents $\eta_m = \eta_m(x_m)$ are given on the m-th illuminated regions (off the $\mathcal{O}(k^{-1/3})$ shadow boundaries) by*

$$\eta_0 = 2ike^{ik\alpha \cdot x^0} \ \alpha \cdot \nu_0 \ \left(1 + \mathcal{O}\left(k^{-1}\right)\right),$$

and for $m = 1, 2, \ldots$

$$\eta_m = e^{ik|x^m - x^{m-1}|} \ \frac{x^m - x^{m-1}}{|x^m - x^{m-1}|} \cdot \nu_m \ |\det H_m|^{-1/2} \ \eta_{m-1} \left(1 + \mathcal{O}\left(k^{-1}\right)\right)$$

where H_i's are defined recursively as

$$H_1 = 2\ |x^1 - x^0|\ \frac{x^1 - x^0}{|x^1 - x^0|} \cdot \nu_0 \begin{pmatrix} \kappa_0^1 & 0 \\ 0 & \kappa_0^2 \end{pmatrix} + E_1$$

and, for $1 < i \leq m$,

$$\begin{aligned} H_i = {} & 2\ |x^i - x^{i-1}|\ \frac{x^i - x^{i-1}}{|x^i - x^{i-1}|} \cdot \nu_{i-1} \begin{pmatrix} \kappa_{i-1}^1 & 0 \\ 0 & \kappa_{i-1}^2 \end{pmatrix} \\ & + \left(1 + \frac{|x^i - x^{i-1}|}{|x^{i-1} - x^{i-2}|}\right) E_i - \frac{|x^i - x^{i-1}|}{|x^{i-1} - x^{i-2}|} F_i^T H_{i-1} F_i\ . \end{aligned}$$

Here we used κ_i^1 and κ_i^2 to denote the principal curvatures at the point x^i, and set

$$E_i = \begin{pmatrix} 1 - \left(\frac{x^i - x^{i-1}}{|x^i - x^{i-1}|} \cdot \frac{x_{t_{i-1}}^{i-1}}{|x_{t_{i-1}}^{i-1}|}\right)^2 & F(t_{i-1}, \tau_{i-1}; i-1, i) \\ F(t_{i-1}, \tau_{i-1}; i-1, i) & 1 - \left(\frac{x^i - x^{i-1}}{|x^i - x^{i-1}|} \cdot \frac{x_{\tau_{i-1}}^{i-1}}{|x_{\tau_{i-1}}^{i-1}|}\right)^2 \end{pmatrix},$$

and

$$F_i = \begin{pmatrix} F(t_{i-2}, t_{i-1}; i-2, i-1) & F(t_{i-2}, \tau_{i-1}; i-2, i-1) \\ F(\tau_{i-2}, t_{i-1}; i-2, i-1) & F(\tau_{i-2}, \tau_{i-1}; i-2, i-1) \end{pmatrix},$$

where

$$F(t_i, t_j; k, l) = \frac{x_{t_i}^i}{|x_{t_i}^i|} \cdot \frac{x_{t_j}^j}{|x_{t_j}^j|} - \frac{x^k - x^l}{|x^k - x^l|} \cdot \frac{x_{t_i}^i}{|x_{t_i}^i|} \frac{x^k - x^l}{|x^k - x^l|} \cdot \frac{x_{t_j}^j}{|x_{t_j}^j|}\ .$$

On the other hand, the iterated current η_m vanishes to first order in wavelength on the m-th shadow region (off the $\mathcal{O}(k^{-1/3})$ shadow boundaries).

The proof of Theorem 5.0.1 is parallel to that of Theorem 4.0.1, and we shall skip most of the details in order to prevent repetition. In particular, as in previous Chapter, it can be shown that the contributions to the integrals in (3.2.10) and (3.2.11) coming from the critical points other than the stationary points of phases are of the form $\eta_m \mathcal{O}(k^{-1})$, and are therefore negligible. Consequently, the derivation of the expansions in Theorem 5.0.1 require only the application of the method of stationary phase for the evaluation of the integrals in (3.2.10) and (3.2.11), and this, in turn, entails the characterization of the stationary points and Hessians at these stationary points of the phases.

5.1 Properties of Phase Functions

This section provides the three dimensional versions of the computations carried in §4.1. As the ideas behind these calculations is the same in all dimensions, we shall only state the results, and provide minor explanations so that, if desired, one can fill in the details.

Now, as in the two-dimensional case, suppose that we are given a sequence of obstacles $\{K_m\}_{m\geq 0}$. We assume that the boundary surfaces ∂K_m possess regular analytic local parametric representations of the form

$$x^i = x^i(t_i, \tau_i),$$

where t_i and τ_i are principle directions. For a *fixed* $x^{m+1} = x^{m+1}(t_{m+1}, \tau_{m+1}) \in \partial K_{m+1}$, with $m \geq 0$, consider the phase functions

$$\varphi_{t_{m+1},\tau_{m+1}}(t_m, \tau_m) = \alpha \cdot x^0 + \sum_{i=0}^{m} |x^{i+1} - x^i|, \tag{5.1.1}$$

of the RHS integrals in (3.2.15) where the points $x^0, \dots, x^m$ are assumed to be on the same optical ray path and belong to the illuminated regions of their corresponding boundary surfaces.

As in the two dimensional case, phase functions corresponding to the creeping waves can also be considered; these phases must be defined as integrals on the geodesics along which the creeping rays travel. Calculating the derivatives of these phases with respect to the geodesic coordinates, it can be easily deduced that these phases are stationary at a point if and only if the creeping ray diffracts tangentially at this point. Consequently, as in the previous Chapter, we shall concentrate on the phases (5.1.1).

5.1.1 First Order Partial Derivatives

The next result should be compared with Lemma 4.1.1.

Lemma 5.1.1 *For $m = 0$, we have*

$$\frac{\partial}{\partial t_0}\varphi_{t_1,\tau_1}(t_0,\tau_0) = \left(\alpha - \frac{x^1 - x^0}{|x^1 - x^0|}\right) \cdot x^0_{t_0} \tag{5.1.2}$$

$$\frac{\partial}{\partial \tau_0}\Phi_{t_1,\tau_1}(t_0,\tau_0) = \left(\alpha - \frac{x^1 - x^0}{|x^1 - x^0|}\right) \cdot x^0_{\tau_0}, \tag{5.1.3}$$

and, for $m \geq 1$, we have

$$\frac{\partial}{\partial t_m}\varphi_{t_{m+1},\tau_{m+1}}(t_m,\tau_m) = \left(\frac{x^m - x^{m-1}}{|x^m - x^{m-1}|} - \frac{x^{m+1} - x^m}{|x^{m+1} - x^m|}\right) \cdot x^m_{t_m} \tag{5.1.4}$$

$$\frac{\partial}{\partial \tau_m}\varphi_{t_{m+1},\tau_{m+1}}(t_m,\tau_m) = \left(\frac{x^m - x^{m-1}}{|x^m - x^{m-1}|} - \frac{x^{m+1} - x^m}{|x^{m+1} - x^m|}\right) \cdot x^m_{\tau_m}. \tag{5.1.5}$$

Proof. The proofs of (5.1.2) and (5.1.3) are trivial. To prove (5.1.4), first we differentiate (5.1.1):

$$\begin{aligned}\frac{\partial}{\partial t_m}\varphi_{t_{m+1},\tau_{m+1}}(t_m,\tau_m) = \alpha \cdot \left(x^0_{t_0}\frac{\partial t_0}{\partial t_m} + x^0_{\tau_0}\frac{\partial \tau_0}{\partial t_m}\right)& \\ + \sum_{i=0}^{m-1} \frac{x^{i+1} - x^i}{|x^{i+1} - x^i|} \cdot \left(x^{i+1}_{t_{i+1}}\frac{\partial t_{i+1}}{\partial t_m} + x^{i+1}_{\tau_{i+1}}\frac{\partial \tau_{i+1}}{\partial t_m} - x^i_{t_i}\frac{\partial t_i}{\partial t_m} - x^i_{\tau_i}\frac{\partial \tau_i}{\partial t_m}\right)& \\ - \frac{x^{m+1} - x^m}{|x^{m+1} - x^m|} \cdot \left(x^m_{t_m}\frac{\partial t_m}{\partial t_m} + x^m_{\tau_m}\frac{\partial \tau_m}{\partial t_m}\right).&\end{aligned}$$

We then rearrange the terms to obtain

$$
\begin{aligned}
\frac{\partial}{\partial t_m}\varphi_{t_{m+1},\tau_{m+1}}(t_m,\tau_m) = \alpha\cdot\left(x^0_{t_0}\frac{\partial t_0}{\partial t_m}+x^0_{\tau_0}\frac{\partial \tau_0}{\partial t_m}\right) \\
-\sum_{i=0}^{m-1}\frac{x^{i+1}-x^i}{|x^{i+1}-x^i|}\cdot\left(x^i_{t_i}\frac{\partial t_i}{\partial t_m}+x^i_{\tau_i}\frac{\partial \tau_i}{\partial t_m}\right) \\
+\sum_{i=0}^{m-1}\frac{x^{i+1}-x^i}{|x^{i+1}-x^i|}\cdot\left(x^{i+1}_{t_{i+1}}\frac{\partial t_{i+1}}{\partial t_m}+x^{i+1}_{\tau_{i+1}}\frac{\partial \tau_{i+1}}{\partial t_m}\right) \\
-\frac{x^{m+1}-x^m}{|x^{m+1}-x^m|}\cdot\left(x^m_{t_m}\frac{\partial t_m}{\partial t_m}+x^m_{\tau_m}\frac{\partial \tau_m}{\partial t_m}\right),
\end{aligned}
$$

and a further rearrangement gives

$$
\begin{aligned}
\frac{\partial}{\partial t_m}\varphi_{t_{m+1},\tau_{m+1}}(t_m,\tau_m) = \left(\alpha-\frac{x^1-x^0}{|x^1-x^0|}\right)\cdot\left(x^0_{t_0}\frac{\partial t_0}{\partial t_m}+x^0_{\tau_0}\frac{\partial \tau_0}{\partial t_m}\right) \\
+\sum_{i=0}^{m-2}\left(\frac{x^{i+1}-x^i}{|x^{i+1}-x^i|}-\frac{x^{i+2}-x^{i+1}}{|x^{i+2}-x^{i+1}|}\right)\cdot\left(x^{i+1}_{t_{i+1}}\frac{\partial t_{i+1}}{\partial t_m}+x^{i+1}_{\tau_{i+1}}\frac{\partial \tau_{i+1}}{\partial t_m}\right) \\
+\left(\frac{x^m-x^{m-1}}{|x^m-x^{m-1}|}-\frac{x^{m+1}-x^m}{|x^{m+1}-x^m|}\right)\cdot\left(x^m_{t_m}\frac{\partial t_m}{\partial t_m}+x^m_{\tau_m}\frac{\partial \tau_m}{\partial t_m}\right).
\end{aligned}
$$

Therefore, since the points $x_0,\ldots,x_m$ are assumed to be on the same optical ray path, we obtain (5.1.4). The proof of (5.1.5) follows the same lines. ■

5.1.2 Characterization of Stationary Points

The following Lemma shows that the characterization of the stationary points in three dimensions is the same as in two dimensions (see Lemma 4.1.2); that is, the phase function $\varphi_{t_{m+1},\tau_{m+1}}(t_m,\tau_m)$ is stationary at a point x^m if and only if the points $x^0,\ldots,x^m,x^{m+1}$ are on the same optical ray path.

Corollary 5.1.2 i) (First Reflections) *For $m=0$, the phase given by (5.1.1) is stationary at a point x^0 with $x^0 = x^0(t_0,\tau_0)$ if and only if*

$$
\frac{x^1-x^0}{|x^1-x^0|} = \alpha + 2\frac{x^1-x^0}{|x^1-x^0|}\cdot\nu_0\ \nu_0 \qquad (5.1.6)
$$

or

$$\frac{x^1 - x^0}{|x^1 - x^0|} = \alpha. \tag{5.1.7}$$

ii) (Further Reflections) *For $m \geq 1$, the phase given by (5.1.1) is stationary at a point x^m with $x^m = x^m(t_m, \tau_m)$ if and only if*

$$\frac{x^{m+1} - x^m}{|x^{m+1} - x^m|} = \frac{x^m - x^{m-1}}{|x^m - x^{m-1}|} + 2\frac{x^{m+1} - x^m}{|x^{m+1} - x^m|} \cdot \nu_m \ \nu_m \tag{5.1.8}$$

or

$$\frac{x^{m+1} - x_m}{|x^{m+1} - x^m|} = \frac{x^m - x^{m-1}}{|x^m - x^{m-1}|}. \tag{5.1.9}$$

Proof. Using Lemma 5.1.1, we obtain

$$\left(\frac{\partial}{\partial t_0}\varphi_{t_1,\tau_1}(t_0,\tau_0), \frac{\partial}{\partial \tau_0}\varphi_{t_1,\tau_1}(t_0,\tau_0)\right) = 0$$

if and only if

$$\alpha - \frac{x^1 - x^0}{|x^1 - x^0|} = \lambda_0 \nu_0$$

for some λ_0; and

$$\left(\frac{\partial}{\partial t_m}\varphi_{t_{m+1},\tau_{m+1}}(t_m,\tau_m), \frac{\partial}{\partial \tau_m}\varphi_{t_{m+1},\tau_{m+1}}(t_m,\tau_m)\right) = 0$$

if and only if

$$\frac{x^m - x^{m-1}}{|x^m - x^{m-1}|} - \frac{x^{m+1} - x^m}{|x^{m+1} - x^m|} = \lambda_m \nu_m$$

for some λ_m. The rest of the proof follows the same lines with the proof of Lemma 4.1.2. ■

5.1.3 Hessians at Stationary Points

For $i \geq 0$, we define

$$\mathbb{H}_{i+1} = |x^{i+1} - x^i| \begin{pmatrix} \dfrac{\frac{\partial^2}{\partial t_i^2}\varphi_{t_{i+1},\tau_{i+1}}(t_i,\tau_i)}{|x^i_{t_i}|^2} & \dfrac{\frac{\partial^2}{\partial t_i \partial \tau_i}\varphi_{t_{i+1},\tau_{i+1}}(t_i,\tau_i)}{|x^i_{t_i}||x^i_{\tau_i}|} \\ \dfrac{\frac{\partial^2}{\partial t_i \partial \tau_i}\varphi_{t_{i+1},\tau_{i+1}}(t_i,\tau_i)}{|x^i_{t_i}||x^i_{\tau_i}|} & \dfrac{\frac{\partial^2}{\partial \tau_i^2}\varphi_{t_{i+1},\tau_{i+1}}(t_i,\tau_i)}{|x^i_{\tau_i}|^2} \end{pmatrix}.$$

In stating the next result, we use the notation in Theorem 5.0.1.

Theorem 5.1.3 i) (Hessian in First Reflections) *For $m = 0$, if (5.1.6) holds, then*

$$\mathbb{H}_1 = H_1 = 2\ |x^1 - x^0|\ \frac{x^1 - x^0}{|x^1 - x^0|} \cdot \nu_0 \begin{pmatrix} \kappa_0^1 & 0 \\ 0 & \kappa_0^2 \end{pmatrix} + E_1\ , \tag{5.1.10}$$

while if (5.1.7) holds, then

$$\mathbb{H}_1 = E_1\ . \tag{5.1.11}$$

ii) (Hessian in Further Reflections) *For $m \geq 1$, if (5.1.8) holds, then*

$$\begin{aligned} \mathbb{H}_m = H_m = 2\ |x^m - x^{m-1}|\ \frac{x^m - x^{m-1}}{|x^m - x^{m-1}|} \cdot \nu_{m-1} \begin{pmatrix} \kappa_{m-1}^1 & 0 \\ 0 & \kappa_{m-1}^2 \end{pmatrix} \\ + \left(1 + \frac{|x^m - x^{m-1}|}{|x^{m-1} - x^{m-2}|}\right) E_m - \frac{|x^m - x^{m-1}|}{|x^{m-1} - x^{m-2}|} F_m^T H_{m-1} F_m\ , \end{aligned} \tag{5.1.12}$$

while if (5.1.9) holds, then

$$\mathbb{H}_m = \left(1 + \frac{|x^m - x^{m-1}|}{|x^{m-1} - x^{m-2}|}\right) E_m - \frac{|x^m - x^{m-1}|}{|x^{m-1} - x^{m-2}|} F_m^T H_{m-1} F_m\ . \tag{5.1.13}$$

We skip the proof of Theorem 5.1.3 as it is parallel to that of Theorem 4.1.4.

5.2 Integration around Stationary Points

In this section, we describe the main ideas in applying Theorem 5.1.3 in conjunction with the stationary phase method to obtain the asymptotic expansions provided in Theorem 5.0.1. To begin, we note that, in three-dimensions, the integral equations (3.2.14) and (3.2.15) take on the form

$$\rho_0(x) - \frac{1}{2\pi} e^{-ik\alpha\cdot x} \int_{\partial K_0} e^{ik(\alpha\cdot y+|x-y|)} \frac{1-ik|x-y|}{|x-y|^2} \frac{x-y}{|x-y|} \cdot \nu(x)\rho_0(y)dS(y) = 2ik\alpha\cdot\nu(x),$$

and, for $m \geq 1$,

$$\begin{aligned} &\rho_m(x) - \frac{1}{2\pi} e^{-ik\varphi_m(x)} \int_{\partial K_m} e^{ik(\varphi_m(y)+|x-y|)} \frac{1-ik|x-y|}{|x-y|^2} \frac{x-y}{|x-y|} \cdot \nu(x)\rho_m(y)dS(y) \\ &\quad = \frac{1}{2\pi} e^{-ik\varphi_m(x)} \int_{\partial K_{m-1}} e^{ik(\varphi_{m-1}(y)+|x-y|)} \frac{1-ik|x-y|}{|x-y|^2} \frac{x-y}{|x-y|} \cdot \nu(x)\rho_{m-1}(y)dS(y), \end{aligned}$$

respectively. Asymptotically, these equations can be written as

$$\begin{aligned} &\rho_0(x) + \frac{1}{2\pi} e^{-ik\alpha\cdot x} \int_{\partial K_0} e^{ik(\alpha\cdot y+|x-y|)} \frac{ik}{|x-y|} \frac{x-y}{|x-y|} \cdot \nu(x)\rho_0(y)dS(y) \\ &\qquad \sim 2ik\alpha\cdot\nu(x) \end{aligned} \tag{5.2.1}$$

and, for $m \geq 1$,

$$\begin{aligned} &\rho_m(x) + \frac{1}{2\pi} e^{-ik\varphi_m(x)} \int_{\partial K_m} e^{ik(\varphi_m(y)+|x-y|)} \frac{ik}{|x-y|} \frac{x-y}{|x-y|} \cdot \nu(x)\rho_m(y)dS(y) \\ &\sim -\frac{1}{2\pi} e^{-ik\varphi_m(x)} \int_{\partial K_{m-1}} e^{ik(\varphi_{m-1}(y)+|x-y|)} \frac{ik}{|x-y|} \frac{x-y}{|x-y|} \cdot \nu(x)\rho_{m-1}(y)dS(y). \end{aligned} \tag{5.2.2}$$

Accordingly, as we explained in Chapter 4, if the target point $x = x^m \in \partial K_m$, $m \geq 0$, is in the m-th illuminated region off the $\mathcal{O}(k^{-1/3})$ shadow boundary, then equations (5.2.1) and (5.2.2) reduce to

$$\rho_0(x^0)(1+\mathcal{O}(k^{-1})) = 2ik\alpha\cdot\nu(x^0),$$

and, for $m \geq 1$,

$$\rho_m(x^m)(1+\mathcal{O}(k^{-1})) = -\frac{1}{2\pi}e^{-ik\varphi_m(x^m)} \int_{\partial K_{m-1}(x^{m-1})} e^{ik(\varphi_{m-1}(y)+|x^m-y|)}\frac{ik}{|x^m-y|}\frac{x^m-y}{|x^m-y|}\cdot\nu(x^m)\rho_{m-1}(y)dS(y),$$

where, for $m \geq 1$, the neighborhood $\partial K_{m-1}(x^{m-1})$ of the stationary point x^{m-1} is chosen so that, except for x^{m-1}, it contains no critical points of the integration kernel.

On the other hand, for a target point $x = x_s^m \in \partial K_m$, $m \geq 0$, in the m-th shadow region off the $\mathcal{O}(k^{-1/3})$ shadow boundary, in addition to the stationary point $x^{m-1} \in \partial K_{m-1}$ of the RHS integral, the LHS integral possesses a stationary point $x^m \in \partial K_m$ that belongs to the m-th illuminated region. Consequently, for the target point x_s^m, equations (5.2.1) and (5.2.2) reduce to

$$\rho_0(x_s^0) + \frac{1}{2\pi}e^{-ik\alpha\cdot x_s^0}\int_{\partial K_0(x^0)} e^{ik(\alpha\cdot y+|x_s^0-y|)}\frac{ik|x_s^0-y|}{|x_s^0-y|^2}\frac{x_s^0-y}{|x_s^0-y|}\cdot\nu(x_s^0)\rho_0(y)dS(y) \sim 2ik\alpha\cdot\nu(x_s^0),$$

and, for $m \geq 1$,

$$\rho_m(x_s^m) + \frac{1}{2\pi}e^{-ik\varphi_m(x_s^m)}\int_{\partial K_m(x^m)} e^{ik(\varphi_m(y)+|x_s^m-y|)}\frac{ik}{|x_s^m-y|}\frac{x_s^m-y}{|x_s^m-y|}\cdot\nu(x_s^m)\rho_m(y)dS(y)$$
$$\sim -\frac{1}{2\pi}e^{-ik\varphi_m(x_s^m)}\int_{\partial K_{m-1}(x^{m-1})} e^{ik(\varphi_{m-1}(y)+|x_s^m-y|)}\frac{ik}{|x_s^m-y|}\frac{x_s^m-y}{|x_s^m-y|}\cdot\nu(x_s^m)\rho_{m-1}(y)dS(y).$$

where, as with $\partial K_{m-1}(x^{m-1})$, the neighborhood $\partial K_m(x^m)$ is chosen so that it contains no critical points of the kernel of the LHS integral other than x^m.

We derive the asymptotic expansions of these integrals utilizing the method of stationary phase and appealing to Theorem 5.1.3. More precisely, in evaluating the RHS integrals, equations (5.1.10) and (5.1.12) must be used. On the other hand, LHS integrals must be evaluated using equations (5.1.11) and (5.1.13). To exemplify this procedure, let us consider the evaluation of the RHS integral for a target point $x^m \in \partial K_m$, $m \geq 1$. Then, writing this integral in parametric form, and applying the method of stationary phase yields

$$\begin{aligned} \frac{1}{2\pi} \int_{\partial K_{m-1}(x^{m-1})} & e^{ik(\varphi_{m-1}(y)+|x^m-y|)} \frac{ik}{|x^m-y|} \frac{x^m-y}{|x^m-y|} \cdot \nu(x^m) \rho_{m-1}(y) |y_u \times y_v| du dv \\ & \sim \frac{i}{k} \frac{e^{ik\varphi_m(x^m)}}{\sqrt{|\det \mathrm{Hess}\,[\varphi_{t_m,\tau_m}(t_{m-1},\tau_{m-1})]\,|}} \\ & \qquad \frac{ik}{|x^m-x^{m-1}|} \frac{x^m-x^{m-1}}{|x^m-x^{m-1}|} \cdot \nu(x^m) |x^{m-1}_{t_{m-1}} \times x^{m-1}_{\tau_{m-1}}| \rho_{m-1}(x^{m-1}). \end{aligned}$$

Therefore, choosing the directions t_{m-1} and τ_{m-1} to be the principal directions at the point x^{m-1} gives

$$\begin{aligned} \frac{1}{2\pi} \int_{\partial K_{m-1}(x^{m-1})} & e^{ik(\varphi_{m-1}(y)+|x^m-y|)} \frac{ik}{|x^m-y|} \frac{x^m-y}{|x^m-y|} \cdot \nu(x^m) \rho_{m-1}(y) |y_u \times y_v| du dv \\ & \sim - \frac{e^{ik\varphi_m(x^m)}}{\sqrt{|\det \mathrm{Hess}\,[\varphi_{t_m,\tau_m}(t_{m-1},\tau_{m-1})]\,|}} \\ & \qquad \frac{1}{|x^m-x^{m-1}|} \frac{x^m-x^{m-1}}{|x^m-x^{m-1}|} \cdot \nu(x^m) |x^{m-1}_{t_{m-1}}||x^{m-1}_{\tau_{m-1}}| \rho_{m-1}(x^{m-1}) \\ & = - \frac{e^{ik\varphi_m(x^m)}}{\sqrt{|\det \mathbb{H}_m|}} \frac{x^m-x^{m-1}}{|x^m-x^{m-1}|} \cdot \nu(x^m) \rho_{m-1}(x^{m-1}). \end{aligned}$$

The LHS integrals corresponding to target points at the shadow regions are evaluated in a similar manner. As we did in §4.3, it can then be verified that the currents vanish to first order in wavelength in the shadow regions.

Chapter 6

Convergence of Multiple Scattering Iterations in HF-IEM

As is apparent from the asymptotic expansions developed in Chapters 4 and 5, in the high-frequency regime, the convergence of the Neumann series (3.2.5) depends solely on the geometrical characteristics of the scatterers. Moreover, appealing to Theorems 4.0.1 and 5.0.1, one can easily find sufficient conditions, in terms of the distances between scatterers and curvatures of the objects, guaranteeing the convergence of the series. The natural question that arises is whether one can find a condition that is both necessary and sufficient for convergence. In this Chapter, we consider this question in the setting of Chapters 4 and 5. That is, we consider a finite collection of convex obstacles satisfying the visibility condition.

In this regard, we establish that, when a collection of obstacles are transversed periodically, the ratios of the (asymptotic expansions of) multiple scattering iterations that differ by one period converge uniformly to a certain complex number. This number is independent of incidence, and in the limit of infinite frequency it depends solely on the geometrical arrangement.

To derive these results, our strategy begins with the use of Theorems 4.0.1 and 5.0.1 to deduce that if a ray arrives at a point on the boundary of a scatterer after n-

bounces, then (asymptotically) the iterated current at that point equals the current at the (n - 1)-th reflection-point of the ray times a continued fraction (of 2×2 matrices in three-dimensional case) determined by geometric properties of the corresponding ray path. Then we analyze optical ray paths to deduce that if a group of rays transverse the objects periodically for a large number of reflections, then -except for the first and last few reflections- their reflection points accumulate on certain specific regions of the boundaries of the scatterers. Finally, we demonstrate that, when a p-periodic orbit is transversed indefinitely, the ratio of iterated currents differing by one period converges uniformly to the product of a number p of limit p-periodic continued fractions; the convergence rate is then deduced utilizing the theory of limit p-periodic continued fractions [44].

6.1 Rate of Convergence on Periodic Orbits

To clarify the intuition behind these ideas, let us consider a p-periodic orbit $\{K_m\}_{m\geq 0}$; that is, $K_i = K_{i+qp}$ for $i = 1, \ldots, p$ and all $q \geq 0$. As is apparent from Figures 3.5 and 3.8, the paths of the reflected rays start to stabilize after a few reflections for a periodic orbit ($p = 2$ in these figures). As we shall explain shortly, this is an immediate consequence of Fermat's principle which states that "The actual path between two points taken by a beam of light is the one which is transversed in the least time". Indeed, considering the phase function

$$\varphi(x_1, \ldots, x_p) = |x_p - x_1| + \sum_{m=1}^{p-1} |x_{m+1} - x_m| \tag{6.1.1}$$

defined for $(x_1, \ldots, x_p) \in \partial K = \partial K_1 \times \ldots \times \partial K_p$, we have:

Lemma 6.1.1 *The tuple* $(a_1, \ldots, a_p) \in \partial K_1 \times \ldots \times \partial K_p$ minimizing *the phase (6.1.1)* *is uniquely determined, and it satisfies*

$$\frac{a_{i+1} - a_i}{|a_{i+1} - a_i|} = \frac{a_i - a_{i-1}}{|a_i - a_{i-1}|} - 2\left(\frac{a_i - a_{i-1}}{|a_i - a_{i-1}|} \cdot \nu_i\right)\nu_i \ , \qquad i = 1, \ldots, p.$$

That is, a ray starting from a_i and arriving at a_{i+1} traverses the path formed by the points $(a_1, \ldots, a_p)$ indefinitely.

Proof. Suppose that the boundaries ∂K_i are parametrized by $x_i = x_i(t_i)$. Then

$$\frac{d\varphi}{dt_i} = \frac{d}{dt_i}\left(|x_{i+1} - x_i| + |x_i - x_{i-1}|\right) = \left(\frac{x_i - x_{i-1}}{|x_i - x_{i-1}|} - \frac{x_{i+1} - x_i}{|x_{i+1} - x_i|}\right) \cdot \dot{x}_i$$

so that $d\varphi/dt_i = 0$ if and only if

$$\frac{x_{i+1} - x_i}{|x_{i+1} - x_i|} = \frac{x_i - x_{i-1}}{|x_i - x_{i-1}|} \qquad \text{or} \qquad \frac{x_{i+1} - x_i}{|x_{i+1} - x_i|} = \lambda_i \nu_i + \frac{x_i - x_{i-1}}{|x_i - x_{i-1}|}$$

for some λ_i. The first case is not possible by the visibility assumption. In the second case,

$$1 = \frac{x_{i+1} - x_i}{|x_{i+1} - x_i|} \cdot \frac{x_{i+1} - x_i}{|x_{i+1} - x_i|} = \lambda_i^2 + 2\left(\frac{x_i - x_{i-1}}{|x_i - x_{i-1}|} \cdot \nu_i\right)\lambda_i + 1$$

so that

$$\lambda_i = -2\frac{x_i - x_{i-1}}{|x_i - x_{i-1}|} \cdot \nu_i \qquad \text{or} \qquad \lambda_i = 0 \ .$$

The visibility assumption prevents the case $\lambda_i = 0$. The proof in three-dimensions follows the same lines. ■

Intuitively then, this result combined with Fermat's principle tells us that, as the number of reflections m grows, the paths of the rays arriving at any point $x \in \partial K$ at the m-th reflection have the property that (except for the first and last few reflections) they are *almost* identical with $(a_1, \ldots, a_p)$; and to a good approximation, the only difference between the optical path arriving at a point $x \in \partial K$ at the m-th reflection and $(m+p)$-th reflection is the addition of the path formed by the points $(a_1, \ldots, a_p)$ somewhere in the sequence of points.

Now, for $x_m \in \partial K_m$, let $(x_0, \ldots, x_{m-1}) \in \partial K_0 \times \ldots \times \partial K_{m-1}$ be the uniquely determined tuple on the optical ray path arriving at $x = x_m$ after $m-1$ reflections. Concentrating, for instance, on a two-dimensional setting, we see that

$$\eta_m(x_m) \sim 2ik(-1)^m \frac{x_m - x_{m-1}}{|x_m - x_{m-1}|} \cdot \nu_m e^{ik\varphi_m(x_m)} \left(\prod_{i=0}^{m-1} R_i^m(x_m) \right)^{-1/2}, \quad m \geq 1$$

on account of Theorem 4.0.1. Here, we set

$$\begin{aligned} R_0^m(x_m) &= 1 + \frac{2\kappa_0 |x_1 - x_0|}{\cos\alpha_0} \\ R_i^m(x_m) &= 1 + \frac{2\kappa_i |x_{i+1} - x_i|}{\cos\alpha_i} + \frac{|x_{i+1} - x_i|}{|x_i - x_{i-1}|} \left(1 - \frac{1}{R_{i-1}^m(x_m)} \right), \quad 1 \leq i \leq m-1 \end{aligned}$$

where

$$\alpha_i := cos^{-1} \left(\frac{x_{i+1} - x_i}{|x_{i+1} - x_i|} \cdot \nu_i \right).$$

Therefore, appealing to the explanations above, for a fixed j with $1 \leq j \leq p$ (assuming without loss of generality that j is the smallest index such that $K_j = K_m$ for some obstacle in the p-periodic orbit $\{K_m\}_{m \geq 0}$), and for a fixed point $x \in \partial K_j$, we obtain

$$\frac{\eta_{m+p}(x)}{\eta_m(x)} \sim (-1)^p e^{ik\varphi(a_1,\ldots,a_p)} \left(\prod_{i=0}^{m+p-1} R_i^{m+p}(x) \right)^{-1/2} \left(\prod_{i=0}^{m-1} R_i^m(x) \right)^{1/2} \tag{6.1.2}$$

as $m = j + qp$ grows. Accordingly, it is necessary to study the convergence of the ratio $\prod_{i=0}^{m+p-1} R_i^{m+p}(x) / \prod_{i=0}^{m-1} R_i^m(x)$ as $m \to \infty$. To this end, we choose n with $n \approx m/2$, write it as

$$\begin{aligned} \frac{\prod_{i=0}^{m+p-1} R_i^{m+p}(x)}{\prod_{i=0}^{m-1} R_i^m(x)} = &\left(1 + \left(\prod_{i=0}^{n} \frac{R_i^{m+p}(x)}{R_i^m(x)} - 1 \right) \right) \\ &\left(1 + \left(\prod_{i=n+1}^{m-1} \frac{R_{i+p}^{m+p}(x)}{R_i^m(x)} - 1 \right) \right) \prod_{i=n+1}^{n+p} R_i^{m+p}(x) . \end{aligned}$$

Thus, we need to study the convergence properties of the quantities

$$\prod_{i=0}^{n} \frac{R_i^{m+p}(x)}{R_i^m(x)} - 1, \quad \prod_{i=n+1}^{m-1} \frac{R_{i+p}^{m+p}(x)}{R_i^m(x)} - 1, \text{ and } \prod_{i=n+1}^{n+p} R_i^{m+p}(x) \tag{6.1.3}$$

as $m = j + qp$ goes to infinity. Indeed, when the sets of points $x_0^m, \ldots, x_m^m$ (with $x = x_m^m$ and $m = j + qp$) forming the continued fractions $R_i^m(x)$ are considered, it holds that each of the sequences $x_i^j, x_{i+p}^{j+p}, x_{i+2p}^{j+2p}, \ldots$ converge. Moreover, since $n \approx m/2$, the points forming the continued fractions in the third term of (6.1.3) form p sequences converging to the points $a_1, \ldots, a_p$. Accordingly, the analysis of the quantities in (6.1.3) can be based on an extension of the theory of limit periodic p-periodic continued fractions.

As is to be expected then, an analysis of the optical ray paths combined with the techniques of the theory of limit p-periodic continued fractions can be used to show that the first and second terms in (6.1.3) do converge to zero uniformly for $x \in \partial K$. In the same way, the product of the p (almost) limit p-periodic continued fractions forming the third term in (6.1.3) can be shown to converge to a limit s. Note that, however, the behavior of this third term is independent of the direction of the incidence and of the point $x \in \partial K$. Consequently, the limit s is uniform and is independent of the direction of incidence. In fact, as we shall explain shortly, s depends only and explicitly on the distances $|a_{i+1} - a_i|$, the curvatures κ_i at the points a_i of the surfaces ∂K_i and the scalar products $\frac{a_{i+1}-a_i}{|a_{i+1}-a_i|} \cdot \nu_i$ $(i = 1, \ldots, p)$ where $(a_1, \ldots, a_p) \in \partial K_1 \times \ldots \times \partial K_p$ are the unique points minimizing the phase (6.1.1). Indeed, dropping the upper indices in the representations of R_i^m, and concentrating on the set of points $x_0, \ldots, x_n$ where $n \approx m/2$, we see that the sequences $\{x_{i+qp}\}_{q \geq 0}$ converge to the points a_i, $i = 1, \ldots, p$. Therefore, replacing x_i's with their limiting values yields the p equations

$$L_i = d_i - \frac{c_i}{L_{i-1}}, \quad 1 \leq i \leq p \tag{6.1.4}$$

where we have set, for $1 \le i \le p$,

$$L_i = \lim_{m\to\infty} R^m_{n+i}, \quad b_i = 1 + \frac{2\kappa_i|a_{i+1} - a_i|}{\cos\alpha_i}, \quad c_i = \frac{|a_{i+1} - a_i|}{|a_i - a_{i-1}|}, \quad \text{and} \quad d_i = b_i + c_i.$$

Equivalently, equations (6.1.4) can be written, for $i = 1, \ldots, p$, as

$$L_i = L_{i+p} = d_{i+p} - \cfrac{c_{i+p}}{d_{i+p-1} - \cfrac{c_{i+p-1}}{\ddots \; \overline{\qquad\qquad} \atop d_{i+1} - \cfrac{c_{i+1}}{L_i}}} \tag{6.1.5}$$

and equations (6.1.5), in turn, can be used to obtain quadratic equations in L_i, $i = 1, \ldots, p$.

Using the fact that each of the terms R_i satisfy $R_i > 1$, it can be easily shown that $L_i \ge 1$ for $i = 1, \ldots, p$, and that this is possible only if L_i's are taken to be the larger roots of the corresponding quadratic equations.

For instance, when the period is $p = 2$, solutions of these quadratic equations yield

$$L_1 = (1 + d\kappa_1)\left[1 \pm \sqrt{1 - \frac{1}{(1 + d\kappa_1)(1 + d\kappa_2)}}\,\right]$$

and

$$L_2 = (1 + d\kappa_2)\left[1 \pm \sqrt{1 - \frac{1}{(1 + d\kappa_1)(1 + d\kappa_2)}}\,\right].$$

When the signs in these formulas are taken to be negative, the conditions $L_i \ge 1$ are easily seen to imply

$$(1 + d\kappa_1)^{-1} + (1 + d\kappa_2)^{-1} \ge 2$$

which is not possible due to the convexity assumption. It follows that, for $p = 2$,

$$s = \prod_{i=1}^{p} L_i = \left(\sqrt{\gamma} + \sqrt{\gamma - 1}\right)^2 \tag{6.1.6}$$

where $\gamma = (1 + d\kappa_1)(1 + d\kappa_2)$.

Using the asymptotic expansions given in Theorem 5.0.1, which is the three-dimensional analog of Theorem 4.0.1, convergence factors similar to (6.1.6) can be derived for any periodic orbit in three-dimensions. As is to be expected, the formulas for these convergence factors are significantly complicated. Even for a 2-periodic orbit, they depend on the angle of rotation between the axes determined by principal directions at the points a_i minimizing the distance between the two obstacles. Nevertheless, for a two-periodic orbit, when these axes are parallel to each other, the convergence factor takes on the relatively simple form

$$s = \left(\sqrt{\gamma_1} + \sqrt{\gamma_1 - 1}\right)^2 \left(\sqrt{\gamma_2} + \sqrt{\gamma_2 - 1}\right)^2$$

where $\gamma_i = (1 + d\kappa_i^1)(1 + d\kappa_i^2)$, κ_i^1 and κ_i^2 are the principal curvatures at the points a_i, and $d = |a_1 - a_2|$.

6.2 Analysis of Products of Continued Fractions

The starting point in the analysis of the first and second quantities in (6.1.3) is the next recursion.

Lemma 6.2.1 *For $m \geq 1$, we have:*

$$\begin{aligned} A_0^m \cdots A_m^m &= A_0^m \cdots A_{m-1}^m \\ &\quad + |x_{m+1} - x_m| \left(\frac{2\kappa_m}{\cos\alpha_m} A_0^m \cdots A_{m-1}^m + \cdots + \frac{2\kappa_1}{\cos\alpha_1} A_0^m + \frac{2\kappa_0}{\cos\alpha_0} \right). \end{aligned}$$

Proof. For $m \geq 0$, let

$$d_m = |x_{m+1} - x_m|, \quad \gamma_m = \frac{2\kappa_m}{\cos\alpha_m}, \quad \beta_m = \frac{2\kappa_m |x_{m+1} - x_m|}{\cos\alpha_m} = \gamma_m d_m,$$

and, for $m \geq 1$, let

$$r_m = \frac{|x_{m+1} - x_m|}{|x_m - x_{m-1}|} = \frac{d_m}{d_{m-1}}.$$

With this notation, we have

$$\begin{aligned} A_0 &= 1 + \gamma_0 d_0 = 1 + \beta_0 \\ A_m &= 1 + \gamma_m d_m + r_m \left(1 - \frac{1}{A_{m-1}}\right) = 1 + \beta_m + r_m \left(1 - \frac{1}{A_{m-1}}\right), \quad m \geq 1. \end{aligned}$$

Now, a direct calculation yields

$$\begin{aligned} A_0 A_1 &= (1 + \beta_1) A_0 + \beta_0 r_1 = A_0 + \beta_1 A_0 + \beta_0 r_1 = A_0 + \gamma_1 d_1 A_0 + \gamma_0 d_0 r_1 \\ &= A_0 + \gamma_1 d_1 A_0 + \gamma_0 d_1 = A_0 + d_1 (\gamma_1 A_0 + \gamma_0). \end{aligned}$$

Then, by induction,

$$\begin{aligned} &A_0 \cdots A_{m+1} \\ &\quad = \left(1 + \beta_{m+1} + r_{m+1}\left(1 - \frac{1}{A_m}\right)\right) A_0 \cdots A_m \\ &\quad = A_0 \cdots A_m + \beta_{m+1} A_0 \cdots A_m + r_{m+1} (A_m - 1) A_0 \cdots A_{m-1} \\ &\quad = A_0 \cdots A_m + (\beta_{m+1} + r_{m+1}) A_0 \cdots A_m - r_{m+1} A_0 \cdots A_{m-1} \\ &\quad = A_0 \cdots A_m + \left(\gamma_{m+1} d_{m+1} + \frac{d_{m+1}}{d_m}\right) A_0 \cdots A_m - \frac{d_{m+1}}{d_m} A_0 \cdots A_{m-1} \\ &\quad = A_0 \cdots A_m + \gamma_{m+1} d_{m+1} A_0 \cdots A_m + \frac{d_{m+1}}{d_m} (A_0 \cdots A_m - A_0 \cdots A_{m-1}) \\ &\quad = A_0 \cdots A_m + \gamma_{m+1} d_{m+1} A_0 \cdots A_m + \frac{d_{m+1}}{d_m} d_m (\gamma_m A_0 \cdots A_{m-1} + \cdots + \gamma_1 A_0 + \gamma_0) \\ &\quad = A_0 \cdots A_m + d_{m+1} (\gamma_{m+1} A_0 \cdots A_m + \gamma_m A_0 \cdots A_{m-1} + \cdots + \gamma_1 A_0 + \gamma_0) \end{aligned}$$

finishing the proof. ■

Now, fix a point $x \in \partial K$, and denote by x_i and $\widetilde{x}_i$ the points in the respective optical paths used to define

$$A_i = A_i^{m+p}(x) \qquad \text{and} \qquad B_i = A_i^{m}(x)$$

respectively, and utilize the notation

$$\alpha_i := \cos^{-1}\left(\frac{x_{i+1}-x_i}{|x_{i+1}-x_i|}\cdot \nu_i\right), \quad \widetilde{\alpha}_i := \cos^{-1}\left(\frac{\widetilde{x}_{i+1}-\widetilde{x}_i}{|\widetilde{x}_{i+1}-\widetilde{x}_i|}\cdot \widetilde{\nu}_i\right), \quad \theta_i - \widetilde{\theta}_i := \cos^{-1}\left(\nu_i \cdot \widetilde{\nu}_i\right)$$

where ν_i and $\widetilde{\nu}_i$ denote the outward unit normal to $\partial\Omega$ at the points x_i and $\widetilde{x}_i$ respectively. Note that then

$$\begin{aligned} A_0\cdots A_n - B_0\cdots B_n &= A_0\cdots A_{n-1} - B_0\cdots B_{n-1} \\ &+ 2|x_{n+1}-x_n|\left(\frac{\kappa_n}{\cos\alpha_n}A_0\cdots A_{n-1} - \frac{\widetilde{\kappa}_n}{\cos\widetilde{\alpha}_n}B_0\cdots B_{n-1} + \right. \\ &\qquad\qquad \left. \cdots + \frac{\kappa_1}{\cos\alpha_1}A_0 - \frac{\widetilde{\kappa}_1}{\cos\widetilde{\alpha}_1}B_0 + \frac{\kappa_0}{\cos\alpha_0} - \frac{\widetilde{\kappa}_0}{\cos\widetilde{\alpha}_0}\right) \\ &+ \left(|x_{n+1}-x_n| - |\widetilde{x}_{n+1}-\widetilde{x}_n|\right)\left(\frac{2\widetilde{\kappa}_n}{\cos\widetilde{\alpha}_n}B_0\cdots B_{n-1} + \cdots + \frac{2\widetilde{\kappa}_1}{\cos\widetilde{\alpha}_1}B_0 + \frac{2\widetilde{\kappa}_0}{\cos\widetilde{\alpha}_0}\right) \ , \end{aligned}$$

and this yields

$$\begin{aligned} A_0\cdots A_n - B_0\cdots B_n &= A_0\cdots A_{n-1} - B_0\cdots B_{n-1} \\ &+ 2|x_{n+1}-x_n|\left(\frac{\kappa_n}{\cos\alpha_n}(A_0\cdots A_{n-1} - B_0\cdots B_{n-1}) + \cdots + \frac{\kappa_1}{\cos\alpha_1}(A_0 - B_0)\right) \\ &+ 2|x_{n+1}-x_n|\left(\left(\frac{\kappa_n}{\cos\alpha_n} - \frac{\widetilde{\kappa}_n}{\cos\widetilde{\alpha}_n}\right)B_0\cdots B_{n-1} + \right. \\ &\qquad\qquad \left. \cdots + \left(\frac{\kappa_1}{\cos\alpha_1} - \frac{\widetilde{\kappa}_1}{\cos\widetilde{\alpha}_1}\right)B_0 + \left(\frac{\kappa_0}{\cos\alpha_0} - \frac{\widetilde{\kappa}_0}{\cos\widetilde{\alpha}_0}\right)\right) \\ &+ \left(|x_{n+1}-x_n| - |\widetilde{x}_{n+1}-\widetilde{x}_n|\right)\left(\frac{2\widetilde{\kappa}_n}{\cos\widetilde{\alpha}_n}B_0\cdots B_{n-1} + \cdots + \frac{2\widetilde{\kappa}_1}{\cos\widetilde{\alpha}_1}B_0 + \frac{2\widetilde{\kappa}_0}{\cos\widetilde{\alpha}_0}\right), \end{aligned}$$

or equivalently

$$
\begin{aligned}
A_0 \cdots A_n - B_0 \cdots B_n = {} & A_0 \cdots A_{n-1} - B_0 \cdots B_{n-1} \\
& + 2|x_{n+1} - x_n| \left(\frac{\kappa_n}{\cos \alpha_n} (A_0 \cdots A_{n-1} - B_0 \cdots B_{n-1}) + \cdots + \frac{\kappa_1}{\cos \alpha_1} (A_0 - B_0) \right) \\
& + 2|x_{n+1} - x_n| \left(\kappa_n \frac{\cos \widetilde{\alpha}_n - \cos \alpha_n}{\cos \widetilde{\alpha}_n \cos \alpha_n} B_0 \cdots B_{n-1} + \right. \\
& \qquad \left. \cdots + \kappa_1 \frac{\cos \widetilde{\alpha}_1 - \cos \alpha_1}{\cos \widetilde{\alpha}_1 \cos \alpha_1} B_0 + \kappa_0 \frac{\cos \widetilde{\alpha}_0 - \cos \alpha_0}{\cos \widetilde{\alpha}_0 \cos \alpha_0} \right) \\
& + 2|x_{n+1} - x_n| \left(\frac{\kappa_n - \widetilde{\kappa}_n}{\cos \widetilde{\alpha}_n} B_0 \cdots B_{n-1} + \cdots + \frac{\kappa_1 - \widetilde{\kappa}_1}{\cos \widetilde{\alpha}_1} B_0 + \frac{\kappa_0 - \widetilde{\kappa}_0}{\cos \widetilde{\alpha}_0} \right) \\
& + \left(|x_{n+1} - x_n| - |\widetilde{x}_{n+1} - \widetilde{x}_n| \right) \left(\frac{2\widetilde{\kappa}_n}{\cos \widetilde{\alpha}_n} B_0 \cdots B_{n-1} + \cdots + \frac{2\widetilde{\kappa}_1}{\cos \widetilde{\alpha}_1} B_0 + \frac{2\widetilde{\kappa}_0}{\cos \widetilde{\alpha}_0} \right).
\end{aligned}
$$

Therefore, in this last identity, utilizing the approximations

$$
\begin{aligned}
\frac{\cos \widetilde{\alpha}_i - \cos \alpha_i}{\cos \alpha_i} &= (\alpha_i - \widetilde{\alpha}_i) \tan \alpha_i + \mathcal{O}(\alpha_i - \widetilde{\alpha}_i)^2, \\
\widetilde{\kappa}_i - \kappa_i &= \left(\widetilde{\theta}_i - \theta_i \right) \kappa_i' + \mathcal{O} \left(\widetilde{\theta}_i - \theta_i \right)^2,
\end{aligned}
$$

and appealing to Lemma 6.2.1 yields

$$
\begin{aligned}
A_0 \cdots A_n - B_0 \cdots B_n \sim {} & A_0 \cdots A_{n-1} - B_0 \cdots B_{n-1} \\
& + 2|x_{n+1} - x_n| \left(\frac{\kappa_n}{\cos \alpha_n} (A_0 \cdots A_{n-1} - B_0 \cdots B_{n-1}) + \cdots + \frac{\kappa_1}{\cos \alpha_1} (A_0 - B_0) \right) \\
& + 2|x_{n+1} - x_n| \left(\frac{\kappa_n \tan \alpha_n}{\cos \widetilde{\alpha}_n} (\alpha_n - \widetilde{\alpha}_n) B_0 \cdots B_{n-1} + \right. \\
& \qquad \left. \cdots + \frac{\kappa_1 \tan \alpha_1}{\cos \widetilde{\alpha}_1} (\alpha_1 - \widetilde{\alpha}_1) B_0 + \frac{\kappa_0 \tan \alpha_0}{\cos \widetilde{\alpha}_0} (\alpha_0 - \widetilde{\alpha}_0) \right) \\
& + 2|x_{n+1} - x_n| \left(\frac{\kappa_n'}{\cos \widetilde{\alpha}_n} \left(\theta_n - \widetilde{\theta}_n \right) B_0 \cdots B_{n-1} + \right. \\
& \qquad \left. \cdots + \frac{\kappa_1'}{\cos \widetilde{\alpha}_1} \left(\theta_1 - \widetilde{\theta}_1 \right) B_0 + \frac{\kappa_0'}{\cos \widetilde{\alpha}_0} \left(\theta_0 - \widetilde{\theta}_0 \right) \right) \\
& + \frac{|x_{n+1} - x_n| - |\widetilde{x}_{n+1} - \widetilde{x}_n|}{|\widetilde{x}_{n+1} - \widetilde{x}_n|} \left(B_0 \cdots B_n - B_0 \cdots B_{n-1} \right).
\end{aligned}
$$

Dividing through by $B_0 \cdots B_n$ gives :

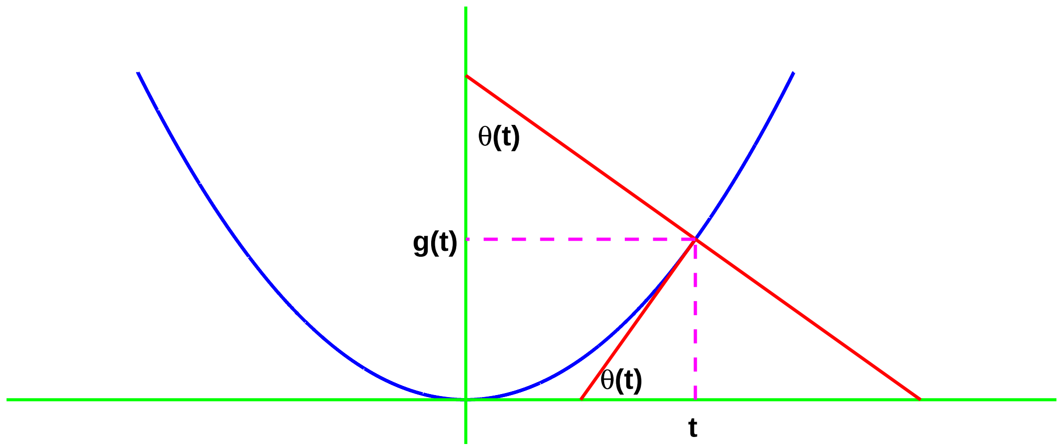

Figure 6.1: Local parametrization of a convex curve.

Lemma 6.2.2 *We have*

$$
\begin{aligned}
\frac{A_0\cdots A_n}{B_0\cdots B_n}-1 &\sim \frac{1}{B_n}\left(\frac{A_0\cdots A_{n-1}}{B_0\cdots B_{n-1}}-1\right)\\
&+\frac{2|x_{n+1}-x_n|}{B_n}\left(\frac{\kappa_n}{\cos\alpha_n}\left(\frac{A_0\cdots A_{n-1}}{B_0\cdots B_{n-1}}-1\right)+\cdots+\frac{\kappa_1}{\cos\alpha_1}\frac{1}{B_1\cdots B_{n-1}}(\frac{A_0}{B_0}-1)\right)\\
&+\frac{2|x_{n+1}-x_n|}{B_n}\left(\frac{\kappa_n\tan\alpha_n}{\cos\widetilde{\alpha}_n}(\alpha_n-\widetilde{\alpha}_n)+\cdots+\frac{1}{B_0\cdots B_{n-1}}\frac{\kappa_0\tan\alpha_0}{\cos\widetilde{\alpha}_0}(\alpha_0-\widetilde{\alpha}_0)\right)\\
&+\frac{2|x_{n+1}-x_n|}{B_n}\left(\frac{\kappa_n'}{\cos\widetilde{\alpha}_n}\left(\theta_n-\widetilde{\theta}_n\right)+\cdots+\frac{1}{B_0\cdots B_{n-1}}\frac{\kappa_0'}{\cos\widetilde{\alpha}_0}\left(\theta_0-\widetilde{\theta}_0\right)\right)\\
&+\frac{|x_{n+1}-x_n|-|\widetilde{x}_{n+1}-\widetilde{x}_n|}{|\widetilde{x}_{n+1}-\widetilde{x}_n|}\left(1-\frac{1}{B_n}\right).
\end{aligned}
$$

Therefore, one needs to find relations among the angles α_n, $\widetilde{\alpha}_n$, θ_n and $\widetilde{\theta}_n$. We do this analysis next.

6.3 Analysis of Reflected Rays

For simplicity of presentation, we shall concentrate on the case $p = 2$, however, the techniques and approximations we shall present can be easily carried over to calculations for larger periods. We begin with a simple lemma concerning local parametrizations of a convex curve.

Lemma 6.3.1 *In Figure 6.1, if g is convex near $t = 0$, then as $t \to 0$*

$$t = \frac{\theta(t)}{\kappa(0)} + \mathcal{O}(\theta(t))^2 \quad \textit{and} \quad g(t) = \mathcal{O}(\theta(t))^2.$$

Proof. Noting that $g(0) = g'(0) = 0$, for a convex object, we have

$$\kappa(0) = \left. \frac{g''(t)}{(1 + g'(t)^2)^{3/2}} \right|_{t=0} = g''(0).$$

Therefore,

$$\theta(t) = \arctan g'(t) = tg''(0) + \mathcal{O}(t^2) = \kappa(0)t + \mathcal{O}(t^2)$$

so that

$$t = \frac{\theta(t)}{\kappa(0)} + \mathcal{O}(\theta(t))^2.$$

That $g(t) = \mathcal{O}(\theta(t))^2$ is immediate from this and the Taylor expansion of g. ■

We shall concentrate on the rays moving towards the line determined by a_1 and a_2 (see Figure 6.2); analysis for rays moving away from this line is very similar. The next lemma will be used without any further reference in what follows.

Lemma 6.3.2 *In Figure 6.2, the following identities hold:*

$$\alpha_i = \alpha_{i+1} + \theta_{i+1} + \theta_i \ , \qquad \textit{for} \ \ i \geq 0, \tag{6.3.1a}$$

$$\alpha_i = \alpha_0 - \theta_0 - 2\sum_{j=1}^{i-1} \theta_j - \theta_i \ , \qquad \textit{for} \ \ i \geq 1, \tag{6.3.1b}$$

and

$$\alpha_0 - \widetilde{\alpha}_0 = \widetilde{\theta}_0 - \theta_0 \ ,$$

$$\alpha_i - \widetilde{\alpha}_i = 2\sum_{j=0}^{i-1} \left(\widetilde{\theta}_j - \theta_j\right) + \left(\widetilde{\theta}_i - \theta_i\right) \ , \qquad \textit{for} \ \ i \geq 1.$$

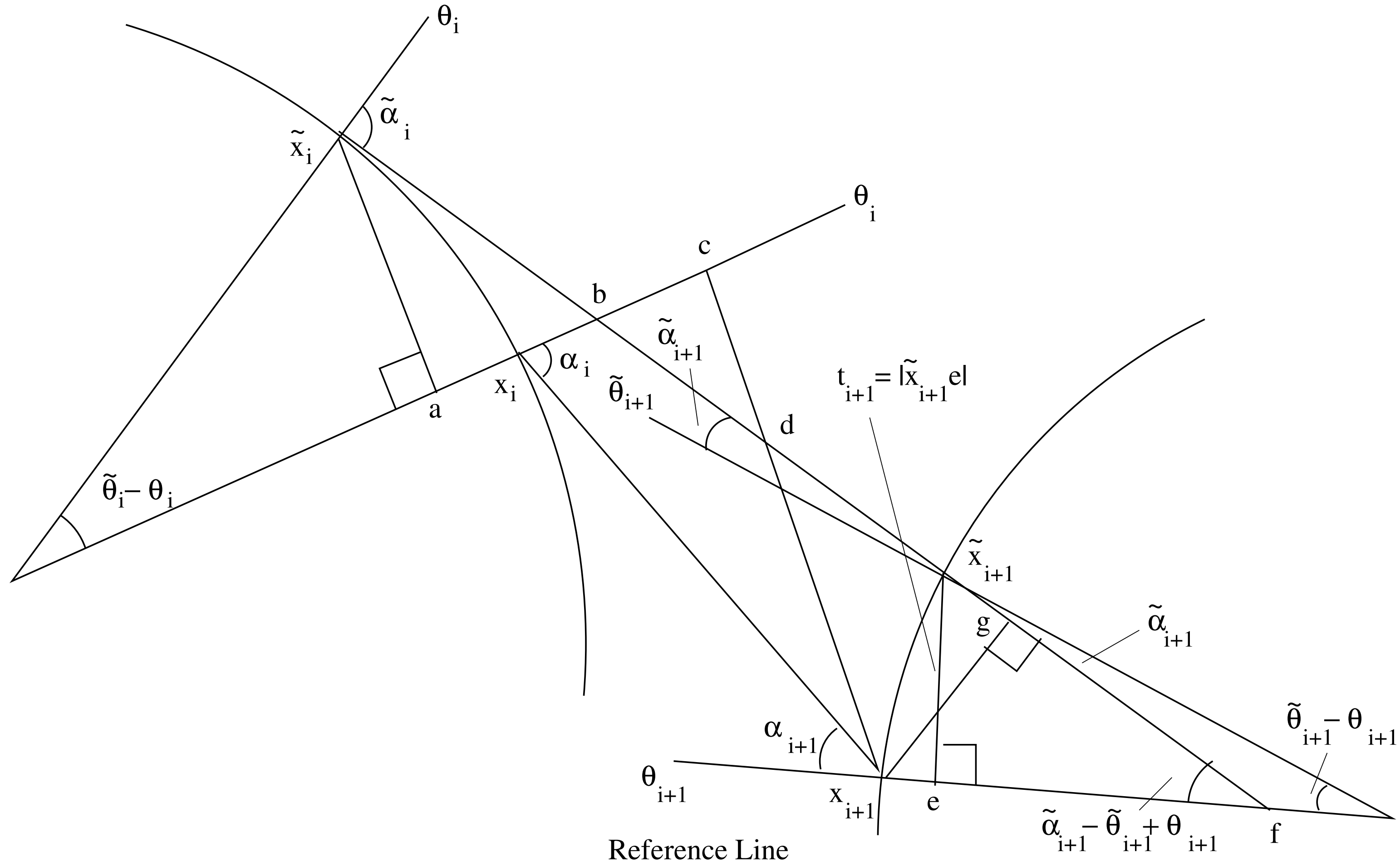

Figure 6.2: Rays moving towards the reference line.

Proof. Equation (6.3.1a) is just a simple geometrical identity concerning triangles. Adding these up yields (6.3.1b). Utilizing the second identity, we obtain

$$\alpha_i - \widetilde{\alpha}_i = (\alpha_0 - \widetilde{\alpha}_0) + \left(\widetilde{\theta}_0 - \theta_0\right) + 2\sum_{j=1}^{i-1}\left(\widetilde{\theta}_j - \theta_j\right) + \left(\widetilde{\theta}_i - \theta_i\right) \ , \qquad i \geq 1.$$

That $\alpha_0 - \widetilde{\alpha}_0 = \widetilde{\theta}_0 - \theta_0$ is an immediate consequence of the fact that the incoming field is a plane wave. ■

Lemma 6.3.3 *In Figure 6.2, the following identity holds :*

$$\begin{aligned}\{|x_{i+1} - x_i| \sin\alpha_i + t_i\} \cos(\widetilde{\alpha}_i + \theta_i - \widetilde{\theta}_i) - \{|x_{i+1} - x_i| \cos\alpha_i + g_i(t_i)\} \sin(\widetilde{\alpha}_i + \theta_i - \widetilde{\theta}_i) \\ = t_{i+1}\cos(\widetilde{\alpha}_{i+1} + \widetilde{\theta}_{i+1} - \theta_{i+1}) + g_{i+1}(t_{i+1}) \sin(\widetilde{\alpha}_{i+1} + \widetilde{\theta}_{i+1} - \theta_{i+1}).\end{aligned}$$

Proof. Using the identity

$$\tan(\widetilde{\alpha}_i + \theta_i - \widetilde{\theta}_i) = \frac{t_i}{|ax_i| + |x_i b|} = \frac{t_i}{g_i(t_i) + |x_i b|} \ ,$$

we obtain

$$|x_i b| = \frac{t_i}{\tan(\widetilde{\alpha}_i + \theta_i - \widetilde{\theta}_i)} - g_i(t_i).$$

Therefore, on account of the equation

$$\frac{|x_i b| + |bc|}{|x_{i+1} - x_i|} = \cos\alpha_i \ ,$$

we get

$$|bc| = |x_{i+1} - x_i| \cos\alpha_i - |x_i b| = |x_{i+1} - x_i| \cos\alpha_i + g_i(t_i) - \frac{t_i}{\tan(\widetilde{\alpha}_i + \theta_i - \widetilde{\theta}_i)}.$$

On the other hand, we have

$$\tan(\widetilde{\alpha}_{i+1} + \widetilde{\theta}_{i+1} - \theta_{i+1}) = \frac{t_{i+1}}{|ef|}$$

so that

$$\begin{aligned}|x_{i+1}g| &= \{g_{i+1}(t_{i+1}) + |ef|\} \sin(\widetilde{\alpha}_{i+1} + \widetilde{\theta}_{i+1} - \theta_{i+1}) \\ &= g_{i+1}(t_{i+1}) \sin(\widetilde{\alpha}_{i+1} + \widetilde{\theta}_{i+1} - \theta_{i+1}) + t_{i+1} \cos(\widetilde{\alpha}_{i+1} + \widetilde{\theta}_{i+1} - \theta_{i+1}).\end{aligned}$$

This gives

$$\begin{aligned}|dx_{i+1}| &= \frac{|x_{i+1}g|}{\sin[\frac{\pi}{2} - (\widetilde{\alpha}_i + \theta_i - \widetilde{\theta}_i)]} = \frac{|x_{i+1}g|}{\cos(\widetilde{\alpha}_i + \theta_i - \widetilde{\theta}_i)} \\ &= \frac{g_{i+1}(t_{i+1}) \sin(\widetilde{\alpha}_{i+1} + \widetilde{\theta}_{i+1} - \theta_{i+1}) + t_{i+1} \cos(\widetilde{\alpha}_{i+1} + \widetilde{\theta}_{i+1} - \theta_{i+1})}{\cos(\widetilde{\alpha}_i + \theta_i - \widetilde{\theta}_i)} \ ,\end{aligned}$$

so that the identity

$$\frac{|cd| + |dx_{i+1}|}{|x_{i+1} - x_i|} = \sin \alpha_i$$

implies

$$\begin{aligned}|cd| &= |x_{i+1} - x_i| \sin \alpha_i - |dx_{i+1}| \\ &= \frac{|x_{i+1} - x_i| \sin \alpha_i \cos(\widetilde{\alpha}_i + \theta_i - \widetilde{\theta}_i) - g_{i+1}(t_{i+1}) \sin(\widetilde{\alpha}_{i+1} + \widetilde{\theta}_{i+1} - \theta_{i+1})}{\cos(\widetilde{\alpha}_i + \theta_i - \widetilde{\theta}_i)} \\ &\qquad - \frac{t_{i+1} \cos(\widetilde{\alpha}_{i+1} + \widetilde{\theta}_{i+1} - \theta_{i+1})}{\cos(\widetilde{\alpha}_i + \theta_i - \widetilde{\theta}_i)}.\end{aligned}$$

Finally, utilizing the identity

$$|cd| = |bc| \tan(\widetilde{\alpha}_i + \theta_i - \widetilde{\theta}_i) \ ,$$

we obtain

$$
\begin{aligned}
|x_{i+1} - x_i| \sin\alpha_i \cos(\widetilde{\alpha}_i + \theta_i - \widetilde{\theta}_i) & \\
& - g_{i+1}(t_{i+1}) \sin(\widetilde{\alpha}_{i+1} + \widetilde{\theta}_{i+1} - \theta_{i+1}) - t_{i+1} \cos(\widetilde{\alpha}_{i+1} + \widetilde{\theta}_{i+1} - \theta_{i+1}) \\
& = \sin(\widetilde{\alpha}_i + \theta_i - \widetilde{\theta}_i) \left(|x_{i+1} - x_i| \cos\alpha_i + g_i(t_i) - \frac{t_i}{\tan(\widetilde{\alpha}_i + \theta_i - \widetilde{\theta}_i)} \right) .
\end{aligned}
$$

Rearranging the terms after cancellations delivers the lemma. ■

In what follows, we use the notation

$$
r_i = \frac{1}{\kappa_i}
$$

where κ_i is the curvature at the point x_i.

Corollary 6.3.4 *In Figure 6.2, we have :*

$$
\begin{aligned}
\widetilde{\theta}_{i+1} - \theta_{i+1} = & \frac{r_i \cos\alpha_i}{|x_{i+1} - x_i| + r_{i+1} \cos\alpha_{i+1}} (\widetilde{\theta}_i - \theta_i) \\
& - \frac{|x_{i+1} - x_i|}{|x_{i+1} - x_i| + r_{i+1} \cos\alpha_{i+1}} (\widetilde{\alpha}_{i+1} - \alpha_{i+1}) \\
& + \mathcal{O}(\theta_i - \widetilde{\theta}_i)^2 + \mathcal{O}(\theta_{i+1} - \widetilde{\theta}_{i+1})^2.
\end{aligned}
$$

Proof. First we use trigonometric addition formulas to obtain

$$
\begin{aligned}
\cos(\widetilde{\alpha}_i + \theta_i - \widetilde{\theta}_i) &= \cos\widetilde{\alpha}_i \cos(\theta_i - \widetilde{\theta}_i) - \sin\widetilde{\alpha}_i \sin(\theta_i - \widetilde{\theta}_i) \\
&= \cos\widetilde{\alpha}_i - (\theta_i - \widetilde{\theta}_i) \sin\widetilde{\alpha}_i + \mathcal{O}(\theta_i - \widetilde{\theta}_i)^2 \ ,
\end{aligned}
$$

and

$$
\begin{aligned}
\sin(\widetilde{\alpha}_i + \theta_i - \widetilde{\theta}_i) &= \sin\widetilde{\alpha}_i \cos(\theta_i - \widetilde{\theta}_i) - \cos\widetilde{\alpha}_i \sin(\theta_i - \widetilde{\theta}_i) \\
&= \sin\widetilde{\alpha}_i + (\theta_i - \widetilde{\theta}_i) \cos\widetilde{\alpha}_i + \mathcal{O}(\theta_i - \widetilde{\theta}_i)^2.
\end{aligned}
$$

Also, by Lemma 6.3.1, we have

$$t_i = r_i(\widetilde{\theta}_i - \theta_i) + \mathcal{O}(\theta_i - \widetilde{\theta}_i)^2 \quad \text{and} \quad g_i(t_i) = \mathcal{O}(\theta_i - \widetilde{\theta}_i)^2.$$

Therefore, utilizing Lemma 6.3.3 yields

$$\begin{aligned}
&(|x_{i+1} - x_i| \sin \alpha_i + r_i(\widetilde{\theta}_i - \theta_i))(\cos \widetilde{\alpha}_i - (\theta_i - \widetilde{\theta}_i) \sin \widetilde{\alpha}_i) \\
&\qquad - |x_{i+1} - x_i| \cos \alpha_i (\sin \widetilde{\alpha}_i + (\theta_i - \widetilde{\theta}_i) \cos \widetilde{\alpha}_i) \\
&\qquad\qquad = r_{i+1}(\widetilde{\theta}_{i+1} - \theta_{i+1})(\cos \widetilde{\alpha}_{i+1} - (\widetilde{\theta}_{i+1} - \theta_{i+1}) \sin \widetilde{\alpha}_{i+1}) \\
&\qquad\qquad\qquad + \mathcal{O}(\theta_i - \widetilde{\theta}_i)^2 + \mathcal{O}(\theta_{i+1} - \widetilde{\theta}_{i+1})^2
\end{aligned}$$

so that

$$\begin{aligned}
&|x_{i+1} - x_i|(\sin \alpha_i \cos \widetilde{\alpha}_i - \cos \alpha_i \sin \widetilde{\alpha}_i) \\
&\qquad + (|x_{i+1} - x_i|(\sin \alpha_i \sin \widetilde{\alpha}_i + \cos \alpha_i \cos \widetilde{\alpha}_i) + r_i \cos \widetilde{\alpha}_i)(\widetilde{\theta}_i - \theta_i) \\
&\qquad\qquad = r_{i+1} \cos \widetilde{\alpha}_{i+1}(\widetilde{\theta}_{i+1} - \theta_{i+1}) + \mathcal{O}(\theta_i - \widetilde{\theta}_i)^2 + \mathcal{O}(\theta_{i+1} - \widetilde{\theta}_{i+1})^2.
\end{aligned}$$

This gives

$$\begin{aligned}
&|x_{i+1} - x_i| \sin(\alpha_i - \widetilde{\alpha}_i) + (|x_{i+1} - x_i| \cos(\alpha_i - \widetilde{\alpha}_i) + r_i \cos \widetilde{\alpha}_i)(\widetilde{\theta}_i - \theta_i) \\
&\qquad = r_{i+1} \cos \widetilde{\alpha}_{i+1}(\widetilde{\theta}_{i+1} - \theta_{i+1}) + \mathcal{O}(\theta_i - \widetilde{\theta}_i)^2 + \mathcal{O}(\theta_{i+1} - \widetilde{\theta}_{i+1})^2 \ ,
\end{aligned}$$

so that, in particular,

$$\alpha_i - \widetilde{\alpha}_i = \mathcal{O}(\theta_i - \widetilde{\theta}_i) + \mathcal{O}(\theta_{i+1} - \widetilde{\theta}_{i+1}) \ .$$

Therefore

$$
\begin{aligned}
&|x_{i+1} - x_i|(\alpha_i - \widetilde{\alpha}_i) + (|x_{i+1} - x_i| + r_i \cos\widetilde{\alpha}_i)(\widetilde{\theta}_i - \theta_i) \\
&\qquad\qquad = r_{i+1}\cos\widetilde{\alpha}_{i+1}(\widetilde{\theta}_{i+1} - \theta_{i+1}) + \mathcal{O}(\theta_i - \widetilde{\theta}_i)^2 + \mathcal{O}(\theta_{i+1} - \widetilde{\theta}_{i+1})^2.
\end{aligned}
$$

On the other hand, appealing to the fact that

$$
\begin{aligned}
\cos\widetilde{\alpha}_i &= \cos(\alpha_i + \widetilde{\alpha}_i - \alpha_i) = \cos\alpha_i\cos(\widetilde{\alpha}_i - \alpha_i) - \sin\alpha_i\sin(\widetilde{\alpha}_i - \alpha_i) \\
&= \cos\alpha_i - (\widetilde{\alpha}_i - \alpha_i)\sin\alpha_i + \mathcal{O}(\widetilde{\alpha}_i - \alpha_i)^2 \ ,
\end{aligned}
$$

this identity can be written as

$$
\begin{aligned}
&|x_{i+1} - x_i|(\alpha_i - \widetilde{\alpha}_i) + (|x_{i+1} - x_i| + r_i \cos\alpha_i)(\widetilde{\theta}_i - \theta_i) \\
&\qquad\qquad = r_{i+1}\cos\alpha_{i+1}(\widetilde{\theta}_{i+1} - \theta_{i+1}) + \mathcal{O}(\theta_i - \widetilde{\theta}_i)^2 + \mathcal{O}(\theta_{i+1} - \widetilde{\theta}_{i+1})^2.
\end{aligned}
$$

Since

$$
\alpha_i = \alpha_{i+1} + \theta_{i+1} + \theta_i \quad \text{and} \quad \widetilde{\alpha}_i = \widetilde{\alpha}_{i+1} + \widetilde{\theta}_{i+1} + \widetilde{\theta}_i \ ,
$$

we obtain

$$
\begin{aligned}
\widetilde{\theta}_{i+1} - \theta_{i+1} = &\frac{r_i\cos\alpha_i}{|x_{i+1} - x_i| + r_{i+1}\cos\alpha_{i+1}}(\widetilde{\theta}_i - \theta_i) \\
&- \frac{|x_{i+1} - x_i|}{|x_{i+1} - x_i| + r_{i+1}\cos\alpha_{i+1}}(\widetilde{\alpha}_{i+1} - \alpha_{i+1}) \\
&+ \mathcal{O}(\theta_i - \widetilde{\theta}_i)^2 + \mathcal{O}(\theta_{i+1} - \widetilde{\theta}_{i+1})^2 \ ,
\end{aligned}
$$

completing the proof. ■

Now, we find a relation between the distances $|x_{i+1} - x_i|$ and $|\widetilde{x}_{i+1} - \widetilde{x}_i|$.

Lemma 6.3.5 *In Figure 6.2, the following identity holds :*

$$
\begin{aligned}
|\widetilde{x}_{i+1} - \widetilde{x}_i| \cos(\widetilde{\alpha}_i + \theta_i - \widetilde{\theta}_i) &= |x_{i+1} - x_i| \cos\alpha_i + g_i(t_i) \\
&\qquad + t_{i+1} \sin(\theta_i + \theta_{i+1}) + g_{i+1}(t_{i+1}) \cos(\theta_i + \theta_{i+1}).
\end{aligned}
$$

Proof. It follows from Figure 6.2 that

$$
\begin{aligned}
|\widetilde{x}_{i+1} - \widetilde{x}_i| = \frac{|x_{i+1} - x_i| \cos\alpha_i + g_i(t_i)}{\cos(\widetilde{\alpha}_i + \theta_i - \widetilde{\theta}_i)} &+ |x_{i+1}g| \tan(\widetilde{\alpha}_i + \theta_i - \widetilde{\theta}_i) \\
&- \left(\frac{t_{i+1}}{\sin(\widetilde{\alpha}_{i+1} + \widetilde{\theta}_{i+1} - \theta_{i+1})} - \frac{|x_{i+1}g|}{\tan(\widetilde{\alpha}_{i+1} + \widetilde{\theta}_{i+1} - \theta_{i+1})} \right).
\end{aligned}
$$

Equivalently, this equation can be written as

$$
\begin{aligned}
|\widetilde{x}_{i+1} - \widetilde{x}_i| &= \frac{|x_{i+1} - x_i| \cos\alpha_i + g_i(t_i)}{\cos(\widetilde{\alpha}_i + \theta_i - \widetilde{\theta}_i)} - \frac{t_{i+1}}{\sin(\widetilde{\alpha}_{i+1} + \widetilde{\theta}_{i+1} - \theta_{i+1})} \\
&\quad + \Big(g_{i+1}(t_{i+1}) \sin(\widetilde{\alpha}_{i+1} + \widetilde{\theta}_{i+1} - \theta_{i+1}) + t_{i+1} \cos(\widetilde{\alpha}_{i+1} + \widetilde{\theta}_{i+1} - \theta_{i+1}) \Big) \\
&\quad \times \left(\tan(\widetilde{\alpha}_i + \theta_i - \widetilde{\theta}_i) + \frac{1}{\tan(\widetilde{\alpha}_{i+1} + \widetilde{\theta}_{i+1} - \theta_{i+1})} \right) \\
&= \frac{|x_{i+1} - x_i| \cos\alpha_i + g_i(t_i)}{\cos(\widetilde{\alpha}_i + \theta_i - \widetilde{\theta}_i)} \\
&\quad - \frac{t_{i+1}}{\sin(\widetilde{\alpha}_{i+1} + \widetilde{\theta}_{i+1} - \theta_{i+1})} \Big(1 - \cos^2(\widetilde{\alpha}_{i+1} + \widetilde{\theta}_{i+1} - \theta_{i+1}) \Big) \\
&\quad + t_{i+1} \cos(\widetilde{\alpha}_{i+1} + \widetilde{\theta}_{i+1} - \theta_{i+1}) \tan(\widetilde{\alpha}_i + \theta_i - \widetilde{\theta}_i) \\
&\quad + g_{i+1}(t_{i+1}) \sin(\widetilde{\alpha}_{i+1} + \widetilde{\theta}_{i+1} - \theta_{i+1}) \tan(\widetilde{\alpha}_i + \theta_i - \widetilde{\theta}_i) \\
&\quad + g_{i+1}(t_{i+1}) \cos(\widetilde{\alpha}_{i+1} + \widetilde{\theta}_{i+1} - \theta) \\
&= \frac{|x_{i+1} - x_i| \cos\alpha_i + g_i(t_i)}{\cos(\widetilde{\alpha}_i + \theta_i - \widetilde{\theta}_i)} \\
&\quad + t_{i+1} \Big(\tan(\widetilde{\alpha}_i + \theta_i - \widetilde{\theta}_i) \cos(\widetilde{\alpha}_{i+1} + \widetilde{\theta}_{i+1} - \theta) - \sin(\widetilde{\alpha}_{i+1} + \widetilde{\theta}_{i+1} - \theta) \Big) \\
&\quad + g_{i+1}(t_{i+1}) \Big(\tan(\widetilde{\alpha}_i + \theta_i - \widetilde{\theta}_i) \sin(\widetilde{\alpha}_{i+1} + \widetilde{\theta}_{i+1} - \theta) \\
&\qquad\qquad + \cos(\widetilde{\alpha}_{i+1} + \widetilde{\theta}_{i+1} - \theta) \Big).
\end{aligned}
$$

Therefore

$$
\begin{aligned}
&|\widetilde{x}_{i+1} - \widetilde{x}_i| \cos(\widetilde{\alpha}_i + \theta_i - \widetilde{\theta}_i) \\
&\qquad = |x_{i+1} - x_i| \cos\alpha_i + g_i(t_i) \\
&\qquad\quad + t_{i+1} \Big(\sin(\widetilde{\alpha}_i + \theta_i - \widetilde{\theta}_i) \cos(\widetilde{\alpha}_{i+1} + \widetilde{\theta}_{i+1} - \theta_{i+1}) \\
&\qquad\qquad\qquad\qquad - \cos(\widetilde{\alpha}_i + \theta_i - \widetilde{\theta}_i) \sin(\widetilde{\alpha}_{i+1} + \widetilde{\theta}_{i+1} - \theta_{i+1}) \Big) \\
&\qquad\quad + g_{i+1}(t_{i+1}) \Big(\sin(\widetilde{\alpha}_{i+1} + \widetilde{\theta}_{i+1} - \theta_{i+1}) \sin(\widetilde{\alpha}_i + \theta_i - \widetilde{\theta}_i) \\
&\qquad\qquad\qquad\qquad + \cos(\widetilde{\alpha}_{i+1} + \widetilde{\theta}_{i+1} - \theta_{i+1}) \cos(\widetilde{\alpha}_i + \theta_i - \widetilde{\theta}_i) \Big) ,
\end{aligned}
$$

so that, on account of the trigonometric difference formulas, we obtain

$$
\begin{aligned}
&|\widetilde{x}_{i+1} - \widetilde{x}_i| \cos(\widetilde{\alpha}_i + \theta_i - \widetilde{\theta}_i) \\
&\qquad = |x_{i+1} - x_i| \cos\alpha_i + g_i(t_i) \\
&\qquad\quad + t_{i+1} \sin\Big((\widetilde{\alpha}_i + \theta_i - \widetilde{\theta}_i) - (\widetilde{\alpha}_{i+1} + \widetilde{\theta}_{i+1} - \theta_{i+1}) \Big) \\
&\qquad\quad + g_{i+1}(t_{i+1}) \cos\Big((\widetilde{\alpha}_i + \theta_i - \widetilde{\theta}_i) - (\widetilde{\alpha}_{i+1} + \widetilde{\theta}_{i+1} - \theta_{i+1}) \Big) .
\end{aligned}
$$

Since

$$\widetilde{\alpha}_i = \widetilde{\alpha}_{i+1} + \widetilde{\theta}_{i+1} + \widetilde{\theta}_i \ ,$$

we get

$$
\begin{aligned}
|\widetilde{x}_{i+1} - \widetilde{x}_i| \cos(\widetilde{\alpha}_i + \theta_i - \widetilde{\theta}_i) &= |x_{i+1} - x_i| \cos\alpha_i + g_i(t_i) \\
&\qquad + t_{i+1} \sin(\theta_i + \theta_{i+1}) + g_{i+1}(t_{i+1}) \cos(\theta_i + \theta_{i+1}).
\end{aligned}
$$

completing the proof. ■

Corollary 6.3.6 *In Figure 6.2, we have*

$$\begin{aligned}&\Big(1-(\widetilde{\alpha}_i-\alpha_i+\theta_i-\widetilde{\theta}_i)\tan\alpha_i\Big)\,|\widetilde{x}_{i+1}-\widetilde{x}_i|\\&\quad=|x_{i+1}-x_i|+r_{i+1}(\widetilde{\theta}_{i+1}-\theta_{i+1})\frac{\sin(\theta_i+\theta_{i+1})}{\cos\alpha_i}+\mathcal{O}(\theta_i-\widetilde{\theta}_i)^2+\mathcal{O}(\theta_{i+1}-\widetilde{\theta}_{i+1})^2\ ,\end{aligned}$$

and

$$\begin{aligned}|\widetilde{x}_{i+1}-\widetilde{x}_i|=&\Big(1+(\widetilde{\alpha}_i-\alpha_i+\theta_i-\widetilde{\theta}_i)\tan\alpha_i\Big)\,|x_{i+1}-x_i|\\&+r_{i+1}(\widetilde{\theta}_{i+1}-\theta_{i+1})\frac{\sin(\theta_i+\theta_{i+1})}{\cos\alpha_i}+\mathcal{O}(\theta_i-\widetilde{\theta}_i)^2+\mathcal{O}(\theta_{i+1}-\widetilde{\theta}_{i+1})^2.\end{aligned}$$

Proof. Simply note that

$$\begin{aligned}\cos(\widetilde{\alpha}_i+\theta_i-\widetilde{\theta}_i)&=\cos(\alpha_i+\widetilde{\alpha}_i-\alpha_i+\theta_i-\widetilde{\theta}_i)\\&=\cos\alpha_i\cos(\widetilde{\alpha}_i-\alpha_i+\theta_i-\widetilde{\theta}_i)-\sin\alpha_i\sin(\widetilde{\alpha}_i-\alpha_i+\theta_i-\widetilde{\theta}_i)\\&=\cos\alpha_i-(\widetilde{\alpha}_i-\alpha_i+\theta_i-\widetilde{\theta}_i)\sin\alpha_i+\mathcal{O}(\theta_i-\widetilde{\theta}_i)^2\end{aligned}$$

and

$$t_i=r_i(\widetilde{\theta}_i-\theta_i)+\mathcal{O}(\theta_i-\widetilde{\theta}_i)^2\quad\text{and}\quad g_i(t_i)=\mathcal{O}(\theta_i-\widetilde{\theta}_i)^2.$$

Therefore, utilizing Lemma 6.3.5 finishes the proof. ■

Corollary 6.3.7 *For $i\geq 0$, we have*

$$\widetilde{\theta}_{i+1}-\theta_{i+1}\sim\frac{2|x_{i+1}-x_i|+r_i\cos\alpha_i}{r_{i+1}\cos\alpha_{i+1}}(\widetilde{\theta}_i-\theta_i)+\frac{2|x_{i+1}-x_i|}{r_{i+1}\cos\alpha_{i+1}}\sum_{j=0}^{i-1}\Big(\widetilde{\theta}_j-\theta_j\Big)$$

and

$$\alpha_{i+1}-\widetilde{\alpha}_{i+1}\sim\left(1+\frac{r_{i+1}\cos\alpha_{i+1}}{|x_{i+1}-x_i|}\right)(\widetilde{\theta}_{i+1}-\theta_{i+1})-\frac{r_i\cos\alpha_i}{|x_{i+1}-x_i|}(\widetilde{\theta}_i-\theta_i)$$

Proof. Utilizing Lemma 6.3.4, we get

$$\widetilde{\theta}_{i+1} - \theta_{i+1} \sim \frac{r_i \cos\alpha_i}{|x_{i+1} - x_i| + r_{i+1}\cos\alpha_{i+1}}(\widetilde{\theta}_i - \theta_i) \\ - \frac{|x_{i+1} - x_i|}{|x_{i+1} - x_i| + r_{i+1}\cos\alpha_{i+1}}(\widetilde{\alpha}_{i+1} - \alpha_{i+1})$$

so that, using

$$\alpha_{i+1} - \widetilde{\alpha}_{i+1} = 2\sum_{j=0}^{i}\left(\widetilde{\theta}_j - \theta_j\right) + \left(\widetilde{\theta}_{i+1} - \theta_{i+1}\right),$$

we obtain

$$\begin{aligned}
\widetilde{\theta}_{i+1} - \theta_{i+1} &\sim \frac{r_i \cos\alpha_i}{|x_{i+1} - x_i| + r_{i+1}\cos\alpha_{i+1}}(\widetilde{\theta}_i - \theta_i) \\
&\quad + \frac{|x_{i+1} - x_i|}{|x_{i+1} - x_i| + r_{i+1}\cos\alpha_{i+1}}\left(2\sum_{j=0}^{i}\left(\widetilde{\theta}_j - \theta_j\right) + \left(\widetilde{\theta}_{i+1} - \theta_{i+1}\right)\right) \\
&= \frac{2|x_{i+1} - x_i| + r_i\cos\alpha_i}{|x_{i+1} - x_i| + r_{i+1}\cos\alpha_{i+1}}(\widetilde{\theta}_i - \theta_i) \\
&\quad + \frac{2|x_{i+1} - x_i|}{|x_{i+1} - x_i| + r_{i+1}\cos\alpha_{i+1}}\sum_{j=0}^{i-1}\left(\widetilde{\theta}_j - \theta_j\right) \\
&\quad + \frac{|x_{i+1} - x_i|}{|x_{i+1} - x_i| + r_{i+1}\cos\alpha_{i+1}}\left(\widetilde{\theta}_{i+1} - \theta_{i+1}\right).
\end{aligned}$$

Rearranging the terms gives the first result. Note that then

$$\begin{aligned}
\alpha_{i+1} - \widetilde{\alpha}_{i+1} &= 2\sum_{j=0}^{i}\left(\widetilde{\theta}_j - \theta_j\right) + \left(\widetilde{\theta}_{i+1} - \theta_{i+1}\right) \\
&\sim \frac{r_{i+1}\cos\alpha_{i+1}\left(\widetilde{\theta}_{i+1} - \theta_{i+1}\right) - r_i\cos\alpha_i\left(\widetilde{\theta}_i - \theta_i\right)}{|x_{i+1} - x_i|} + \left(\widetilde{\theta}_{i+1} - \theta_{i+1}\right) \\
&= \left(1 + \frac{r_{i+1}\cos\alpha_{i+1}}{|x_{i+1} - x_i|}\right)(\widetilde{\theta}_{i+1} - \theta_{i+1}) - \frac{r_i\cos\alpha_i}{|x_{i+1} - x_i|}(\widetilde{\theta}_i - \theta_i)\ ,
\end{aligned}$$

finishing the proof. ■

Now, let $d = |a_1 - a_2|$, and let r_1 and r_2 denote the radius of curvature at the points a_1 and a_2 for the remaining part of this section. Then, Corollary 6.3.7 can be used to show that:

Corollary 6.3.8 *For large values of i, we have:*

$$\widetilde{\theta}_{i+1} - \theta_{i+1} \sim \frac{2d + r_i}{r_{i+1}} \left(\widetilde{\theta}_i - \theta_i\right) + \frac{2d}{r_{i+1}} \sum_{j=0}^{i-1} \left(\widetilde{\theta}_j - \theta_j\right),$$

and an equivalent form of this approximation is provided by

$$\widetilde{\theta}_i - \theta_i \sim \left(\widetilde{\theta}_0 - \theta_0\right) \prod_{j=1}^{i} \xi_j \tag{6.3.2}$$

where

$$\begin{aligned} \xi_1 &= \frac{r_0}{r_1} + \frac{2d}{r_1} \\ \xi_i &= 2\frac{d + r_{i-1}}{r_i} - \frac{1}{\xi_{i-1}}, \quad i = 2, 3, \ldots \end{aligned}$$

We also have

$$\alpha_{i+1} - \widetilde{\alpha}_{i+1} \sim \left(\widetilde{\theta}_0 - \theta_0\right) \left(\left(1 + \frac{r_{i+1}}{d}\right) \xi_{i+1} - \frac{r_i}{d}\right) \prod_{j=1}^{i} \xi_j.$$

Lemmas and Corollaries in this section provide a complete analysis of each one of the terms involved in Lemma 6.2.2. On account of these results, although we do not provide the details, we conjecture that

$$\frac{A_0 \cdots A_n}{B_0 \cdots B_n} - 1 = \mathcal{O}\left(\frac{1}{s^{n/2}}\right)$$

uniformly for $x \in \partial\Omega$. On the other hand, the approximations required for the analysis of the rays moving away from the line determined by the points a_1 and

a_2 (minimizing the distance between K_1 and K_2) can be obtained by switching the indices in the approximations obtained above. Consequently, we conjecture that the approximation

$$\frac{\prod_{i=n+p+1}^{m+p} A_i^{m+p}(x)}{\prod_{i=n+1}^{m} A_i^{m}(x)} - 1 = \mathcal{O}\left(\frac{1}{s^{m-n/2}}\right)$$

holds uniformly for $x \in \partial\Omega$. Finally, an extension of the theory of limit p-periodic continued fractions [44] is needed in order to conclude, as we did in §6.1, that

$$\lim_{m\to\infty} \prod_{i=n+1}^{n+p} A_i^{m+p}(x) = s$$

uniformly for $x \in \partial\Omega$. We expect that a combination of these will yield a complete proof that

$$\lim_{m\to\infty} \frac{\prod_{i=0}^{m+p-1} A_i^{m+p}(x)}{\prod_{i=0}^{m-1} A_i^{m}(x)} = \lim_{m\to\infty} \prod_{i=n+1}^{n+p} A_i^{m+p}(x) = s \tag{6.3.3}$$

uniformly for $x \in \partial\Omega$. We numerically verify (6.3.3) in §7.1.

Chapter 7

Numerical Experiments, Acceleration of Convergence and Connections with the Classical Scattering Theory

7.1 Numerical Experiments

In this section, we exemplify our theoretical developments in Chapter 6. To this end, we have arranged four examples concerning two-periodic orbits (see Figures 7.1, 7.2, 7.3, 7.4), and one concerning three-periodic orbits (see Figure 7.5).

In Figures 7.1, 7.2, 7.3, 7.4, top rows provide the corresponding geometrical configurations; middle rows display the ratios $\max|\eta_m|/\max|\eta_{m+2}|$ on a logarithmic scale of the iterated currents on the obstacle located on the top left or top of the upper rows; note that the bottom rows show that these ratios differ from the infinite frequency limit by an error of $\mathcal{O}(k^{-2})$.

We also note that the configurations in Figures 7.1 and 7.2 significantly differ from those in Figures 7.3 and 7.4: the obstacles in the former figures are not occluded with

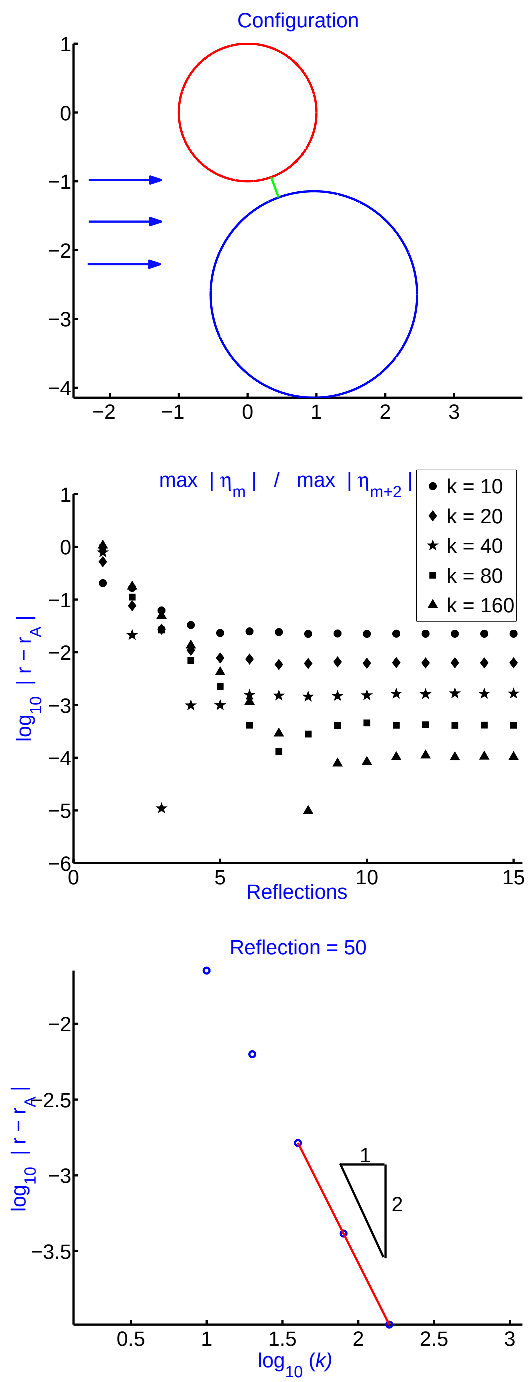

Figure 7.1: A two-periodic example without occlusion; Top: configuration; Middle: logarithmic ratios of periodically iterated currents; Bottom: errors at the 50th reflection.

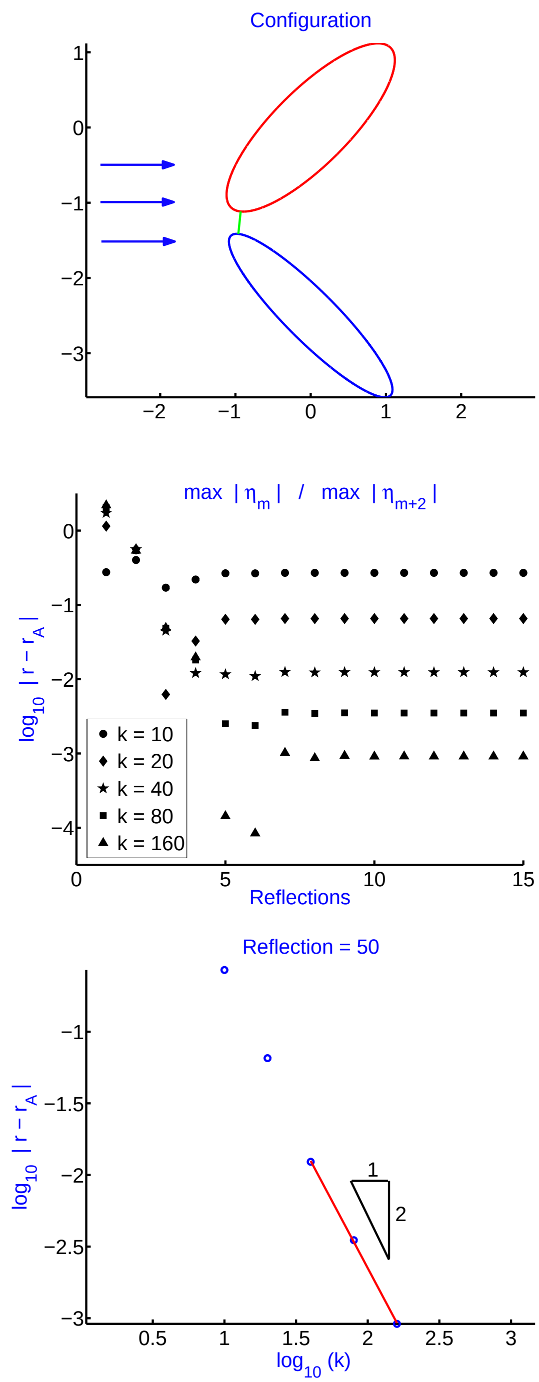

Figure 7.2: A two-periodic example without occlusion; Top: configuration; Middle: logarithmic ratios of periodically iterated currents; Bottom: errors at the 50th reflection.

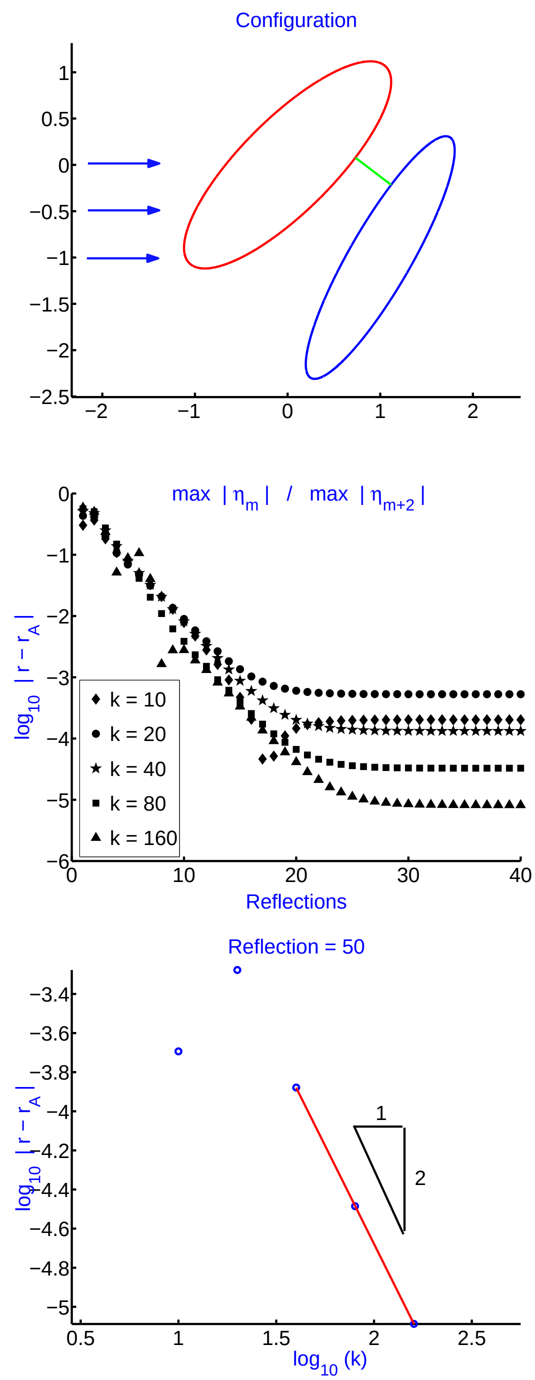

Figure 7.3: A two-periodic example with occlusion; Top: configuration; Middle: logarithmic ratios of periodically iterated currents; Bottom: errors at the 50th reflection.

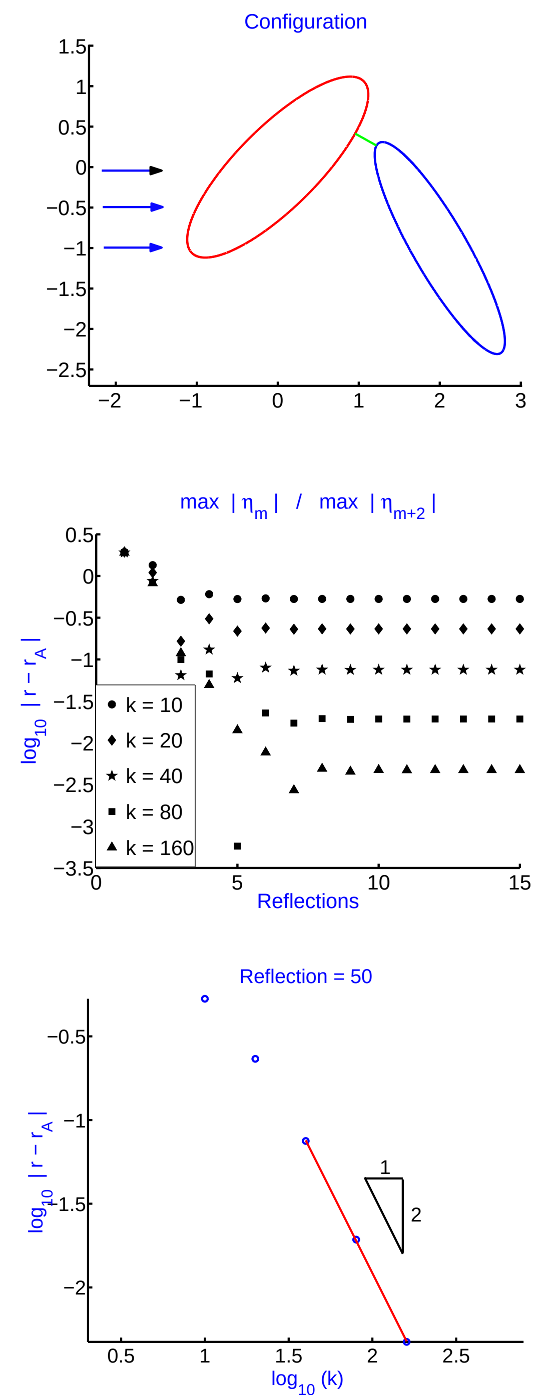

Figure 7.4: A two-periodic example with occlusion; Top: configuration; Middle: logarithmic ratios of periodically iterated currents; Bottom: errors at the 50th reflection.

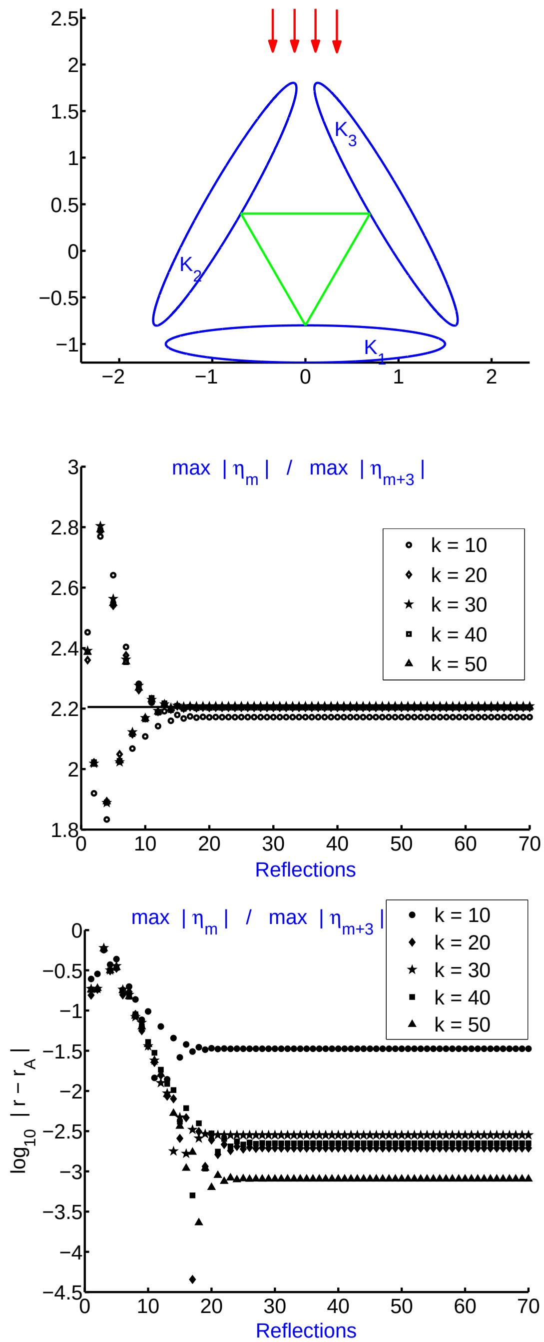

Figure 7.5: A three-periodic example; Top: configuration; Middle: periodic ratios of iterated currents; Bottom: logarithmic ratios of iterated currents.

respect to the direction of incidence, while those in latter figures are. As a consequence, the asymptotic expansions provided in Chapters 4 and 5 are not applicable in the configurations of Figures 7.3 and 7.4. However, in these configurations, similar asymptotic expansions can be derived appealing to the second derivatives of phase functions (4.1.2) at the very first reflections. Consequently, our analysis of the rate of convergence over periodic orbits can be easily extended to include the possibility of occlusion with respect to the direction of incidence yielding the same rate as before. Figures 7.3 and 7.4 verify this finding.

Finally, in Figure 7.5, we exemplify our rate of convergence formula on a three-periodic orbit: we plotted the ratios $\max|\eta_m|/\max|\eta_{m+3}|$ of the iterated currents on the obstacle $K_1 = K_{3m+1}$, $m \geq 0$, on the bottom left; bottom right provides the same plot in a logarithmic scale.

7.2 Acceleration of Convergence

Although, as our work has shown, the series converges spectrally, it is clearly desirable to design mechanisms to accelerate its convergence. Here, we provide an explanation for the enhanced convergence properties of one such procedure, namely Pade approximation [6] in this context. Indeed, as is apparent from Figures 7.1, 7.2, 7.3, 7.4 and 7.5, the ratios of iterated currents differing by one period stabilizes after a certain number of reflections. Accordingly, once stabilized, the behavior of the series resembles that of a geometric series which, in turn, can be exactly represented as a rational function. This observation suggests that beyond the point where currents become stationary, Pade approximation will deliver significantly more accurate solutions than those provided by the summation of the series. Figure 7.6, which displays the Pade algorithm applied to the configurations given in Figures 3.5 and 3.8, verify this observation.

Indeed, on account of the approximation (6.3.2), the point where the currents sta-

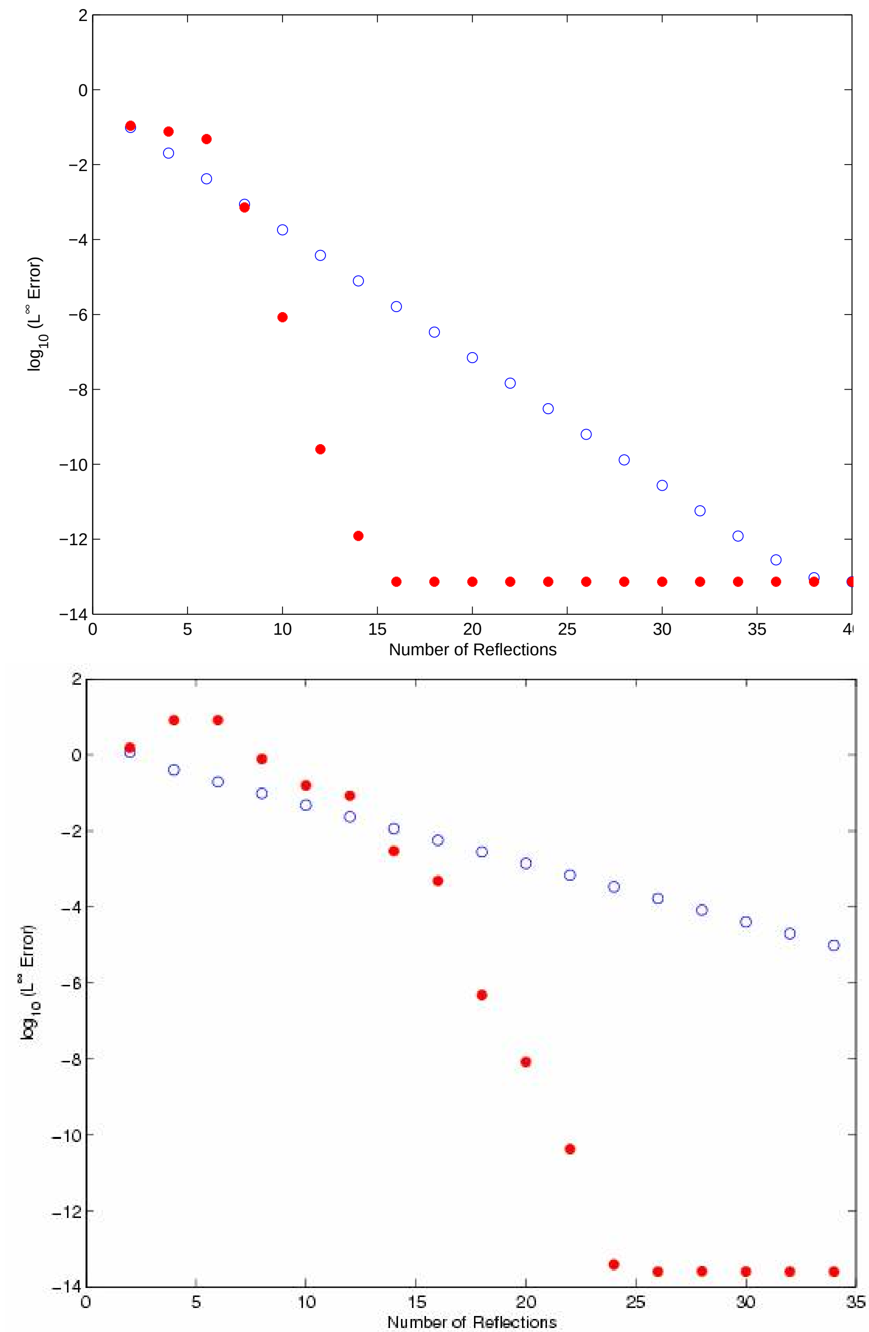

Figure 7.6: Series (hollow circles) versus Pade approximants (bold circles) in connection with the configurations given in Figures 3.5 (top) and 3.8 (bottom).

bilize can be calculated within a small error. Considering, for instance, a configuration consisting two convex obstacles, denote by r_i the radii of curvatures at the points $a_i \in \partial K_i$ minimizing the distance between the obstacles K_i, and let $d = |a_1 - a_2|$. Then the number n given by

$$n \approx \frac{4}{\log s} \max_{i=1,2} \log \frac{\theta_i}{\theta_0} \ ,$$

provides a good approximation for the point of stabilization. Here θ_0 is a fixed small angle, and

$$\theta_1 = \arcsin \frac{r_2}{r1 + r_2 + d} \ , \quad \text{and} \quad \theta_2 = \arcsin \frac{r_1}{r1 + r_2 + d} \ .$$

For instance, for the configuration in Figure 3.8, the choice of $\theta_0 = 5^o$ gives $n = 7$. This should be compared with Figure 7.1.

7.3 Poles of the Scattering Operator

As an interesting consequence of our analysis in Chapters 6 and 7, we shall show here that Theorems 4.0.1 and 5.0.1 can be used to obtain information on the poles of a fundamental object in scattering theory, namely the *scattering operator* which we now define.

To begin with, we note that the solution v of the exterior boundary value problem for the Helmholtz equation

$$\left(\Delta + k^2\right) v = 0 \quad \text{in} \ \ \Omega \tag{7.3.1}$$

$$v = f \quad \text{on} \ \ \partial K \tag{7.3.2}$$

$$\lim_{r\to\infty} r \left(\frac{\partial v}{\partial r} - ikv\right) = 0 \tag{7.3.3}$$

is uniquely determined and belongs to the spaces $L^2(\Omega, [(1 + |x|^2)^{1/2}]^{-1-\delta} dx)$, for all

$\delta > 0$, and $H^{s+1/2}_{loc}(\Omega)$ whenever $f \in H^s(\partial K)$ with $s \geq 3/2$, and $k > 0$ [75]. Denoting the solution operator by

$$v = \mathcal{B}_+(k) f,$$

we note that $\mathcal{B}_+(k)$ admits an analytic continuation onto the upper half-plane $\{k : \operatorname{Im} k > 0\}$. Moreover, the use of single and double layer potentials, as was described in §2.4 (see equations (2.4.1)-(2.4.5) and (2.4.9)), provides a meromorphic continuation of $\mathcal{B}(k)_+$ to an operator-valued function on $\mathbb{C}$, with some poles in $\{k : \operatorname{Im} k < 0\}$. These poles are known as *scattering poles.*

An important family of functions, called *improper eigenfunctions*, corresponding to the scattering problem (7.3.1)-(7.3.3) are given by

$$u_+(x, \xi) = e^{ix\cdot\xi} - \mathcal{B}_+(k) e^{ix\cdot\xi} \quad \text{on} \quad \Omega \times \mathbb{R}^3$$

where $k^2 = |\xi|^2$.

On the other hand, the *outgoing radiation condition* (7.3.3) has a counter part

$$\lim_{r\to\infty} r \left(\frac{\partial v}{\partial r} + ikv \right) = 0 \tag{7.3.4}$$

known as the *incoming radiation condition*, and clearly there is a parallel treatment of the scattering problem (7.3.1), (7.3.2) and (7.3.4). Denoting the corresponding solution operator as $\mathcal{B}_-(k)$, the related improper eigenfunctions are given by

$$u_-(x, \xi) = e^{ix\cdot\xi} - \mathcal{B}_-(k) e^{ix\cdot\xi} \quad \text{on} \quad \Omega \times \mathbb{R}^3$$

with $k^2 = |\xi|^2$.

Corresponding to these eigenfunctions, we define the following analogues of the Fourier transform:

$$\left(\Phi_\pm f\right)(\xi) = \frac{1}{(2\pi)^{3/2}} \int_\Omega \overline{u_\pm(y, \xi)} f(y) dy,$$

for $f \in C_0^\infty(\Omega)$, and

$$\left(\Phi_\pm^* g\right)(x) = \frac{1}{(2\pi)^{3/2}} \int_{\mathbb{R}^3} u_\pm(x,\xi) g(\xi) d\xi,$$

for $g \in L^\infty_{comp}(\mathbb{R}^3)$. These operators extend to surjective transformations

$$\Phi_\pm : L^2(\Omega) \longrightarrow L^2(\mathbb{R}^3) \quad \text{and} \quad \Phi_\pm^* : L^2(\mathbb{R}^3) \longrightarrow L^2(\Omega)$$

with the property that

$$\Phi_\pm^* = \Phi_\pm^{-1}.$$

From these, one constructs the unitary operator

$$S = \Phi_+ \Phi_-^* : L^2(\mathbb{R}^3) \longrightarrow L^2(\mathbb{R}^3),$$

called the *scattering operator*. This operator too can be continued analytically to $\{k : \operatorname{Im} k > 0\}$, and has a meromorphic continuation to an operator-valued function on $\mathbb{C}$, with poles confined to the set of scattering poles. Moreover, these poles coincide with the poles of the meromorphic continuations of $u_\pm$ [42, 52, 75], and they are precisely the poles arising in connection with the integral equation (3.1.3) for the family of incident fields

$$u^{inc}(x) = e^{ik\alpha \cdot x}, \quad \alpha \in S^2,$$

which is precisely the problem we studied in this thesis.

Now, let us see how equations (6.1.2) and (6.1.3) can be used to obtain information about poles of the scattering operator for a collection of convex obstacles satisfying the visibility assumption. Indeed, as we observed in §7.1, when the obstacles $K_1, \ldots, K_p$ are transversed periodically, the ratios of the iterated currents stabilizes after a certain number of reflections. On account of (6.1.2) and (6.1.3), then, it follows that

$$\sum_{i=0}^{\infty} \eta^{j+ip} \sim \eta_j + \eta_{j+p} + \cdots + \eta_{j+np} \sum_{i=0}^{\infty} \xi^i = \eta_j + \eta_{j+p} + \cdots + \eta_{j+np} \frac{1}{1-\xi}$$

where

$$\xi = (-1)^p e^{ik\varphi_p} s^{-1/2},$$

$$\varphi_p = \min \left\{ \varphi(x_1, \ldots, x_p) : (x_1, \ldots, x_p) \in \partial K_1 \times \cdots \times \partial K_p \right\},$$

and $\varphi(x_1, \ldots, x_p)$ is given by (6.1.1). Now write $k = k_1 + ik_2$, and note that $1 - \xi = 0$ if and only if

$$(-1)^p s^{1/2} e^{k_2 \varphi_p} = e^{ik_1 \varphi_p}.$$

Since the left hand side of this identity is real, so must be the right hand side. But the right hand side cannot be negative; thus, we deduce that p must be even which implies first that $k_1 \varphi_p = 2\pi q$ for some integer q, and this, in turn, gives $k_2 \varphi_p = \log s^{-1/2}$. Therefore, $1 - \xi = 0$ if and only if

$$k = \frac{1}{\varphi_p} \left(2\pi q - \frac{i}{2} \log s \right). \tag{7.3.5}$$

Note that when there are more than two convex obstacles, there are infinitely many periodic orbits, and it is a whole different problem to show that the contributions of the periodic or non-periodic orbits to the Neumann series (3.2.5) do not cause cancellation of the contributions coming from each one of the periodic orbits. Nevertheless, when there are only two convex obstacles, there are only two orbits both of which are necessarily periodic. Since the asymptotic expansions provided in Chapters 4 and 5 are valid for $k = k_1 + ik_2 \in \mathbb{C}$ with $|k_1| \gg 1$, appealing to (7.3.5), we see that the poles of the scattering operator S are

$$k \sim \frac{\pi q}{d} - \frac{i}{4d} \log s, \quad q \in \mathbb{Z}$$

where $|q| \gg 1$, and s is given by (6.1.6) in two-dimensions (and a similar expression can be obtained for s in three-dimensional configurations as was explained in Chapter 6).

We note that the poles of the scattering operator are correlated with those of the scattering matrix, a fundamental object that arises in connection with the wave equation [52]. Indeed, as was shown by Ikawa [42], the poles of the scattering matrix for two convex obstacles in two-dimensions are

$$k \sim \frac{\pi q}{d} - \frac{i}{4d} \log[(1 + \kappa_1 d)(1 + \kappa_2 d)], \quad q \in \mathbb{Z}, \quad |q| \gg 1.$$

Chapter 8

Conclusions and Future Directions

As we hope is clear from the discussions above, this thesis work suggests a number of interesting and important research directions relating to integral equation formulations of electromagnetic and acoustic scattering problems. More precisely, these include:

1. *Extensions to the full Maxwell system*: Although our work to-date has concentrated on the solution of Helmholtz equation in two- and three-dimensional settings, we expect that the methodology we developed will easily extend to the Maxwell system in three-dimensional configurations.

2. *Analysis of non-periodic orbits*: As was mentioned above, for a complete derivation of the overall convergence rate in the most general geometrical setting, an analysis over the non-periodic orbits analogous to those of the periodic orbits is required. As it turns out, this problem has connections with the decay of solutions of the wave equation [42], the poles of the scattering matrix [52], and open billiard flows [73]. We therefore expect that the study of this problem will produce significant results in connection with these classical theories.

3. *Full-error control*: The details of the proof of (6.3.3), and therefore

of the rate of convergence formula on periodic orbits, is not complete as given in §6.3. To this end, we need to obtain the error-controlled versions of Lemma 6.2.2, and Corollaries 6.3.7 and 6.3.8. As we mentioned in §6.3, once these versions are derived, an *extension* of the theory of limit p-periodic continued fractions is needed to finalize the proof of the rate of convergence formula for periodic orbits.

4. *A new Krylov subspace approach*: As is apparent form our rate of convergence formula, the Neumann series is ill-conditioned, for instance, when the curvatures of the surfaces vanish at the points minimizing the distance between two obstacles. It is therefore desirable to develop a new method for the solution of the operator equation (3.2.4) that does not suffer from geometrical constraints, and yet provides solutions in frequency-independent computational times. As was suggested in [62], one such approach can be based on the use of Krylov subspaces. Indeed, as we explained in connection with the Neumann series, for a given right hand side f in (3.2.4), each one of the scattering returns $A^n f$ can be calculated in an asymptotically bounded computational time; and, in turn, so can the Krylov subspace

$$< B^0 f, B^1 f, \ldots, B^n f >$$

where $B = I - A$. We expect that this new approach will remove the geometrical constraints arising with the use of Neumann series.

Bibliography

[1] Abarbanel S., Gottlieb D.: *A Mathematical Analysis of the PML Method.* Journal of Computational Physics, 134, 357-363, 1997.

[2] Alber H.D.: *Justification of Geometrical Optics for non-convex obstacles.* Journal of Mathematical Analysis and Applications, 80, 372-386, 1981.

[3] AndershD., Moore J., Kosanovich S., Kapp D., Bhalla R., Kipp R., Courtney T., Nolan A., German F., Cook J., Hughes J.: *Xpatch 4: The next generation in high frequency electromagnetic modeling and simulation software.* IEEE National Radar Conference Proceedings, 2000, pp. 844-849.

[4] Andersson U., Ledfelt G.: *Large scale FD-TD—A billion cells.* 15th Annual Review of Progress in Applied Computational Electromagnetics (Monterey, CA), vol. 1, March 1999, pp. 572-577.

[5] Babic V.M., Buldyrev V.S.: *Short-Wavelength Diffraction Theory: Asymptotic Methods.* Springer-Verlag, 1991.

[6] Baker G.A., Graves-Morris P.: *Pade approximants.* 2nd ed., Cambridge University Press, 1996.

[7] Bender C.M., Orszag S.A.: *Advanced Mathematical Methods for Scientists and Engineers.* MacGraw-Hill, 1978.

[8] Berenger J.P.: *A perfectly matched layer for the absorption of electromagnetic waves.* Journal of Computational Physics, 114, 185-200, 1994.

[9] Berenger J.P.: *Three-dimensional perfectly matched layer for the absorption of electromagnetic waves.* Journal of Computational Physics, 127, 363-379, 1996.

[10] Bleistein N., Handelsman R.A.: *Asymptotic Expansions of Integrals.* Dover Publications, 1986.

[11] Blezynski E., Blezynski M., Jaroszewicz T.: *AIM: Adaptive integral method for solving large-scale electromagnetic scattering and radiation problems.* Radio Science, Vol.31, No.5, 1225-1251, September-October 1996.

[12] Born M., Wolf E.: *Principles of Optics.* Cambridge University Press, 1997.

[13] Bouche D., Molinet F., Mittra R.: *Asymptotic Methods in Electromagnetics.* Springer-Verlag, 1997.

[14] Boyd J.P.: *A fast algorithm for Chebyshev, Fourier and sinc interpolation onto an irregular grid.* J. Comput. Phys. 103, 243-257, 1992.

[15] Bruno O.P., Geuzaine C.A., Monroe J.A., Reitich F.: *Prescribed error tolerances within fixed computational times for scattering problems of arbitrarily high frequency: the convex case.* Phil. Trans. Roy. Soc. London, 362, 629-645, 2004.

[16] Bruno O.P., Geuzaine C.A., Reitich F.: *A new high-order high-frequency integral equation method for the solution of scattering problems I: Single-scattering configurations.* Proceedings of the 20th Annual Review of Progress in Applied Computational Electromagnetics (Syracuse, New York), April 2004.

[17] Bruno O.P., Geuzaine C.A., Reitich F.: *A new high-order high-frequency integral equation method for the solution of scattering problems II: Multiple-scattering configurations.* Proceedings of the 20th Annual Review of Progress in Applied Computational Electromagnetics (Syracuse, New York), April 2004.

[18] Bruno O.P., Geuzaine C.A., Reitich F.: *On the $\mathcal{O}(1)$ solution of multiple-scattering problems.* IEEE Trans. Magn., to appear.

[19] Bruno O.P., Kunyansky L.: *Surface scattering in three dimensions: an accelerated high order solver.* R. Soc. Lond. Proc. Ser. A Math. Phys. Eng. Sci., 457, no. 2016, 2921-2934, 2001.

[20] Bruno O.P., Kunyansky L.: *A fast, high-order algorithm for the solution of surface scattering problems: basic implementation, tests and application.* J. Comput. Phys. 169, 80-110, 2001.

[21] Canning F.X.: *Improved Impedance Matrix Localization method.* IEEE Trans. Antenna Propagation, 41, 659-667, 1993.

[22] Coifman R., Rokhlin V., Wandzura S.: *The fast multipole method for the wave equation: A pedestrian prescription.* IEEE Antennas and Propagation Magazine, Vol.35, No.3, June 1993.

[23] Coifman R., Rokhlin V., Wandzura S.: *Faster single-stage multipole method for the wave equation.* 10th Annu. Rev. Progress Appl. Computat. Electromagn., Monterey, CA, 19-24, Mar. 1994.

[24] Colton D., Kress R.: *Integral Equation Methods in Scattering Theory.* John Wiley & Sons, 1983.

[25] Colton D., Kress R.: *Inverse Acoustic and Electromagnetic Scattering Theory.* Springer-Verlag, 1998.

[26] Cui S., Weile D.S.: *Analysis of electromagnetic scattering from periodic structures by FEM truncated by anisotropic PML boundary conditions.* Microwave Opt. Technol. Lett., Vol.48, No.7, 106-110, July 2000.

[27] Cullen J.A.: *Surface currents induced by short-wavelength radiation.* The Physical Review, Second Series, Vol.109, No.6, 1863-1867, March 1958.

[28] Cuvelier F.: *Approximation de Kirchhoff généralisée dans le complémentaire d'une réunion de convexes. (French) [Generalized Kirchhoff approximation outside a union of convex compact sets].* C. R. Acad. Sci. Paris Sér. I Math., Vol.320, No.12, 1501-1506, 1995.

[29] Darve E.: *The fast multipole method: Numerical Implementation.* Journal of Computational Physics, 160, 195-240, 2000.

[30] Dutt A., Rokhlin V.: *Fast Fourier transforms for nonequispaced data.* SIAM Journal of Scientific Computing 14, 1368-1393, 1993.

[31] Fan G.X., Liu Q.H.: *An FDTD algorithm with perfectly matched layers for general dispersive media.* IEEE Trans. Antennas. Propagat., Vol.48, No.5, May 2000.

[32] Feng N.N., Zhou G.R., Xu C.L., Huang W.P.: *Computation of full-vector modes for bending waveguide using cylindrical perfectly matched layers.* J. Lightwave Technol., 20 (11), 1976-1980, Nov 2002.

[33] Fock V.A.: *Electromagnetic Diffraction and Propagation Problems.* Pergamon Press, Oxford, 1965.

[34] Freund R.W., Golub G.H., Nachtical N.M.: *Iterative solution of linear systems.* Acta Numerica, 57-100, 1991.

[35] Greengard L., Rokhlin V.: *A fast algorithm for particle simulations.* Journal of Computational Physics, Vol.73, 325, 1987.

[36] Givoli D., Keller J.B.: *Special finite elements for use with high-order boundary conditions.* Comp. Methods Appl. Mech. Eng., 119, 199-213, 1994.

[37] Givoli D.: *Numerical Methods for Problems in Infinite Domains.* Elsevier, Amsterdam 1992.

[38] Gottlieb D., Hesthaven J.S., Yang B.: *Spectral Simulations of Electromagnetic Wave Scattering.* Journal of Computational Physics, 134, 216-230, 1997.

[39] Hesthaven J., Warburton T.: *Nodal high-order methods on unstructured grids. I. Time-domain solution of Maxwell's equations.* J. Comput. Phys. 181 (2002), no. 1, 186-221.

[40] Hong S.: *Asymptotic theory of electromagnetic and acoustic wave diffraction by smooth convex surfaces of variable curvature.* J. Math. Phys., 8, 1223-1232, 1967.

[41] Ihlenburg F.: *Finite Element Analysis of Acoustic Scattering*. Springer-Verlag, 1998.

[42] Ikawa M.: *Decay of solutions of the wave equation in the exterior of several convex bodies.* Ann. Inst. Fourier (Grenoble) 38 (1988), no.2, 113-146.

[43] Jackson, J.D.: *Classical Electrodynamics.* John Wiley & Sons, 1975.

[44] Jacobsen L., Ruscheweyn S.: *On the domain of meromorphy of limit k-periodic continued fractions.* Arch. Math. (Basel) 48 (1987), no.2, 130-135.

[45] Jin J.M.: *The Finite Element Method in Electromagnetics*. John Wiley & Sons, 1993.

[46] Keller J.B., Lewis R.M.: *Asymptotic methods for partial differential equations: The reduced wave equation and Maxwell's equations.* Reprint in Surv. Appl. Math., 1, 1-82, 1995.

[47] Kress R.: *Minimizing the condition number of boundary integral operators in acoustic and electromagnetic scattering*. Q. Jl. Mech. appl. Math., 38, 323-341, 1985.

[48] Kress R.: *Numerical Analysis.* Springer-Verlag, 1998.

[49] Kress R.: *Linear Integral Equations.* Springer-Verlag, 1999.

[50] Kunz K.S., Luebbers R.J.: *The Finite Difference Time Domain Method for Electromagnetics.* CRC, 1993.

[51] Labreuche C.A.: *A convergence theorem for the Fast Multipole Method for 2 dimensional scattering problems.* Mathematics of Computation, Vol.67, No.222, 553-591, April 1998.

[52] Lax P., Phillips R.: *Scattering theory.* Second edition. Pure and Applied Mathematics, 26. Academic Press, Inc., Boston, MA, 1989.

[53] Lu C.C., Chew W.C.: *Fast algorithm for solving hybrid integral equations.* Proc. Inst. Elect. Eng., Vol.140, pt.H, No.6, 455-460, Dec. 1993.

[54] Martensen E.: *Uber eine methode zum raumlichen Neumannschen problem mit einer anwendung fur torusartige berandungen.* Acta Math., 109, 75-135, 1963.

[55] Melrose R.B., Taylor M.E.: *Near peak scattering and the corrected Kirchhoff approximation for a convex obstacle.* Adv. in Math., 55, 242-315, 1985.

[56] Mittra R., Ramahi O.: *Absorbing boundary conditions for the direct solution of partial differential equations arising in electromagnetic scattering problems.* In Progress in Electromagnetics Research: Finite Element and Finite Difference Methods in Electromagnetic Scattering, (Editor M.A. Morgan), Elsevier, Chapter 4, 1990.

[57] Peterson A.F., Ray S.L., Mittra R.: *Computational Methods for Electromagnetics.* IEEE Press, 1998.

[58] Petkov V.M.: *High frequency asymptotics of the scattering amplitude for non-convex bodies.* Communications in Partial Differential Equations, 5(3), 293-329, 1980.

[59] Press W.H., Teukolsky S.A., Vetterling W.T., Flannery B.P.: *Numerical Recipes.* Cambridge University Press, 1992.

[60] Quarteroni A., Sacco R., Saleri F.: *Numerical Mathematics.* Springer-Verlag, 2000.

[61] Rao S.M.: *Time Domain Electromagnetics.* Academic Press, 1999.

[62] Reitich F.: Private communication.

[63] Reitich F., Tamma K.K.: *State-of-the-art, trends, and directions in Computational Electromagnetics.* CMES, Vol.4, No.4, 1-8, 2003.

[64] Rokhlin V.: *Rapid solution of integral equations of classical potential theory.* Journal of Computational Physics, Vol.60, No.2, 187-207, 1985.

[65] Rokhlin V.: *Rapid solution of integral equations of scattering theory in two dimensions.* Journal of Computational Physics, Vol.186, No.2, 414-439, 1990.

[66] Rokhlin V.: *Diagonal forms of translation operators for the Helmholtz equation in three dimensions.* Applied and Computational Harmonic Analysis 1, 82-93, 1993.

[67] Saad Y.: *Iterative Methods for Sparse Linear Systems.* PWS Pub. Co., Boston, 1996.

[68] Saad Y., Schultz M.H.: *GMRES : a generalized minimal residual algorithm for solving non-symmetric linear systems.* SIAM J. Sci. Stat. Comput., Vol.7, No.3, 856-869, 1986.

[69] Seaborn J.: *Hypergeometric Functions and Their Applications.* Springer-Verlag, 1991.

[70] Song J., Lu C.C., Chew W.C.: *Fast multipole method solution of the combined field integral equation. 11th* Annu. Rev. Progress Appl. Computat. Electromagn., Monterey, CA, 629-636, Mar. 1995.

[71] Song J., Lu C.C., Chew W.C.: *Multilevel fast multipole algorithm for electromagnetic scattering by large complex objects.* IEEE Trans. Antennas. Propagat., Vol. 45, No. 10, 1488-1493, Oct. 1997.

[72] Steinberg B.Z., Leviatan Y.: *On the use of Wavelet expansions in the method of moments.* IEEE Trans. Antenna Propagation, 41, 610-619, 1993.

[73] Stoyanov L.: *Spectrum of the Ruelle operator and exponential decay of correlations for open billiard flows.* Amer. J. Math. 123 (2001), no.4, 715-759.

[74] Taflove A.: *Computational Electrodynamics : The Finite-Difference Time Domain Method,* Artech House, 1995.

[75] Taylor M.: *Partial Differential Equations II: Qualitative Studies of Linear Equations.* Sipringer-Verlag Newyork, Inc., 1996.

[76] Taylor M.: *Pseudodifferential Operators.* Princeton University Press, 1981.

[77] Wagner R.L., Chew W.C.: *A study of wavelets for the solution of electromagnetic integral equations.* IEEE Trans. Antennas Propagat., Vol.43, 802-810, Aug. 1995.